

**NIST GCR 07-912**

**Flame Retardant Mechanism of the  
Nanotubes-based Nanocomposites.  
Final Report**

Takashi Kashiwagi  
Department of Fire Protection Engineering  
University of Maryland  
College Park, MD 20742

**NIST**  
**National Institute of  
Standards and Technology**  
U.S. Department of Commerce



**NIST GCR 07-912**

# **Flame Retardant Mechanism of the Nanotubes-based Nanocomposites. Final Report**

Prepared for  
*U.S. Department of Commerce  
Building and Fire Research Laboratory  
National Institute of Standards and Technology  
Gaithersburg, MD 20899*

By  
Takashi Kashiwagi  
Department of Fire Protection Engineering  
University of Maryland  
College Park, MD 207042

September 2007



U.S. Department of Commerce  
*Carlos M. Gutierrez, Secretary*

National Institute of Standards and Technology  
*James M. Turner, Acting Director*

### Notice

**This report was prepared for the Building and Fire Research Laboratory of the National Institute of Standards and Technology under Grant number 60NANB5D1022. The statement and conclusions contained in this report are those of the authors and do not necessarily reflect the views of the National Institute of Standards and Technology or the Building and Fire Research Laboratory.**

# **Flame Retardant Mechanism of the Nanotubes-based Nanocomposites**

## **Final Report**

60NANB5D1022

Takashi Kashiwagi  
Department of Fire Protection Engineering, University of Maryland

## Table of Contents

Summary .....	3
Paper “Nanotube networks reduce flammability of polymer nanocomposites” <i>Nature Materials</i> , <b>4</b> , 928-932, 2005 .....	5
Paper “Relationship between dispersion metric and properties of PMMA/SWNT nanocomposites” <i>Polymer</i> , <b>48</b> , 4855-4866, 2007 .....	11
Paper “Effects of aspect ratio of MWNT on the flammability properties of polymer nanocomposites” <i>Polymer</i> , <b>48</b> , 6086-6096, 2007 .....	23
Chapter 10 “New fire retardant nanocomposites” in Flame retardant Polymer Nanocomposites edited by A.B. Morgan and C.A. Wilkie, Wiley-Interscience, 2007 .....	34

## Summary

This project was started from April 1, 2005 and is ending on September 30, 2007 with a total budget of \$ 105,392.

One weak aspect of synthetic polymer materials compared with steel and other metals is that these materials are combustible under certain conditions. Thus, the majority of polymer-containing end products must pass some type of regulatory test to assure public safety from fire. Although halogenated flame retardants are highly effective for reducing heat release rates of commodity polymers, the future use of some of these retardants is becoming highly questionable in Europe and possibly worldwide. Therefore, new, highly effective flame retardants are urgently needed as a possible alternative to conventional halogenated flame retardants. The main objective is to determine the flame retardant (FR) effectiveness of various polymer/nanotube nanocomposites and to understand their FR mechanisms.

Four different nanotubes are used; they are multi-walled carbon nanotube (MWNT), single-walled carbon nanotube (SWNT), carbon nano-fiber (CNF), and alumina silicate nanotube (ASNT). The selected resins are polystyrene (PS) and poly(methyl methacrylate) (PMMA). The study consists of five parts aimed at understanding the FR mechanisms of these nanocomposites, (1) effects of nanotube type and of concentration of the nanotubes in the nanocomposites, (2) effects of the dispersion of the nanotubes in the nanocomposites, (3) effects of molecular weight of the resin, and (4) effects of viscoelastic characteristics of the nanocomposites, (5) effects of aspect ratio (length divided by outer diameter of tubes). A cone calorimeter and the nitrogen gasification device are used for measuring flammability properties of the samples. The results of the first, the third, and the fourth parts were published in *Nature Materials* and the paper is included in this report. The results of the second part (effects of dispersion) were published in *Polymer* and also the results of the fifth part (effects of aspect ratio) are being published in *Polymer*. Both papers are included in this report. Finally, a review of flammability of carbon nanotube based polymer nanocomposites was published as one of chapters in "Flame Retardant Polymer Nanocomposites" edited by A. Morgan and C. Wilkie, Wiley Interscience, 2007 and this review is also included in this report.

Nanocomposites based on ASNT with PMMA were prepared for mass concentrations of 1 %, 2 %, and 4 % of ASNT. However, ASNT was not well dispersed (translucent instead of transparent) and special functional component was attached to ASNT surface to improve the dispersion of ASNT. Although some improvement in the dispersion of ASNT was made, no significant reduction in flammability properties of PMMA was observed.

Another attempt was made to enhance char formation using functionalized nanotubes for making crosslinks with carbon in the resin by the collaboration with Professor Jim Tour at Rice University. His group prepared PS nanocomposites with 1 % mass concentration of bromo benzene functionalized SWNT and also with 1 % mass concentration of bisphenol C functionalized SWNT. Unfortunately, thermal gravimetric

analysis (TGA) and nitrogen gasification test did not show any significant increase in char yield and consequently mass loss rates of PS were not significantly reduced with the specifically functionalized SWNTs.

# Nanoparticle networks reduce the flammability of polymer nanocomposites

TAKASHI KASHIWAGI<sup>1\*</sup>, FANGMING DU<sup>2</sup>, JACK F. DOUGLAS<sup>3\*</sup>, KAREN I. WINEY<sup>2</sup>, RICHARD H. HARRIS Jr<sup>1</sup> AND JOHN R. SHIELDS<sup>1</sup>

<sup>1</sup>Fire Research Division, National Institute of Standards and Technology, Gaithersburg, Maryland 20899-8665, USA

<sup>2</sup>Chemical and Biomolecular Engineering, University of Pennsylvania, Philadelphia, Pennsylvania 19104-6272, USA

<sup>3</sup>Polymers Division, National Institute of Standards and Technology, Gaithersburg, Maryland 20899-8544, USA

\*e-mail: takashi.kashiwagi@nist.gov; jack.douglas@nist.gov

Published online: 23 October 2005; doi:10.1038/nmat1502

Synthetic polymeric materials are rapidly replacing more traditional inorganic materials, such as metals, and natural polymeric materials, such as wood. As these synthetic materials are flammable, they require modifications to decrease their flammability through the addition of flame-retardant compounds. Environmental regulation has restricted the use of some halogenated flame-retardant additives, initiating a search for alternative flame-retardant additives. Nanoparticle fillers are highly attractive for this purpose, because they can simultaneously improve both the physical and flammability properties of the polymer nanocomposite. We show that carbon nanotubes can surpass nanoclays as effective flame-retardant additives if they form a jammed network structure in the polymer matrix, such that the material as a whole behaves rheologically like a gel. We find this kind of network formation for a variety of highly extended carbon-based nanoparticles: single- and multiwalled nanotubes, as well as carbon nanofibres.

The burning process of a polymeric material typically begins with heating to a temperature at which thermal degradation initiates. The boiling temperatures of most of the thermal degradation products of polymers are much lower than the thermal degradation temperatures of thermoplastics, and the degradation products are then superheated as they form<sup>1</sup>. Bubbles nucleate below the heated polymer surface and grow with the supply of more degradation products by diffusion from the surrounding molten plastic<sup>2</sup>, and they further evolve into the gas phase as fuel vapour. These bubbles agitate the outer layer of polymer melt and can interfere with the formation of a solid, char-like heat-transfer barrier at the boundary<sup>3</sup>. It has been recognized that the use of nanoscale reinforcing fillers, such as nanoclay particles, can help to reduce the flammability of polymeric materials by inhibiting this vigorous bubbling process in the course of degradation during combustion<sup>4</sup>. The addition of these filler particles often leads to the added benefit of enhancing the physical properties of nanocomposites relative to the polymer matrix<sup>3-5</sup>. On the other hand, this flame-retardant effect is not general for all nanocomposite additives. We previously found that poly(methyl methacrylate) (PMMA)/nanocomposites of nanosilica (13% mass fraction) showed vigorous bubbling during burning as in unfilled materials, leading ultimately to a residue consisting of granular, coarse particles<sup>6</sup>. The effect of these symmetric nanoparticles on flammability was only marginal for this class of fillers. In contrast, nanocomposites based on nanoclay particles formed a continuous protective solid layer on the burning surface or extended island structures made of clay and carbonaceous char during burning<sup>7-10</sup>. (Several review papers are available that describe the flame-retardant effect of these additives<sup>11-14</sup>.) The presence of the protective layer is clearly important in the flammability reduction by these additives, but these clay-particle layers tend to develop large lateral surface cracks in which vigorous bubbling still occurs<sup>15</sup>. These extended nanoparticles are clearly promising flame retardants, but further studies are needed to improve the effectiveness of this type of filler and to understand the physical factors responsible for this flame-retardant effect.

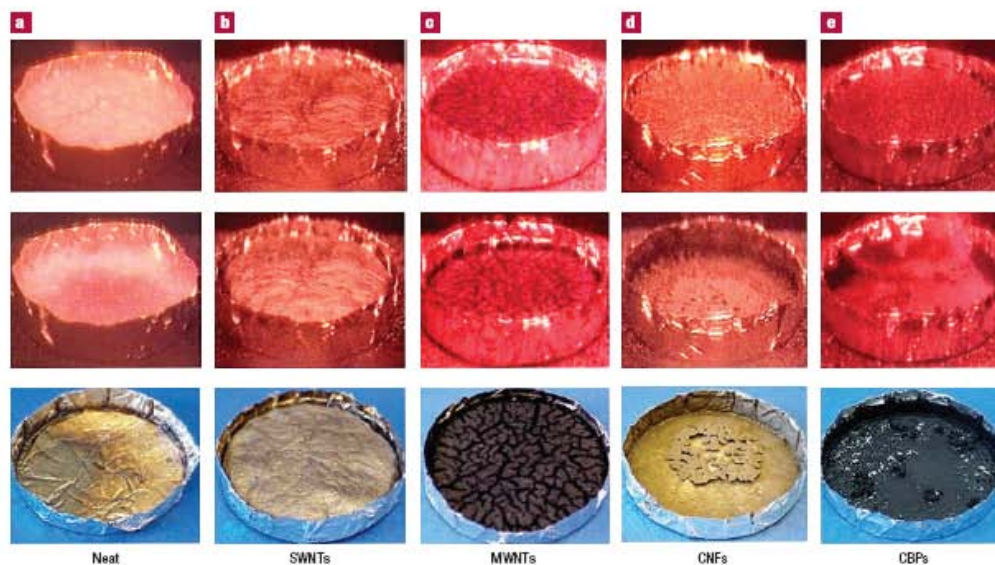


**Figure 1** Selected sequences of sample behaviour during gasification and the collected residues. The top two rows are sample behaviour and the bottom row consists of pictures of the residues. The nanocomposite samples were PMMA with 0.5% mass fraction of each nanoparticle. The tests were conducted at  $50 \text{ kW m}^{-2}$  in nitrogen.

Polymer nanocomposites with low levels of single-walled carbon nanotubes (SWNTs)<sup>16–19</sup>, multiwalled carbon nanotubes (MWNTs)<sup>20–24</sup> or carbon nanofibres (CNFs)<sup>25–28</sup> show significantly increased mechanical properties and electrical conductivity and, similarly to clay, they have a highly extended structure. Thus, carbon-based nanoadditives provide another attractive class of nanoparticle to be examined for flame retardancy. The combination of nanotubes with clay particles provides another class of materials worth exploration as flame-retardant additives<sup>29,30</sup>.

We previously found that nanocomposites based on carbon nanotubes are likewise capable of forming a continuous network-structured protective layer without the formation of cracks that compromise the flame-retardant effectiveness. This resulted in a significant reduction in heat release rate (a flammability measure related to the fire intensity) with a carbon nanotube mass concentration as low as 0.5% (refs 31–33). This protective layer consisted mainly of carbon nanotubes and it seemed to act as a heat shield for the virgin polymer below the layer<sup>32–34</sup>. Poorly dispersed carbon nanotubes resulted in the formation of a discontinuous layer consisting of fragmented islands (with sizes from 1 to 10  $\mu\text{m}$ ) rather than the continuous network protective layer<sup>33</sup>. Very low concentrations of the tubes yielded the same fragmented island structures as found in the clay nanocomposite measurements. The flame-retardant performance of the nanocomposites containing the island structures was much poorer than that of the nanocomposites forming a continuous protective network layer. Thus, the formation of the network-structured protective layer during burning, without any openings or cracks, seems to be crucial for the large reduction in heat release rate. In the present study, we suggest that this network forms in the original sample under appropriate fabrication conditions and that this structure provides the main source of the protective layer that forms during the burning process. This hypothesis is systematically tested with various sizes and concentrations of carbon-based nanoparticles in a PMMA matrix.

The selected nanoparticles all had a common carbon chemistry: SWNTs, MWNTs and CNFs. The effects of the size of the tubes on the physical structure of the protective layer and on the flame-retardant effectiveness were determined. Carbon black particles (CBPs) were also included for comparison to gain insight into the role of particle anisotropy in the flame-retardant effect.

A selected sequence of video images of a sample during gasification tests is shown in Fig. 1 for an external radiant flux of  $50 \text{ kW m}^{-2}$  in nitrogen (no flaming but sample heating similar to fire conditions). The PMMA had a viscosity-average nominal molecular mass of  $100,000 \text{ g mol}^{-1}$  and the mass fraction of SWNTs, MWNTs, CNFs and CBPs was 0.5% in each case. Pristine PMMA behaved like a liquid with vigorous bubbling, and no residue was left in the container at the end of the test. The PMMA/SWNTs(0.5%) nanocomposite was solid-like and did not show noticeable bubbling except for a short period after initial exposure to the external radiant flux. The final residue, although having a slightly undulating surface, had no deep cracks and was slightly thinner than the original sample. The residue mainly consisted of SWNTs with a network structure that was porous, transmitting about 20% of the external radiant flux through the roughly 6-mm-thick layer<sup>32</sup>. On the other hand, numerous small island structures (black spots in Fig. 1c) were formed in the case of the PMMA/MWNTs(0.5%) and the islands coagulated with the progress of the test, leading to the formation of large islands having many deep cracks. Vigorous bubbling was observed through the cracks between the islands. Both the PMMA/CNFs(0.5%) and the PMMA/CBPs(0.5%) formed slightly viscous liquids, with vigorous bubbling occurring under heating. A thin, small, coagulated, network-like residue was left at the bottom of the container of the PMMA/CNFs(0.5%) and a thin black coating over the container surface with several small islands was left after the test on the PMMA/CBPs(0.5%), as shown in Fig. 1e.

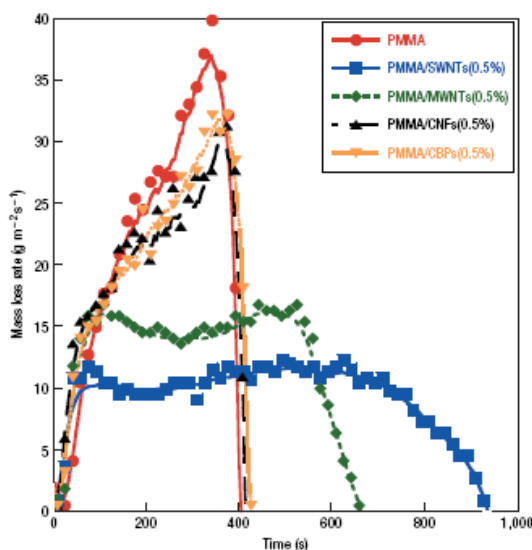


**Figure 2** Effects of the nanoparticle type on mass loss rate. The tests were conducted at an external radiant flux of  $50 \text{ kW m}^{-2}$  in nitrogen.

The mass loss rate of each sample tested in the gasification test was calculated by taking the time derivative of the measured sample mass history; the results are plotted in Fig. 2. Only the PMMA/SWNTs(0.5%) formed the network-structured layer that suppressed bubbling its mass loss rate was the least among the five samples, followed by the PMMA/MWNTs(0.5%). Mass loss rates of both the PMMA/CNFs(0.5%) and the PMMA/CBPs(0.5%) were not appreciably different from that of the pristine PMMA. From these observations, we clearly see that the formation of a network-structured protective layer during burning is crucial for the improvement in flammability properties, as suggested above.

To validate the hypothesis that a jammed network is formed in the initial samples, we performed viscoelastic measurements on the samples as a function of particle type and concentration. The viscoelastic properties of the PMMA nanocomposites containing SWNTs, MWNTs, CNFs or CBPs are presented in Fig. 3 for a range of filler mass fractions. The storage modulus  $G'$  provides a measure of nanocomposite 'stiffness' and its frequency dependence characterizes whether the material is in a liquid-like or solid-like state<sup>24</sup>. At  $200^\circ\text{C}$  and low frequencies, the PMMA/CBPs composites have nearly the same rheological response as pure PMMA, regardless of the CBP concentration, showing the typical rheological response of a newtonian liquid behaviour with  $G' \sim \omega^2$  (where  $\omega$  is the oscillatory frequency) at low frequencies. This scaling was also observed for PMMA/CNFs nanocomposites with intermediate concentration loading (that is, 1%) and for nanocomposites with low loadings of these tubular fillers (that is, 0.1%). However, for the composites containing a higher concentration of these extended fillers, this liquid-like low-frequency scaling of  $G'$  disappeared and  $G'$  became nearly constant at low frequencies. This indicates a transition from a newtonian liquid to an ideal hookean solid, which accompanies the formation of a mechanically stable network structure<sup>24,35</sup> ('jammed network' or 'dispersion gel')<sup>36</sup>. We term the composition at which this rheological state is achieved the 'gel concentration',  $\phi_g$ . Specifically,

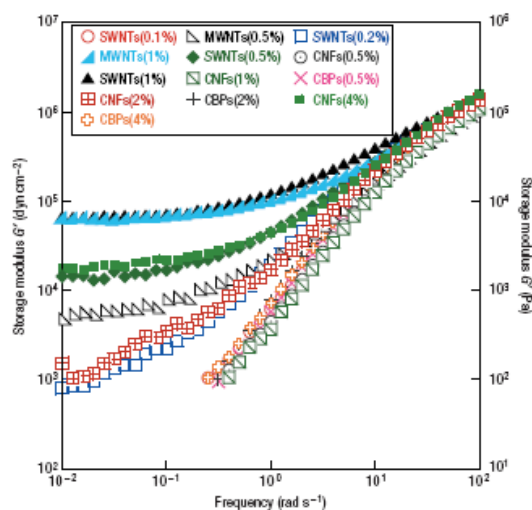


**Figure 3** Effects of the nanoparticle type and concentration on the viscoelastic measurements. The samples with solid symbols show a gel behaviour at low frequencies.

we define  $\phi_g$  as the concentration at which  $G'$  becomes independent of  $\omega$  for an extended low-frequency range.

In addition to the filler type and loading, the filler dimension also had a significant effect on the rheological response of the nanocomposite. With the same 0.5% filler loading, the SWNT nanocomposite had solid-like behaviour, whereas the MWNT nanocomposite had a much reduced elastic response as indicated by the smaller  $G'$  at low frequencies relative to the SWNT nanocomposite and the CNF nanocomposite showed only a liquid-like behaviour. An increase in the concentration of MWNTs and CNFs from 0.5% to 1% and 0.5% to 4%, respectively, yielded a gel-like rheological response for both MWNT and CNF nanocomposites. Our estimate of  $\phi_g$  has the same order of magnitude as previously reported values of the percolation concentration for electrical conductivity (0.26 vol% (ref. 37) with SWNTs, and 1% (ref. 24) and 2% (ref. 38) with MWNTs), but our nanoparticle concentration is much less than the reported percolation threshold (a mass fraction of between 10% and 20%) for CNFs<sup>39</sup>. The addition of CBPs for the concentration range considered in this study did not lead to dispersion gelation. A relatively high percolation concentration of 9 vol% has been reported for CBPs<sup>40</sup>.

Previous work has shown that there should be a general tendency of  $\phi_g$  to decrease with decreasing tube diameter in this class of extended particles<sup>36</sup>. We can roughly understand this trend from the increase in the interfacial area and for tube of a smaller diameter. It is estimated that the interface areas of the MWNTs and the CNFs are about 70% and about 10% of that of the SWNTs, respectively, in 0.5% mass fraction of each type of tubes in PMMA. The fact that the SWNTs tend to form bundles or ropes of nanotubes mitigates the effect of having a small ratio of the SWNT diameter to the diameter of the MWNTs to some extent. The relationship between flammability properties and the total interfacial area is discussed in Supplementary Information.

The results of the gasification experiments with various concentrations of SWNTs, MWNTs and CBPs in PMMA are

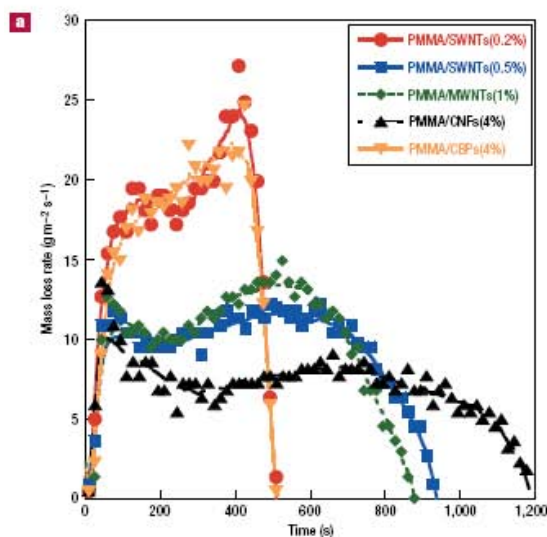


**Figure 4** Effects of the nanoparticle type and concentration on mass loss rate and the configuration of the residues. The tests were conducted at an external radiant flux of 50 kW m<sup>-2</sup> in nitrogen. a, Mass loss rate. b, Pictures of the residues.

shown in Fig. 4a. The PMMA/SWNTs(0.2%), which did not form gelled nanocomposites (see Fig. 3), formed island structures (Fig. 4b) rather than a continuous network protective layer. Its mass loss rate was also much higher than that of the PMMA/SWNTs(0.5%), which formed a continuous protective layer. The PMMA/MWNTs(1%) and the PMMA/CNFs(4%) also formed a network layer (Fig. 4b) and their mass loss rates were at least as low as that of the PMMA/SWNTs(0.5%). However, the PMMA/CBPs(4%) formed a thin layer consisting of the accumulation of a large amount of coagulated granular particles. In addition, bubbling was observed between the granular

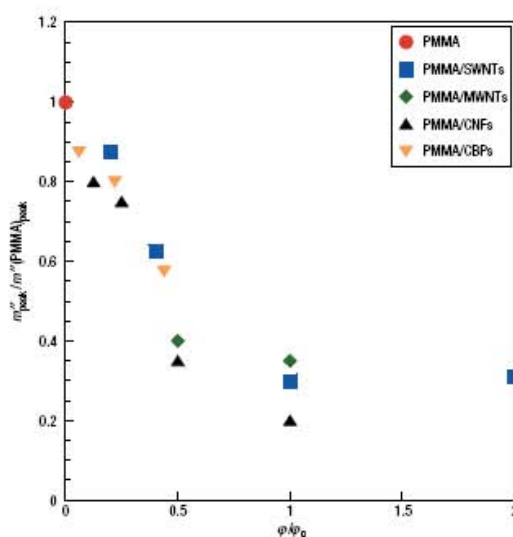


**Figure 5** Relationships between normalized peak mass loss rate and normalized concentration of nanoparticles. Mass loss rates were measured at 50 kW m<sup>-2</sup> in nitrogen. The peak mass loss rate is normalized by the peak mass loss rate of PMMA. The concentration is normalized by the concentration  $\varphi_g$  at which hookan solid gel is formed. The relationship of  $m''_{peak}/m''(PMMA)_{peak} \approx 1 - (2/3)(\varphi/\varphi_g)$  provides a fair representation of our data for the pre-gel concentration range,  $0 \leq \varphi/\varphi_g < 1$ .

particles; this sample's mass loss rate was as high as that of the PMMA/SWNTs(0.2%).

These observations indicate that a large reduction in nanocomposite flammability requires a sufficient nanoparticle concentration  $\varphi_g$  to form a jammed network within the polymer network. We next quantify how this flammability reduction depends on  $\varphi$  (the nanoparticle concentration) to show the transition between the low-flammability reduction regime for small  $\varphi$  and the high-flammability reduction regime for large  $\varphi$ . We normalize the nanoparticle concentration by  $\varphi_g$  for each type of nanoparticle. From Fig. 3 we estimate  $\varphi_g = 0.5\%$  for SWNTs, 1% for MWNTs and 4% for CNFs. Although the CBP concentration used in this study was not sufficient for gelation, we chose a relatively large concentration of this filler ( $\varphi_g = 9\%$ ) to compare with the extended nanoparticle additives. The relationship between the normalized concentration of nanoparticles and the normalized peak mass loss rate is shown in Fig. 5. The peak mass loss rate  $m''_{peak}$  is related to the peak heat release rate, which is a key flammability measure. This figure shows that an increase in the total surface area sharply decreases the peak mass loss rate until the nanocomposite reaches the critical composition  $\varphi_g$ . Then, it seems that a further increase in the concentration of the nanoparticle does not significantly affect the mass loss rate. (A further increase in the concentration of MWNTs in polypropylene actually increased the peak heat release rate, which is probably due to an increase in thermal conductivity of the nanocomposites<sup>2,3</sup>.) These results confirm that achieving  $\varphi_g$  in the initial sample is critical for obtaining maximally reduced flammability properties. Apparently the network structure in the initial sample remains intact during burning, although it was compacted after the PMMA was degraded and its degradation products were gasified.

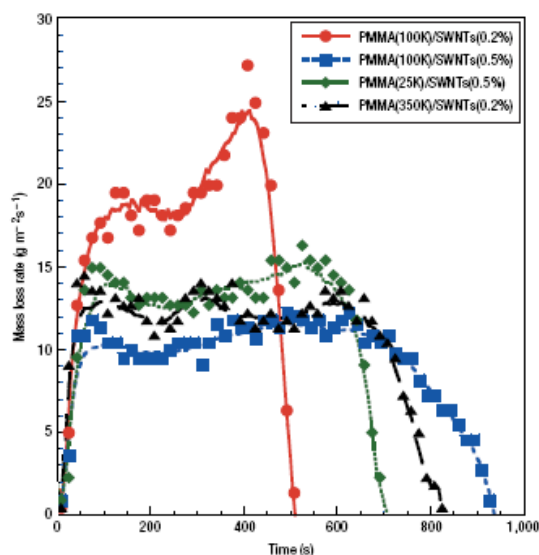


**Figure 6** Effects of  $M_w$  of PMMA on mass loss rate. The tests were conducted at an external radiant flux of  $50 \text{ kW m}^{-2}$  in nitrogen.

The integrity of the network at high temperatures can be expected to be influenced by the molecular mass of the polymer matrix. We thus examine the effect of molecular mass,  $M_w$ , of the resin on the flammability properties of carbon-based nanocomposites. In particular, we anticipate that a high- $M_w$  resin (high viscosity) enhances the formation of the network layer through entanglement couplings of the polymer chains with the nanotube bundles<sup>23</sup>. The low- $M_w$  resin (low viscosity) should have a reduced network integrity owing to the destabilizing effect of the formation and convective motion of bubbles in the molten nanocomposite under burning conditions<sup>24</sup>. The movement of nanoclay particles induced by bubbles was observed in previous measurements on the gasification of polyamid 6–clay nanocomposites<sup>15</sup>. Similar effects could occur for the extended carbon-based nanocomposites if the integrity of the network is not sufficiently strong to resist the movement of bubbles. In order to examine the effects of  $M_w$  on the formation of a network and on flammability properties, PMMA nanocomposites (25,000 and 350,000  $\text{g mol}^{-1}$ ) were prepared with SWNTs; these were subjected to the rheological analysis. The  $G'$  of the PMMA(350K)/SWNTs(0.2%) was roughly an order of magnitude larger than that of the PMMA(100K)/SWNTs(0.2%) and it also showed a weak dependence on frequency in the range of low frequencies ( $<10^{-1} \text{ rad s}^{-1}$ ). The  $G'$  of the PMMA(25K)/SWNTs(0.5%) was roughly an order of magnitude less than that of the PMMA(100K)/SWNTs(0.5%) and showed nearly the same dependence on  $\omega$  as the PMMA(100K)/MWNTs(0.5%).

The measured mass loss rates of the PMMA(350K)/SWNTs(0.2%) and the PMMA(25K)/SWNTs(0.5%) are plotted in Fig. 6, including the PMMA(100K)/SWNTs(0.2%) from Fig. 4 and the PMMA(100K)/SWNTs(0.5%) from Fig. 2 for comparison. Mass loss rates of the nanocomposites with higher  $M_w = 350,000 \text{ g mol}^{-1}$  PMMA were clearly lower than those with

lower  $M_w = 100,000 \text{ g mol}^{-1}$  PMMA. Even with 0.2% of SWNTs, the nanocomposites with  $M_w = 350,000 \text{ g mol}^{-1}$  PMMA formed a very wavy, network-structured layer during burning compared with the formation of islands for  $M_w = 100,000 \text{ g mol}^{-1}$  PMMA. At a mass fraction of 0.5% of SWNTs, the nanocomposite with  $M_w = 25,000 \text{ g mol}^{-1}$  PMMA formed a network layer, but its mass loss rate was about 20% higher than that of the nanocomposite with  $M_w = 100,000 \text{ g mol}^{-1}$  PMMA as shown in Fig. 6. Although the nanocomposites having the characteristic composition of  $\phi_g$  are required for significantly reducing flammability properties, it seems that there is no direct correlation between  $G'_p$  (plateau in  $G'$  at low frequencies) at  $\phi_g$  and the extent of flammability reduction with the nanoparticles. For example, the mass loss rate of the PMMA(100K)/SWNTs(1%) was about the same as that of the PMMA(100K)/SWNTs(0.5%) even though the former  $G'_p$  at  $\phi_g$  was about four times higher than the latter  $G'_p$ . Furthermore, the PMMA(100K)/CNFs(4%) nanocomposite had the lowest mass loss rate, but its  $G'_p$  at  $\phi_g$  was lower than those of PMMA/SWNTs(1%) and PMMA/MWNTs(1%) at  $\phi_g$ .

The propensity to form jammed network structures from extended nanoparticles should not be limited to tubular-shaped additives and in future work we plan to examine our network hypothesis for the reduced flammability of polymer nanocomposites in the case of clay (plate) and carbon sheet additives. We also plan to investigate the role of particle flexibility and size polydispersity on the critical concentration  $\phi_g$  describing the gel concentration. Finally, we point out that our observations suggest that we screen for promising flame-retarded polymer nanocomposites by performing viscoelastic measurements on the initially fabricated samples.

## METHODS

Certain commercial equipment, instruments, materials, services or companies are identified in this article to specify adequately the experimental procedure. This in no way implies endorsement or recommendation by NIST.

The matrix polymer is PMMA (Polyscience). The SWNTs were synthesized by HiPCo and provided from Carbon Nanotechnologies Incorporated and Foster Miller Company. The MWNTs were purchased from Nano Laboratory and the CNFs (PR-1) were purchased from Applied Science. The CBPs were N299 provided by Sid Richardson Carbon. The coagulation method was used to produce all samples<sup>35</sup>. Dimethylformamide was chosen to dissolve the PMMA and to permit dispersion of the particles by sonication for 24 h. A concentration of  $0.2 \text{ mg ml}^{-1}$  (particles/dimethylformamide) was used to make sure that all of the samples had good dispersion of the particles in the sample. Rheology measurements were performed on a Rheometric Solid Analyzer (RSAII) in oscillatory shear with a sandwich fixture. Samples  $12.5 \text{ mm} \times 16 \text{ mm} \times 0.5 \text{ mm}$  were run at  $200 \text{ }^\circ\text{C}$  with a strain of 0.5%. Results were reproducible after one frequency sweep, indicating that there was no chain degradation or further filler alignment during measurement.

A radiant gasification apparatus was designed and constructed at NIST to study the gasification processes of samples (75 mm diameter and 8 mm thick) by measuring sample mass and recording the sample behaviour using a video camera. The apparatus consists of a stainless-steel cylindrical chamber that is 1.70 m tall and 0.61 m in diameter. All tests were conducted at  $50 \text{ kW m}^{-2}$  in nitrogen; more detailed discussion of the apparatus is given in our previous study<sup>41</sup>. The standard uncertainty of the measured mass loss rate is  $\pm 10\%$ . The peak mass loss rate  $m''_{\text{peak}}$  is related to the peak heat release rate, which is a key flammability measure. One peak was observed without the formation of a protective network layer, whereas two peaks were observed with samples having a jammed network, as shown in Figs 2 and 4a. The second, late-stage peak occurs after the formation of the protective network layer and in this case we chose this peak to define  $m''_{\text{peak}}$ .

Received 1 July 2005; accepted 18 August 2005; published 23 October 2005.

## References

1. Kashiwagi, T. Polymer combustion and flammability — Role of the condensed phase. *Proc. Combust. Inst.* 28, 1423–1437 (1994).
2. Clift, R., Grace, J.R. & Weber, M.E. *Bubbles, Drops, and Particles* (Academic, New York, 1978).

3. Kojima, Y. *et al.* Mechanical properties of nylon 6-clay hybrid. *J. Mater. Res.* 8, 1185–1189 (1993).
4. Giannelis, E. P. Polymer layered silicate nanocomposites. *Adv. Mater.* 8, 29–35 (1996).
5. Wang, Z. & Pinnavaia, T. I. Hybrid organic-inorganic nanocomposites: Exfoliation of magadite nanolayers in an elastomeric epoxy polymer. *Chem. Mater.* 10, 1820–1826 (1998).
6. Kashwagi, T. *et al.* Thermal and flammability properties of a silica-poly(methylmethacrylate) nanocomposite. *J. Appl. Polym. Sci.* 89, 2072–2078 (2003).
7. Gilman, J. W. & Kashwagi, T. Nanocomposites: A revolutionary new flame retardant approach. *SAMPE J.* 33, 40–46 (1997).
8. Gilman, J. W. *et al.* Flammability properties of polymer-layered-silicate nanocomposites. Polypropylene and polystyrene nanocomposites. *Chem. Mater.* 12, 1866–1873 (2000).
9. Zhu, J., Morgan, A. B., Lamelas, F. J. & Wilkie, C. A. Fire properties of polystyrene-clay nanocomposites. *Chem. Mater.* 13, 3774–3780 (2001).
10. Zanetti, M., Kashwagi, T., Falqui, L. & Camino, G. Cone calorimeter combustion and gasification studies of polymer layered silicate nanocomposites. *Chem. Mater.* 14, 881–887 (2002).
11. Gilman, J. W. Flammability and thermal stability studies of polymer layered-silicate (clay) nanocomposites. *Appl. Clay Sci.* 15, 31–49 (1999).
12. Porter, D., Metcalfe, E. & Thomas, M. J. K. Nanocomposite fire retardants — A review. *Fire Mater.* 24, 45–52 (2000).
13. Wilkie, C. A. In *Fire Retardancy of Polymers* (eds Le Bras, M., Wilkie, C. A. & Bourgiot, S.) Ch. 1 (Royal Society of Chemistry, Cambridge, 2005).
14. Kashwagi, T. In *Fire Retardancy of Polymers* (eds Le Bras, M., Wilkie, C. A. & Bourgiot, S.) Ch. 6 (Royal Society of Chemistry, Cambridge, 2005).
15. Kashwagi, T. *et al.* Flame retardant mechanism of polyamid 6-clay nanocomposites. *Polymer* 45, 881–891 (2004).
16. Ajayan, P. M., Schadler, L. S., Giannaris, C. & Rubio, A. Single-walled carbon nanotube-polymer composites: strength and weakness. *Adv. Mater.* 12, 750–753 (2000).
17. Park, C. *et al.* Dispersion of single wall carbon nanotubes by in situ polymerization under sonication. *Chem. Phys. Lett.* 364, 303–308 (2002).
18. Chauvet, O., Benoit, J. M. & Corraze, B. Electrical, magneto-transport and localization of charge carriers in nanocomposites based on carbon nanotubes. *Carbon* 42, 949–952 (2004).
19. Chang, T. E. *et al.* Microscopic mechanism of reinforcement in single-wall carbon nanotube/polypropylene nanocomposites. *Polymer* 46, 439–444 (2005).
20. Stephan, C. *et al.* Raman spectroscopy and conductivity measurements on polymer-multi-walled carbon nanotubes composites. *J. Mater. Res.* 17, 396–400 (2002).
21. Barrau, S., Demont, P., Peigney, A., Laurent, C. & Lacabanne, C. DC and AC conductivity of carbon nanotubes-polyepoxy composites. *Macromolecules* 36, 5187–5194 (2003).
22. Ruan, S. L., Gao, P., Yang, X. G. & Yu, T. X. Toughening high performance ultrahigh molecular weight polyethylene using multiwalled carbon nanotubes. *Polymer* 44, 5643–5654 (2003).
23. Meinke, O. *et al.* Mechanical properties and electrical conductivity of carbon-nanotube filled polyamide-6 and its blends with acrylonitrile/butadiene/styrene. *Polymer* 45, 739–748 (2004).
24. Kharchenko, S. B., Douglas, J. E., Obrzut, J., Grulke, E. A. & Milger, K. B. Flow-induced properties of nanotube-filled polymer materials. *Nature Mater.* 3, 564–568 (2004).
25. Lozano, K., Yang, S. & Zeng, Q. Rheological analysis of vapor-grown carbon nanofiber-reinforced polyethylene composites. *J. Appl. Polym. Sci.* 93, 155–162 (2004).
26. Zeng, J., Szlystak, B., Johnson, W. S., Schiraldi, D. A. & Kumar, S. Processing and properties of poly(methyl methacrylate)/carbon nano fiber composites. *Composites B* 35, 173–178 (2003).
27. Xu, Y., Higgins, B. & Brittain, W. I. Bottom-up synthesis of PS-CNF nanocomposites. *Polymer* 46, 799–810 (2005).
28. Gauthier, C., Chazeau, L., Prasse, T. & Cavaille, J. Y. Reinforcement effects of vapor grown carbon nanofibers as fillers in rubbery matrixes. *Compos. Sci. Technol.* 65, 335–343 (2005).
29. Peeterbroeck, S. *et al.* Polymer-layered silicate-carbon nanotube nanocomposites: unique nanofiller synergistic effect. *Compos. Sci. Technol.* 64, 2317–2323 (2004).
30. Beyer, G. Filler blend of carbon nanotubes and organoclays with improved char as a new flame retardant system for polymers and cable applications. *Fire Mater.* 29, 61–69 (2005).
31. Kashwagi, T. *et al.* Thermal degradation and flammability properties of poly(propylene)/carbon nanotube composites. *Macromol. Rapid Commun.* 23, 761–765 (2002).
32. Kashwagi, T. *et al.* Thermal and flammability properties of polypropylene/carbon nanotube nanocomposites. *Polymer* 45, 4227–4239 (2004).
33. Kashwagi, T. *et al.* Flammability properties of polymer nanocomposites with single-walled carbon nanotubes: effects of nanotube dispersion and concentration. *Polymer* 46, 471–481 (2005).
34. Scharif, R., Pötschke, P., Knoll, U. & Abdel-Goad, M. Fire behavior of polyamide 6/multiwall carbon nanotube nanocomposites. *Eur. Polym. J.* 41, 1061–1070 (2005).
35. Du, F. *et al.* Nanotube networks in polymer nanocomposites: rheology and electrical conductivity. *Macromolecules* 37, 9048–9055 (2004).
36. Bicerano, J., Douglas, J. E. & Brune, D. A. Model for the viscosity of particle dispersions. *J.M.S.-Rev. Macromol. Chem. Phys. C* 39, 561–642 (1999).
37. Hough, L. A., Islam, M. F., Janney, P. A. & Yodanis, A. G. Viscosity of single wall carbon nanotube suspensions. *Phys. Rev. Lett.* 93, 168102 (2004).
38. Pötschke, P., Fornes, T. D. & Paul, D. R. Rheological behavior of multiwalled carbon nanotube/polycarbonate composites. *Polymer* 43, 3247–3255 (2002).
39. Lazano, K., Yang, S. & Zeng, Q. Rheological analysis of vapor-grown carbon nanofiber-reinforced polyethylene composites. *J. Appl. Polym. Sci.* 93, 155–162 (2004).
40. Yurekli, K. *et al.* Structure and dynamics of carbon black-filled elastomers. *J. Polym. Sci. B* 39, 256–275 (2001).
41. Austin, P. I., Buch, R. R. & Kashwagi, T. Gasification of silicone fluids under external thermal radiation Part I. Gasification rate and global heat of gasification. *Fire Mater.* 22, 221–237 (1998).

#### Acknowledgements

We thank S. Kharchenko of Masco Corporation for valuable discussion and Carbon Nanotechnologies Incorporated, Foster Miller Company for providing SWNTs and Sid Richardson Carbon Company for providing CBPs. T.K. acknowledges funding from NIST by 5D1022 and E.D. and K.L.W. acknowledge funding from the Office of Naval Research by ONR Grant N00014-02-1-0890. This is a publication of the National Institute of Standards and Technology (NIST), an agency of the US Government, and by statute is not subject to copyright in the United States. Correspondence and requests for materials should be addressed to T.K. or J.E.D. Supplementary Information accompanies this paper on [www.nature.com/naturematerials](http://www.nature.com/naturematerials).

#### Competing financial interests

The authors declare that they have no competing financial interests.

Reprints and permission information is available online at <http://ngp.nature.com/reprintsandpermissions/>



## Relationship between dispersion metric and properties of PMMA/SWNT nanocomposites<sup>☆</sup>

Takashi Kashiwagi<sup>a,\*</sup>, Jeffrey Fagan<sup>b</sup>, Jack F. Douglas<sup>b</sup>, Kazuya Yamamoto<sup>a</sup>, Alan N. Heckert<sup>c</sup>, Stefan D. Leigh<sup>c</sup>, Jan Obrzut<sup>b</sup>, Fangming Du<sup>d</sup>, Sheng Lin-Gibson<sup>b</sup>, Minfang Mu<sup>d</sup>, Karen I. Winey<sup>d</sup>, Reto Haggenmueller<sup>a</sup>

<sup>a</sup> Fire Research Division, National Institute of Standards and Technology, Gaithersburg, MD 20899, USA

<sup>b</sup> Polymers Division, National Institute of Standards and Technology, Gaithersburg, MD 20899, USA

<sup>c</sup> Statistical Engineering Division, National Institute of Standards and Technology, Gaithersburg, MD 20899, USA

<sup>d</sup> Department of Chemical and Biomolecular Engineering, University of Pennsylvania, Philadelphia, PA 19104, USA

Received 30 April 2007; received in revised form 4 June 2007; accepted 5 June 2007

Available online 13 June 2007

### Abstract

Particle spatial dispersion is a crucial characteristic of polymer composite materials and this property is recognized as especially important in nanocomposite materials due to the general tendency of nanoparticles to aggregate under processing conditions. We introduce dispersion metrics along with a specified dispersion scale over which material homogeneity is measured and consider how the dispersion metrics correlate quantitatively with the variation of basic nanocomposite properties. We then address the general problem of quantifying nanoparticle spatial dispersion in model nanocomposites of single-walled carbon nanotubes (SWNTs) dispersed in poly(methyl methacrylate) (PMMA) at a fixed SWNT concentration of 0.5% using a 'coagulation' fabrication method. Two methods are utilized to measure dispersion, UV–vis spectroscopy and optical confocal microscopy. Quantitative spatial dispersion levels were obtained through image analysis to obtain a 'relative dispersion index' (RDI) representing the uniformity of the dispersion of SWNTs in the samples and through absorbance. We find that the storage modulus, electrical conductivity, and flammability property of the nanocomposites correlate well with the RDI. For the nanocomposites containing the same amount of SWNTs, the relationships between the quantified dispersion levels and physical properties show about four orders of magnitude variation in storage modulus, almost eight orders of magnitude variation in electric conductivity, and about 70% reduction in peak mass loss rate at the highest dispersion level used in this study. The observation of such a profound effect of SWNT dispersion indicates the need for objective dispersion metrics for correlating and understanding how the properties of nanocomposites are determined by the concentration, shape and size of the nanotubes.

Published by Elsevier Ltd.

**Keywords:** Particle dispersion metric; Carbon nanotubes; Nanocomposite

### 1. Introduction

Since the discovery of carbon nanotubes (CNTs) by Iijima [1], extensive studies have been conducted exploring their unique electronic, thermal, optical, and mechanical properties

and their potential use in greatly enhancing the physical properties of polymer nanocomposites [2–6], as summarized in recent review articles [7,8]. The outstanding properties are in part attributed to their extremely high aspect ratio (length-to-outer diameter ratio) of up to 1000. It is often stated that the full realization of the reinforcement potential of CNTs requires good spatial dispersion of the CNTs in the polymer and efficient interfacial stress transfer between the CNTs and the polymer matrix [7]. To address this general problem, we must first define some objective method defining what 'good dispersion' means. In particular, we need some kind

<sup>☆</sup>This was carried out by the National Institute of Standards and Technology (NIST), an agency of the US Government and is not subject to copyright in the US.

\* Corresponding author.

E-mail address: [takashi.kashiwagi@nist.gov](mailto:takashi.kashiwagi@nist.gov) (T. Kashiwagi).

of dispersion metric to evaluate the role of dispersion on nanocomposite properties.

In attempts to achieve well-dispersed CNTs in a polymer, functionalization of the CNT walls [9,10], use of surfactants [11], controlled duration of sonication of mixtures of CNTs in various solvents [12–16], in situ polymerization under sonication [17], in situ bulk polymerization [18], high speed mechanical stirring [19,20], and compounding using a twin screw extruder [21,22] have been used. The dispersion of the CNTs in the polymer was mainly determined by taking images using transmission electron microscopy (TEM), scanning electron microscopy (SEM), or optical microscopy. Most studies provide only a *qualitative* measure of dispersion of the CNTs, without a specification of the length scale over which these characterizations are made along with the scale over which this metrics applied. A *quantitative* measure of spatial dispersion of nanoparticles is critically needed to understand the relationship between the original sample characterization and the physical properties of nanocomposites [23]. Further improvement in the physical properties of nanocomposite could be achieved from such a relationship [24].

To develop such a quantitative relationship, papers describing quantitative characterizations of the dispersion of nanoparticles have been recently published. Four different methods using small-angle neutron scattering, near-infrared fluorescence measurement, optical absorption spectroscopy, and resonant Raman scattering were applied to determine the dispersion of DNA-wrapped single-walled carbon nanotubes (SWNTs) in poly(acrylic acid) [25]. The morphology of dispersed SWNT was determined by light scattering [12] and the length and the diameter of multi-walled carbon nanotubes (MWNTs) suspended in an aqueous solution were determined by analysis of the images taken by field emission gun scanning microscope [15]. The dispersion level of SWNTs in poly(methyl methacrylate) (PMMA) was characterized by producing a Raman map over a  $40\ \mu\text{m} \times 40\ \mu\text{m}$  domain by measuring Raman scattering intensity [13]. A value of the mean standard deviation (SD) of the Raman scattering intensity over the map was used as a quantitative dispersion index of the SWNTs in the PMMA. (A small value of standard deviation in the intensity represents good dispersion.) A similar approach measuring intensity variation of a fluorescence signal from Nile blue dye distributed in polystyrene of PS/MWNT nanocomposites using a laser scanning confocal microscope was reported for determining the quantitative level of dispersion over a large domain size of about  $150\ \mu\text{m}^2$  [26]. An extensive image analysis of TEM images of PMMA/montmorillonite and PMMA/bentonite nanocomposites was conducted to determine quantitative degree of exfoliation of the clay particles [27]. The dispersion of SWNT in surfactants was determined by optical absorption spectroscopy but the relation with physical properties was not obtained [28]. Other detailed, statistical analyses of the dispersion of montmorillonites in polyvinylchloride [29] and of carbon blacks (CB) in polyamide 6 [30] over a  $5\ \mu\text{m} \times 5\ \mu\text{m}$  domain were conducted by the quantitative image analysis of the SEM images utilizing the quadrat method of Morishita [31]. The dispersion pattern of CBs, including

small and large aggregates, was estimated by the analysis and Morishita's index was introduced as a quantitative measure of the dispersion of CBs.

Although many quantitative physical properties of CNT nanocomposites have been previously subjected to experimental investigation, the dispersion characteristic of nanocomposites has not been measured, except in the few cases discussed above where some limited quantification is considered. The objective of this study is to determine the *quantitative* relationship between quantitative dispersion levels and the physical properties of CNT nanocomposites. And, more generally, to establish a sound approach to this problem when the spatial scales of dispersion are prescribed in the measurements of dispersion determined. In this study, multiple dispersion levels of PMMA/SWNT nanocomposites are prepared using the coagulation method, which is chosen since it can lead to highly variable status of particle dispersion. The level of dispersion of SWNTs in PMMA for each nanocomposite is quantitatively determined by two different methodologies. Physical properties such as viscoelastic properties, electrical conductivity, and flammability properties are then measured for each nanocomposite and the relationships between the physical properties and the measures of dispersion determined. This approach allows for a more rational comparison of the reinforcement performance of polymer by different types of nanoparticles with the measured dispersion indices of the nanoparticles.

## 2. Experimental section

### 2.1. Sample preparation

The matrix polymer used in this paper is poly(methyl methacrylate) (PMMA) (Polysciences,<sup>1</sup>  $M_w$ : 100,000 g/mol). SWNTs for the nanocomposites, synthesized by the high-pressure carbon monoxide method (HiPCo) [32], were provided by Carbon Nanotechnologies Inc. and Foster Miller Co. The metal residue in the SWNTs is less than 13 mass%. The coagulation method was used to produce the PMMA/SWNT nanocomposites [33]. In the coagulation method, dimethylformamide (DMF) was chosen to dissolve the PMMA and to permit dispersion of the SWNTs by bath sonication for 24 h. To obtain good nanotube dispersion, the nanotube concentration in DMF is critical. We can observe nanotube agglomerates by the naked eye at a concentration higher than 0.4 mg/ml, while the 0.2 mg/ml suspension is visually homogeneous. Therefore, we can control the nanotube dispersion in the nanocomposites by changing the nanotube concentration in DMF, assuming that the state of nanotube dispersion is comparable in DMF before coagulation and in the polymer matrix after coagulation suspension [13]. Concentrations of 0.05 mg/ml, 0.1 mg/ml, 0.2 mg/ml, 0.4 mg/ml, 0.8 mg/ml,

<sup>1</sup> Certain commercial equipments, instruments, materials, services or companies are identified in this paper in order to specify adequately the experimental procedure. This in no way implies endorsement or recommendation by NIST.

and 1.2 mg/ml were used to make nanocomposites with various levels of dispersion. The concentration of SWNTs in PMMA was 0.5 mass% for all samples. All samples for the physical measurement were compression molded at 200 °C under a pressure of about 1.4 MPa for a duration of 15 min.

## 2.2. Development of an objective dispersion metric

Two different methodologies were used to characterize the quantitative dispersion level of SWNTs in PMMA. One was to take images of a thin film of each PMMA/SWNT sample using confocal microscopy which allows a large observation domain size of about 100  $\mu\text{m}$  compared to much smaller domain size of about 1  $\mu\text{m}$  by TEM or SEM. The other method was absorption measurement on a thin film of the sample using UV–vis and near-infrared spectroscopy. Its observation size of about 3 mm  $\times$  10 mm  $\times$  200  $\mu\text{m}$  thickness was much larger than that achieved by confocal microscopy. All films were made by compression molding. A small amount of sample was placed between thin Kapton films which covered two mechanically buffed brass plates. A 200  $\mu\text{m}$  thick shim plate (with a round hole in the center) was inserted between the two plates to produce a uniform film.

A laser scanning confocal microscope (Model LSM510, Carl Zeiss Inc.) was used to image the SWNTs in the PMMA matrix. The confocal microscope utilizes coherent laser light and collects reflected light exclusively from a single plane with a thickness of about 100 nm (a pinhole sits conjugated to the focal plane and rejects light out of the focal plane). However, the smooth front surface was required to define the surface location. A red laser ( $\lambda = 633$  nm) was used as the coherent light and images were taken at 100 $\times$  magnification with an Epiplan-Neofluar 100 $\times$ /1.30 oil-pool objective. An LP385 (Rapp OptoElectronic) filter was used to limit the lower spectra of reflected light. One hundred two-dimensional images (optical slices with 1024 pixels  $\times$  1024 pixels), with scan size 92.1  $\times$  92.1  $\mu\text{m}$ , were taken at a spacing of 100 nm by moving the focal plane.

Several different spatial statistical analyses were conducted with our sample of 100 images. As a first assay of distance from uniformity, the standard  $\chi^2$  statistic [34]

$$\chi^2 = \sum_{\text{cells}} \frac{[\text{Observed} - \text{Uniform}]^2}{\text{Uniform}} \quad (1)$$

was computed for each sample across a range of cubic cell sizes, ranging from the size of 0.46  $\mu\text{m}$   $\times$  0.46  $\mu\text{m}$   $\times$  0.50  $\mu\text{m}$  to about 9.2  $\mu\text{m}$   $\times$  9.6  $\mu\text{m}$   $\times$  10  $\mu\text{m}$ . The cubic cell gridding scheme was consistently applied, for all samples, to the observation domain consisting of 100 slices of a 1024  $\times$  1024 pixel image. Initial computations were done in the gray scale presented by the data. Ultimately, however, comparison to an estimated background and recoding of pixels as “nanotube present” or “nanotube not present” (1 or 0) was employed to the computation of this and other statistics. In each case, for each density and cube size, the expected “Uniform” density cell content was computed as the total number of pixels

with nanotube present divided by the total number of cubes scanned. Portions of the solid rectangle of data being binned and scanned that did not fall within the binning scheme, boundary areas, were excluded from the counting.

Another, more direct, approach to quantify the degree of non-conformance of the distribution of carbon nanotubes in the PMMA matrix to a uniform distribution is to compute a distance between the empirical and ideal (uniform) distributions. The ideal is derived directly from the masses of materials used in the preparation of the composite. The empirical is computed by tallying nanotubes present in a volume partition of composite material. The variational distance is commonly employed in mathematical statistics, for example in determining rates of convergence of one distribution to another. Among multiple equivalent definitions

$$d = \frac{1}{2} \sum_{k=0}^{\infty} |P(\text{UNIF} = k) - P(\text{EMPIR} = k)| \quad (2)$$

is the simplest to apply [35]. Domain by domain, one evaluates the difference between the uniform-predicted probability of occurrence of a nanotube and the observed probability. One sums the absolute values of all such differences and divides by two. The functional described by the formula is a true distance, symmetric in its two arguments, and satisfying the triangle inequality. The factor  $\frac{1}{2}$  ensures that the distance takes values between 0 and 1.

We prefer to work here in terms of a linearly transformed variational distance, which we term ‘relative dispersion index’,

$$\text{RDI} = 100 \times (1 - d) \quad (3)$$

Relative dispersion of 100 connotes perfect conformance to uniform, with successively lower values, down to zero, indicating less and less conformity.

UV–vis and near-infrared absorption measurements were performed on PMMA/SWNT composites over the wavelength range of 190–2750 nm, using a Perkin Elmer Lambda 950 UV–vis-NIR spectrophotometer in transmission mode. The recorded spectra were corrected for the instrument background and dark current, as well as for absorbance of the PMMA polymer. The polymer signal was subtracted using the Beer–Lambert law,<sup>2</sup>

$$A = \varepsilon(c, \text{dispersion}) \times C \times L \quad (4)$$

in which  $A = \ln(I_0/I)$  is the absorbance,  $C$  the concentration,  $L$  the path length, and  $\varepsilon$  is a parameter that depends on the concentration and dispersion of the SWNTs. Subtraction was performed by matching the absorbance of a pure PMMA blank and the PMMA components of the PMMA/SWNT composites over the 2700–1800 nm wavelength range. In particular, the

<sup>2</sup> Homogeneity of the sample is assumed in the Beer–Lambert law. In this instance, however, the composites are inhomogeneous, any extinction coefficient calculated should not be viewed as intrinsic to the SWNTs, but rather as a function of the processing variables that led to the observed dispersion of the SWNTs within the polymer.

magnitude of the PMMA blank subtraction was set by the elimination of a spectral feature at 2245 nm due solely to the polymer matrix. (Since absorbance has a linear relation to the film thickness, the difference in thickness between PMMA and PMMA/SWNTs is corrected by subtracting the spectral feature at 2245 nm. No actual thickness measurement was conducted. We estimate accuracy of  $\pm 2\%$  for this procedure.) For PMMA in this situation  $\epsilon$  and  $C$  are constants.

### 2.3. Property measurements

Thermal gravimetric analyses (TGA) were conducted using a TA Instruments TGA Q 500 and a platinum pan at  $5^\circ\text{C}/\text{min}$  from  $90^\circ\text{C}$  to  $500^\circ\text{C}$  in nitrogen (flow rate of  $60\text{ cm}^3/\text{min}$ ). The standard uncertainty of the sample mass measurement is  $\pm 1\%$ .

Viscoelastic measurements were performed on a Rheometric solid analyzer (RSAII) in oscillatory shear with a sandwich fixture. Frequency sweep with the sample size of  $12.5\text{ mm} \times 16\text{ mm} \times 0.5\text{ mm}$  was performed at  $200^\circ\text{C}$  with a strain of  $0.5\%$ . Results were reproducible after one frequency sweep, indicating that there was no degradation of the sample or additional nanotube alignment during the measurement.

Electrical conductivities of the nanocomposites were measured at room temperature. A thin film, typically about  $100\text{ }\mu\text{m}$  thickness, was made by compression molding at  $200^\circ\text{C}$  under the pressure of  $1.4\text{ MPa}$  for the duration of  $15\text{ min}$ . Gold electrodes with a thickness of  $0.1\text{ }\mu\text{m}$  were prepared by sputtering in argon. We used a parallel plate electrode configuration where the diameter of the top electrode was  $10.0\text{ mm}$  while the diameter of the bottom electrode was about  $13\text{ mm}$ . The conductivity was obtained from the complex impedance measurements (impedance magnitude  $Z^*$  and the corresponding phase angle  $\theta$ ), which were carried out in a frequency range of  $40\text{--}50\text{ MHz}$  through a four-terminal technique using an Agilent 4294A Precision Impedance Analyzer. The output AC voltage was  $0.5\text{ V}$ . The complex electrical conductivity  $\sigma^*$  was obtained from the measured complex impedance  $Z^*$  normalized by the geometry of the test sample  $\sigma^* = t/(Z^*a)$ , where  $t$  is the specimen thickness and  $a$  is the area of the top electrode. The combined relative experimental uncertainty of the measured complex conductivity magnitude was within  $8\%$ , while the relative experimental uncertainty of the dielectric phase angle measurements was about  $1\%$ .

A radiant gasification apparatus, similar to a cone calorimeter, was designed and constructed at NIST to study the gasification processes of samples by measuring mass loss rate and temperatures of the sample exposed to a fire-like heat flux in a nitrogen atmosphere (no burning). A disc shaped sample was mounted horizontally and its top surface was exposed to a well-characterized thermal radiant flux from an electrical heating element. The weight of the sample was continuously measured by a sensitive weight device and mass loss rate was calculated by taking the time derivative of the weight. The observed mass loss rate in this device correlates well with heat release rate (a direct measure of the size of a fire) of polymer/CNT nanocomposites [22,36] and polymer/clay

nanocomposites [37]. The apparatus consists of a stainless-steel cylindrical chamber that is  $1.70\text{ m}$  tall and  $0.61\text{ m}$  in diameter. In order to maintain a negligible background heat flux, the interior walls of the chamber are painted black and the chamber walls are water-cooled to  $25^\circ\text{C}$ . All experiments were conducted at an incident radiant flux of  $50\text{ kW}/\text{m}^2$ . The unique nature of this device is twofold: (1) observation and results obtained from it are based solely on the condensed phase processes due to the absence of any gas phase oxidation reactions and processes; (2) it enables visual observation of gasification behavior of a sample using a video camera under a radiant flux similar to that of a fire without any interference from a flame. A more detailed discussion of the apparatus is given in our previous study [38]. The standard uncertainty of the measured mass loss rate is  $\pm 10\%$ .

## 3. Results

### 3.1. Application of dispersion metric to model PMMA/SWNT nanocomposites

Three-dimensional reconstructions of the confocal microscopy images of each sample with the concentration of SWNT in DMF at  $0.2\text{ mg}/\text{ml}$ ,  $0.4\text{ mg}/\text{ml}$ ,  $0.8\text{ mg}/\text{ml}$ , and  $1.2\text{ mg}/\text{ml}$  are shown in Fig. 1. These images show SWNT bundles and agglomerates. Transparent areas correspond to PMMA. The image of  $1.2\text{ mg}/\text{ml}$  shows numerous, large agglomerates, but such agglomerates are hardly seen in the images of  $0.2\text{ mg}/\text{ml}$  and  $0.4\text{ mg}/\text{ml}$ .

Quantitative spatial uniformity of SWNT in PMMA was determined by calculating the variational distance described in the previous section. Domain by domain, one evaluates the difference between the uniform-predicted probability of occurrence of a nanotube and the observed probability. The ideal uniform distance of SWNT bundle was calculated from an estimated total number of SWNT bundles in the observation area of the confocal microscopy. The average size of SWNT bundles was about  $7\text{ nm}$  in diameter and  $310\text{ nm}$  in length [13] and it was assumed that the bundle size was same for all samples. With  $0.5\text{ wt}\%$  of SWNT in the observation area of  $92\text{ }\mu\text{m} \times 92\text{ }\mu\text{m} \times 10\text{ }\mu\text{m}$ , there were about  $2 \times 10^7$  SWNT bundles. The variational distance was calculated by Eq. (2) and subsequently relative dispersion index, RDI, representing the quantitative uniformity of the dispersion of SWNT bundles within the nanocomposite was calculated by Eq. (3). RDI varies from  $100\%$  for a perfect uniform distribution to a poorest value of  $0\%$ . The RDI values of the six samples are shown in Fig. 2 as a function of the domain size. Here, one domain size ( $92\text{ }\mu\text{m}$  divided by  $1092$  and  $10\text{ }\mu\text{m}$  divided by  $100$ ) is about  $90\text{ nm} \times 90\text{ nm} \times 100\text{ nm}$ . All RDI values increase gradually with the domain size. The highest RDI is about  $85\%$  for  $0.4\text{ mg}/\text{ml}$  and the lowest is about  $15\%$  for  $1.2\text{ mg}/\text{ml}$ .

The corresponding values of  $\chi^2$  were calculated for the six samples as an additional indication of quantitative uniformity of the dispersion of SWNT bundles within the nanocomposite. The results are shown in Fig. 3. A lower value of  $\chi^2$  indicates better uniformity. The trend of the three different levels of the

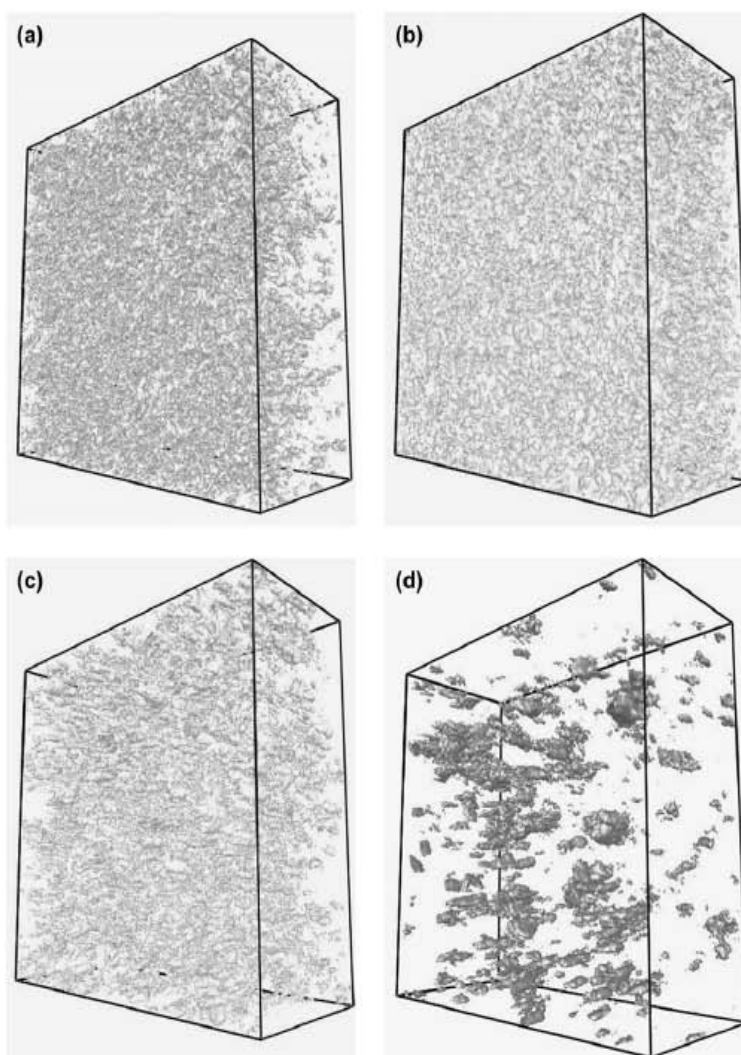


Fig. 1. Three-dimensional images constructed from confocal microscopy images of the PMMA/SWNT (0.5%) nanocomposite samples prepared with various SWNT concentrations in DMF: (a) 0.2 mg/ml, (b) 0.4 mg/ml, (c) 0.8 mg/ml, and (d) 1.2 mg/ml. The size of the observation domain is  $23 \mu\text{m} \times 23 \mu\text{m} \times 9.2 \mu\text{m}$  depth.

uniformity, best with 0.2 mg/ml and 0.4 mg/ml, middle group of 0.05 mg/ml, 0.1 mg/ml, and 0.8 mg/ml, and the poorest with 1.2 mg/ml, is similar to the pattern with RDI shown in Fig. 2. However, the 0.2 mg/ml sample displays the best uniformity by the  $\chi^2$  analysis compared to 0.4 mg/ml for the RDI analysis.

The absorption spectra of the polymer/SWNT composites vary systematically with the initial loading concentration of the SWNTs in DMF, as shown in Fig. 4. Each absorption spectrum was scaled by the known path length through the sample to a constant thickness equal to that of the PMMA blank. Composite films cast from the most dilute suspensions (0.1 mg/ml and 0.2 mg/ml) show higher total absorption and sharper definition of the SWNT van-Hove transitions than the films cast from higher concentrated suspensions (0.8 mg/ml and 1.2 mg/ml).

In a poorly dispersed film containing large aggregates, a large fraction of the total nanotube mass is contained within a small volume of the composite. This leaves regions of low nanotube content, in which a large fraction of the photons are transmitted. Due to the logarithmic relation between the total transmitted light over the transmission area and the measured absorption given by Eq. (5), a few regions of high transmittance will dominate the observed absorbance.

$$A = -\log_{10} \left( \int_{\text{area}} T d(\text{area}) \right) \quad (5)$$

This effect is illustrated schematically in Fig. 5(a). Due to the logarithmic scaling, nanotubes within aggregates tend not

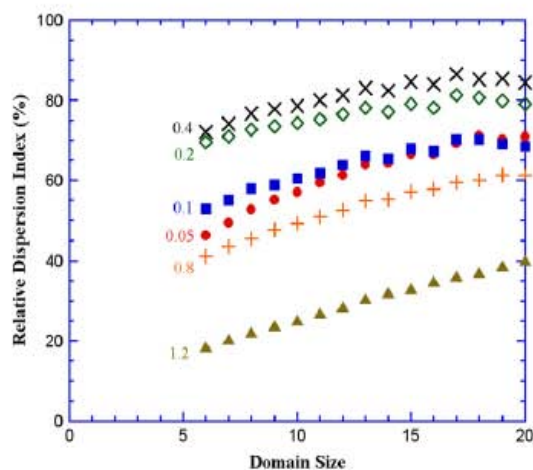


Fig. 2. Relative dispersion indices (RDI) of SWNT in PMMA/SWNT (0.5%) nanocomposites prepared with various concentrations of SWNT in DMF (mg/ml) vs the domain size.

to contribute as significantly to the measured spectrum. A larger absorbance for a constant film thickness and nanotube concentration is thus indicative of a better uniformity of SWNT dispersion within the nanocomposite. The composite films used for the UV–vis–NIR measurements are shown in Fig. 5(b). The trend in opacity of the samples seen in this figure is apparent in the photograph. Although some variation in the films is apparent, this is primarily due to variations in the local thickness of the films. Multiple spectra were recorded for each film and most of the variation was removed by normalization to the thickness of the PMMA blank. The data shown in

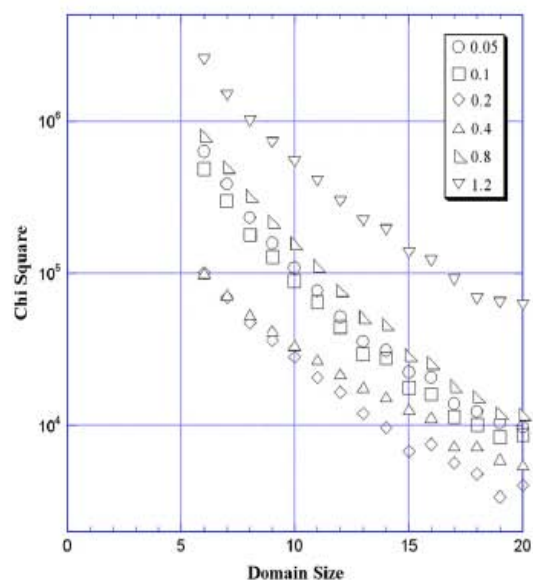


Fig. 3.  $\chi^2$  values describing the dispersion level of SWNT in PMMA/SWNT (0.5%) nanocomposites prepared with various concentrations of SWNT in DMF (mg/ml) vs the domain size.

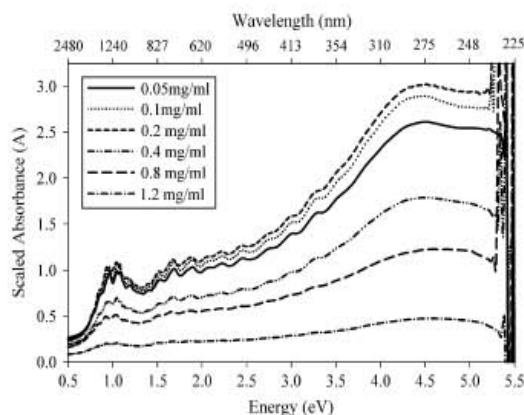


Fig. 4. Scaled absorption spectra of the six PMMA/SWNT (0.5%) samples prepared with different concentrations of SWNT in DMF.

Fig. 4 are the averages of the scaled spectra for the individual samples.

As shown in Figs. 2 and 3, the values of RDI and  $\chi^2$  are not constant and depend on multiple parameter choices. Therefore, the values of these parameters must be specified as RDI (spatial resolution, statistical analysis domain size, observation image size, and a number of observations at selected locations in a sample) to carefully characterize under what conditions these values are obtained. In this study, spatial resolution is  $0.1 \mu\text{m}$ , statistical analysis domain size is selected at  $1 \mu\text{m}^3$  corresponding to the domain (cell) size of 12 in the two figures, observation image size is  $92 \mu\text{m} \times 92 \mu\text{m} \times 10 \mu\text{m}$ , and the number of observations in a physical measurement sample is 1 (only one location).

The calculated values of scaled absorbance at 275 nm, RDI ( $0.1 \mu\text{m}$ ,  $1 \mu\text{m}^3$ ,  $84,640 \mu\text{m}^3$ , 1) and  $\chi^2$  ( $0.1 \mu\text{m}$ ,  $1 \mu\text{m}^3$ ,  $84,640 \mu\text{m}^3$ , 1) with respect to SWNT concentrations in DMF are listed in Table 1. It was anticipated that a lower concentration of SWNT in DMF would lead to an improved dispersion of SWNTs in the polymer. However, it appears that the dispersion does not get better beyond about the

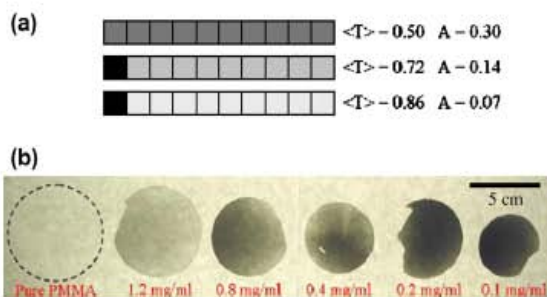


Fig. 5. (a) The average transmittance and corresponding absorbance for three illustrated lateral distributions of an absorbing material. The distribution affects the apparent concentration calculated using the assumption of homogeneity implicit in Eq. (4). (b) Photograph of the PMMA/SWNT (0.5%) films used for the absorbance measurement. The differences in opacity are due primarily to the relative level of dispersion in each film.

Table 1

SWNT concentration in DMF vs scaled absorbance (at 275 nm), relative dispersion index ( $0.1 \mu\text{m}$ ,  $1 \mu\text{m}^3$ ,  $84,640 \mu\text{m}^3$ , 1) and  $\chi^2$  ( $0.1 \mu\text{m}$ ,  $1 \mu\text{m}^3$ ,  $84,640 \mu\text{m}^3$ , 1)

SWNT concentration in DMF (mg/ml)	Absorbance	RDI (%)	$\chi^2 (\times 10^5)$
0.05	2.75	61	6.3
0.1	2.60	64	1.4
0.2	3.06	77	1.1
0.4	1.80	81	1.0
0.8	1.20	53	8.0
1.2	0.56	28	25

concentration of 0.2 mg/ml in DMF. This might be due to poor interaction of the tubes with polymer chains in a large volume of DMF at a low concentration.

The relationship between the RDI ( $0.1 \mu\text{m}$ ,  $1 \mu\text{m}^3$ ,  $84,640 \mu\text{m}^3$ , 1),  $\chi^2$  ( $0.1 \mu\text{m}$ ,  $1 \mu\text{m}^3$ ,  $84,640 \mu\text{m}^3$ , 1) value, and the absorbance is shown in Fig. 6. The absorbance is selected at 275 nm, whose value is near the largest as shown in Fig. 5. The trend shown in Fig. 6 is not significantly modified by selecting a different domain size for determining RDI and  $\chi^2$  value and absorbance at a different wavelength such as 426 nm. The correlation coefficient between RDI ( $0.1 \mu\text{m}$ ,  $1 \mu\text{m}^3$ ,  $84,640 \mu\text{m}^3$ , 1) and  $\chi^2$  ( $0.1 \mu\text{m}$ ,  $1 \mu\text{m}^3$ ,  $84,640 \mu\text{m}^3$ , 1) value is 0.999. This strong correlation could be due to the use of the same images taken by confocal microscopy and the fact that both analysis assay the uniformity of the distribution. However, the correlation coefficient between RDI ( $0.1 \mu\text{m}$ ,  $1 \mu\text{m}^3$ ,  $84,640 \mu\text{m}^3$ , 1) and absorbance is 0.735. This poor correlation appears to be due to the RDI value of the 0.4 mg/ml sample. Without this sample, the correlation coefficient increases from 0.735 to 0.927. In Section 3, the relationships

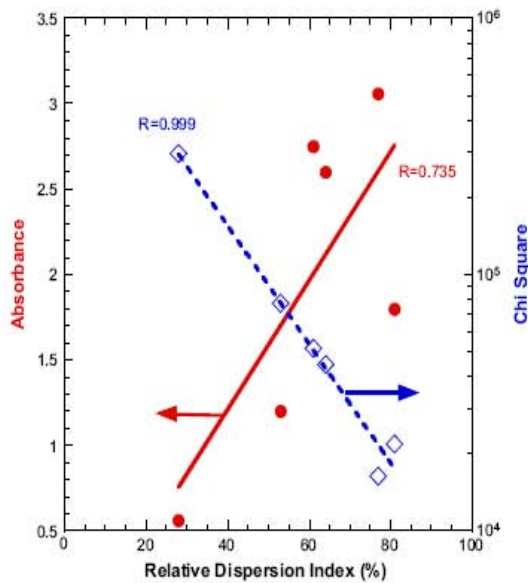


Fig. 6. Relationship between relative dispersion index ( $0.1 \mu\text{m}$ ,  $1 \mu\text{m}^3$ ,  $84,640 \mu\text{m}^3$ , 1),  $\chi^2$  ( $0.1 \mu\text{m}$ ,  $1 \mu\text{m}^3$ ,  $84,640 \mu\text{m}^3$ , 1) with open squares, and absorbance at 275 nm with solid circles.  $R$  is correlation coefficient.

between the dispersion levels determined by the above three analysis and various physical properties of the nanocomposites are obtained and compared to find which analysis best correlates with the properties.

### 3.2. Basic PMMA/SWNT nanocomposite properties

#### 3.2.1. Thermal stability

Derivative weight loss rates of the six samples with respect to temperature in nitrogen are plotted in Fig. 7. The peak weight loss rate was observed at  $362^\circ\text{C}$  for pristine PMMA (plot not shown),  $364^\circ\text{C}$  for the sample with the SWNT concentration in DMF at 1.2 mg/ml, and at around  $370^\circ\text{C}$  for all other samples. All the curves shown in this figure are close to each other. Thus, morphology difference in PMMA/SWNT nanocomposites does not appear to make an appreciable difference in the thermal stability of the nanocomposites.

#### 3.2.2. Viscoelastic properties

The storage modulus  $G'$  provides a measure of nanocomposite "stiffness" and its frequency dependence characterizes whether the sample is in a liquid-like or solid-like state. Comparison of the relationship of storage modulus as a function of frequency among the six nanocomposite samples is shown in Fig. 8 at  $200^\circ\text{C}$ .  $G'$  of the sample prepared at 1.2 mg/ml in DMF is not significantly different from that of PMMA and it shows the typical rheological response of a Newtonian liquid behavior with  $G' \sim \omega^2$  (where  $\omega$  is the oscillatory frequency) at low frequencies. However,  $G'$  increases significantly with a decrease in SWNT concentration in DMF and the liquid-like scaling of  $G'$  at low frequencies disappears.  $G'$  is about

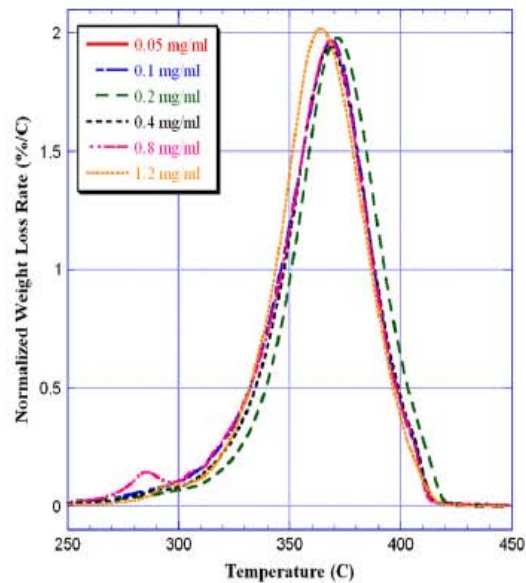


Fig. 7. DTG, dynamic thermogravimetric, curves of the six PMMA/SWNT (0.5%) nanocomposites prepared by different SWNT concentrations in DMF. TGA was conducted in nitrogen at heating rate of  $5^\circ\text{C}/\text{min}$ .

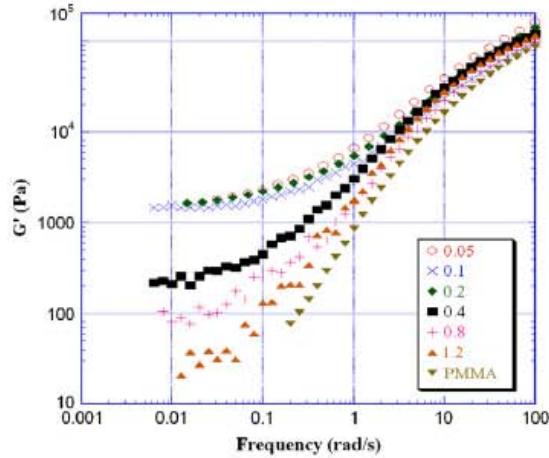


Fig. 8. Storage modulus vs frequency for the PMMA/SWNT (0.5%) nanocomposites prepared with various concentration of SWNT in DMF (mg/ml).

the same for the three samples based on 0.05 mg/ml, 0.1 mg/ml, and 0.2 mg/ml in DMF and  $G'$  becomes nearly constant at low frequencies. This indicates a transition from a Newtonian liquid to an ideal Hookean solid, which accompanies the formation of a mechanically stable network structure [39] ('jammed network' or 'dispersion gel') [40]. The formation of such a structure has significant effects on flammability properties [41] as shown later in this paper.

### 3.2.3. Electrical conductivity

The complex conductivity  $\sigma^*$  of our specimens can be expressed by Eq. (6):

$$\sigma^* = \sigma_0 + j\omega\epsilon_0\epsilon_r^* \quad (6)$$

where  $\sigma_0$  is the direct current conductivity (DC), independent of AC frequency  $f$ ,  $\omega = 2\pi f$ ,  $\epsilon_r^*$  is the complex dielectric permittivity of the composite material,  $\epsilon_r^* = \epsilon_0(\epsilon_r' - j\epsilon_r'')$ , and  $\epsilon_0$  is the dielectric permittivity of free space. At low frequencies the complex admittance term,  $\omega\epsilon_0\epsilon_r^*$ , is small and the total conductivity becomes real ( $\theta \approx 0$ ;  $|\sigma^*| = \sigma_0$ ), independent of frequency, essentially equivalent to DC conductivity. Thus in the low frequency limit  $|Z^*|_{(f \rightarrow 0)} = Z_0$  and  $\sigma_0 = \frac{1}{Z_0} \frac{l}{a}$ .

Fig. 9 shows a log–log plot of complex conductivity of the six nanocomposite samples as a function of frequency. The plateau seen in each plot extending up to a crossover frequency,  $f_c$ , corresponds to the DC conductivity  $\sigma_0$  where  $2\pi f_c \epsilon_0 |\epsilon_r^*| = \sigma_0$ . It is seen that the samples prepared with 1.2 mg/ml in DMF exhibit a purely dielectric character. The linear frequency-dependent increase in complex conductivity on the log–log plot corresponds to a dielectric constant of about 4.1. Similarly, samples with 0.8 mg/ml show a dielectric behavior at frequencies above  $f_c \approx 65$  Hz. However, with increasing dispersion of SWNT the nanocomposites became increasingly conducting while  $f_c$  shifts to higher frequencies. The conductivity  $\sigma_0$  increases from  $10^{-7}$  S/m and reaches a peak value of about  $2.8 \times 10^{-3}$  S/m at SWNT/DMF of

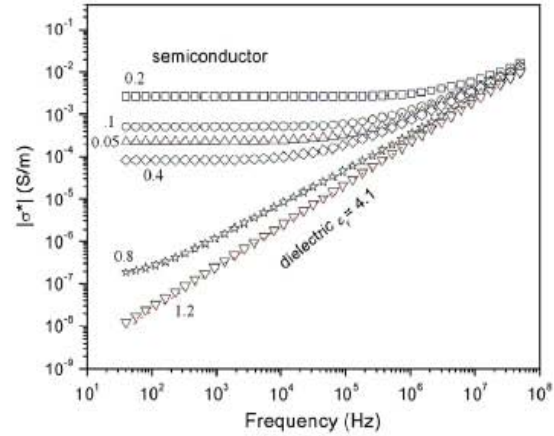


Fig. 9. Complex electrical conductivity vs frequency for the PMMA/SWNT (0.5%) nanocomposites prepared with various concentrations of SWNT in DMF (mg/ml).

0.2 mg/ml, while  $f_c$  increases from 65 Hz to about 1.2 MHz. The conductivity results are summarized in Table 2, which shows significant effect of the dispersion level of SWNT on  $\sigma_0$ .

### 3.2.4. Flammability property

Mass loss rate curves in nitrogen atmosphere at an external flux of  $50 \text{ kW/m}^2$  are shown in Fig. 11. All samples were tested with 4 mm thick samples except for an 8 mm thick sample prepared at 0.2 mg/ml concentration in DMF. This particular sample was tested in our previous study [36]. It is expected that the effect of the difference between 8 mm thickness and 4 mm thickness on mass loss rate curve is not significant, except to give roughly twice longer test time for the 8 mm thick sample than that for the 4 mm thick sample. (This is the reason why the upper time scale, which applies only to the sample prepared with 0.2 mg/ml concentration in DMF (8 mm), is twice long as the lower time scale for all other samples.) Lower mass loss rate implies lower heat release rate during burning and thus lower flammability. Fig. 10 shows the significant effects of the morphology difference on mass loss rate. The mass loss rate of sample prepared with 0.2 mg/ml concentration in DMF is roughly 1/3 of that of pristine PMMA compared to a small reduction of only 10–20% with samples prepared at 0.8 mg/ml and 1.2 mg/ml concentrations in DMF despite there being the same amount of SWNT in all samples. The pictures of the residues collected

Table 2  
Effects of SWNT concentration in DMF on electrical conductivity of PMMA/SWNT (0.5%)

SWNT/DMF (mg/ml)	$\sigma_0$ (S/m)
0.05	$2.8 \times 10^{-4}$
0.1	$5.2 \times 10^{-4}$
0.2	$2.8 \times 10^{-3}$
0.4	$8.6 \times 10^{-5}$
0.8	$2.0 \times 10^{-7}$
1.2	$3.2 \times 10^{-10}$

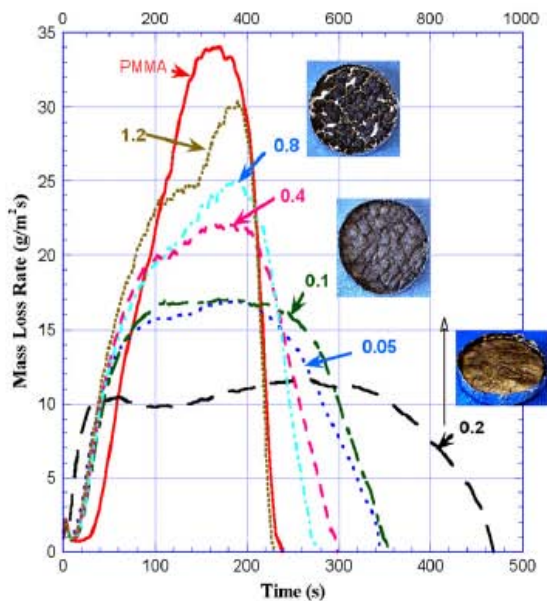


Fig. 10. Mass loss rate curves of PMMA/SWNT (0.5%) nanocomposites prepared with various concentrations of SWNT in DMF (mg/ml). All samples were 4 mm thick except 8 mm thick for 0.2 mg/ml. Tests were conducted at  $50 \text{ kW/m}^2$  in a nitrogen atmosphere.

at the end of the tests show a relatively uniform, smooth surface for the sample prepared at 0.2 mg/ml concentration in DMF compared to many large islands for the sample prepared at 0.8 mg/ml concentration in DMF (Many cracks were formed for 0.1 mg/ml). During the test for the latter sample, vigorous bubbling was observed between the islands but no bubbling was observed except in the very early stages of the test (within first 30 s) for the sample prepared at 0.2 mg/ml concentration in DMF. This observation and the relationship between the formation of a uniform residue vs the formation of islands and the mass loss rate curves are consistent with our previous observation [36,41].

### 3.3. Relationship between quantitative dispersion level and physical properties

As shown above, there are no significant effects of the dispersion level of SWNT in the PMMA/SWNT (0.5%) nanocomposites on thermal stability. Relationships between the dispersion level and physical properties, such as storage modulus, electrical conductivity, and flammability properties of the nanocomposites are obtained. Since the quantified dispersion level by RDI is very similar to that by  $\chi^2$  analysis, as shown in Fig. 6, only the former analysis as well as the absorbance is used as measures of dispersion level.

The relationships between storage modulus at 0.05 rad/s in Fig. 8 and dispersion level quantified by RDI ( $0.1 \mu\text{m}$ ,  $1 \mu\text{m}^3$ ,  $84,640 \mu\text{m}^3$ , 1) and absorbance at wavelength 275 nm in Fig. 5 are plotted in Fig. 11. The second order polynomials fit best as compared to a power fit or an exponential fit. Both fits show

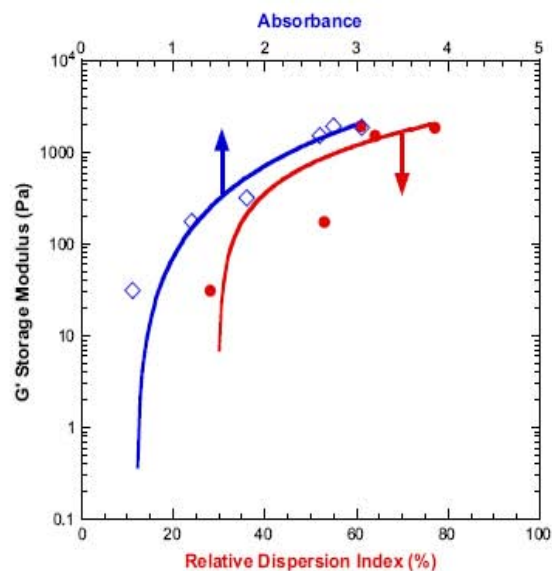


Fig. 11. The relationships between storage modulus of PMMA/SWNT (0.5%) at 0.5 rad/s and quantitative dispersion levels of SWNT described with relative dispersion index ( $0.1 \mu\text{m}$ ,  $1 \mu\text{m}^3$ ,  $84,640 \mu\text{m}^3$ , 1) (solid circles) and with absorbance at 275 nm (open squares). Second order polynomial fits and correlation coefficient,  $R$ , with RDI is 0.84 and that with absorbance is 0.97.

a rapid increase in the storage modulus at low dispersion levels followed by slow increase in storage modulus at high dispersion levels. The storage modulus evidently correlates with the dispersion level determined by absorbance better than with that measured by RDI ( $0.1 \mu\text{m}$ ,  $1 \mu\text{m}^3$ ,  $84,640 \mu\text{m}^3$ , 1). The correlation coefficient of the former is 0.97 compared to 0.84 for the latter. The figure also indicates that storage modulus can vary about four orders of magnitude with dispersion level for a fixed SWNT concentration (0.5%) in the nanocomposites.

The corresponding relationship between dispersion level and electrical conductivity is shown in Fig. 12. Both a power fit and an exponential fit correlate well with either RDI or absorbance. (A polynomial fit was also used but a fit with the highest correlation coefficient was selected in this study.) The correlation coefficient of the power fit with RDI is 0.99 and with absorbance is 0.96. The electrical conductivity varies by roughly  $10^8$  orders with dispersion level for a fixed SWNT concentration, an effect even more drastic than for storage modulus. The electric conductivity increases rapidly with an increase in the dispersion level, but the increase in electrical conductivity with an increase in dispersion level becomes lower when the dispersion level is relatively high.

Next, the effect of dispersion level on normalized peak mass loss rate of the nanocomposites is shown in Fig. 13, given recent interest in SWNT as a fire retardant additive [36]. The abscissa of the figure is the ratio of the peak mass loss rate of PMMA/SWNT (0.5%) nanocomposites divided by the peak mass loss rate of PMMA measured at an external radiant flux of  $50 \text{ kW/m}^2$  in a nitrogen atmosphere. The smaller the ratio the less flammable is the sample. The figure

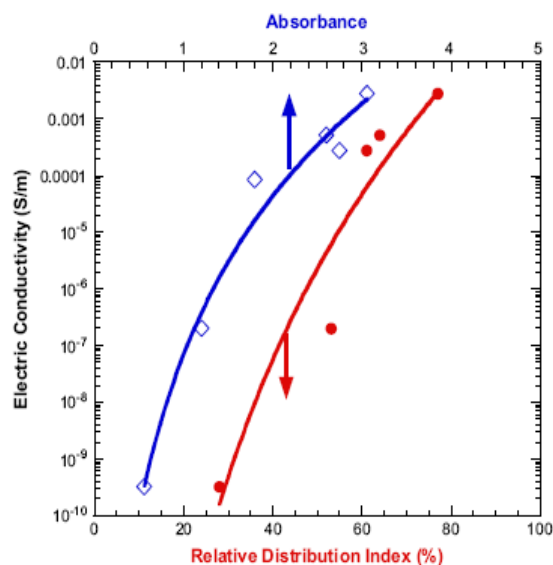


Fig. 12. The relationships between electric conductivity of PMMA/SWNT (0.5%) and electrical conductivity and quantitative dispersion levels of SWNT described with relative dispersion index ( $0.1 \mu\text{m}^3$ ,  $1 \mu\text{m}^3$ ,  $84,640 \mu\text{m}^3$ , 1) (solid circles) and with absorbance at 275 nm (open squares). Power fits and correlation coefficient,  $R$ , with RDI is 0.99 and that with absorbance is 0.96.

shows about an approximately 70% reduction in flammability is achieved with the best dispersed sample tested in this study, so that we again find a large effect of dispersion level on an important property of these nanocomposites. Contrary to the

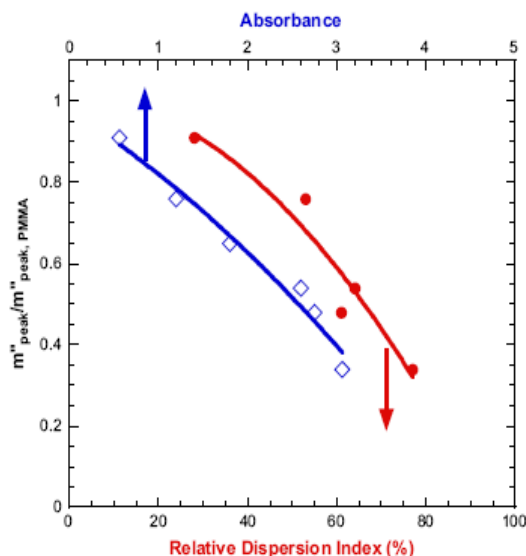


Fig. 13. The relationships between the normalized peak mass loss rate of PMMA/SWNT (0.5%) by the peak mass loss rate of PMMA and quantitative dispersion levels of SWNT described with relative dispersion index ( $0.1 \mu\text{m}^3$ ,  $1 \mu\text{m}^3$ ,  $84,640 \mu\text{m}^3$ , 1) (solid circles) and with absorbance at 275 nm (open squares). Second order polynomial fits and correlation coefficient,  $R$ , with RDI is 0.96 and that with absorbance is 0.99.

above trend observed for storage modulus and electric conductivity, it appears that the peak mass loss rate is monotonically reduced even at the high end of dispersion level (no plateau). The second order polynomial fit correlates best as compared to a power fit and an exponential fit. The correlation coefficient of the fit with absorbance is 0.99 compared to 0.96 with RDI.

#### 4. Discussion

Our measurements of SWNT nanocomposite properties over a wide range of dispersion level indicate a profound variation in the properties of the nanocomposites and the evident need for dispersion metrics to allow some control of these properties and some understanding of why these property changes come about. The majority of studies show few TEM or SEM images comprising only a few nanocomposite samples without any analyses and assume that the dispersion levels of all the samples are same. However, without any quantitative analyses of spatial dispersion in all of the samples, the dispersion level of each sample might differ. At higher concentrations of nanoparticles, distances between nanoparticles become less and nanoparticles tend to agglomerate or bundle with each other. Thus, it tends to get more difficult to achieve good dispersion of nanoparticles in nanocomposites at high concentrations of nanoparticles. This might be one of the reasons why the reported concentrations of nanoparticles needed to attain percolation in electrical conductivity and in storage modulus differ significantly among published papers.

We would like to understand better the sources of uncertainty in estimation of the RDI. There are several possible reasons: (1) the spatial resolution of the images taken by confocal microscopy might not be fine enough to detect smaller bundles of SWNTs or individual SWNTs, although their actual amounts in the samples were not known. The analysis used in this study might be more appropriate for larger tubes. (2) Although the observed volume is relatively large compared to those seen by TEM and SEM, only one location of each sample was analyzed. The three-dimensional image of the sample prepared at  $0.4 \text{ mg/ml}$  concentration in DMF shown in Fig. 1(b) appears to show a more uniform distribution than the other images. There might be larger scale non-uniformity in some of the samples. The same analysis used in this study might need to be applied to a number of statistically selected locations in the sample to get an overall dispersion level. (3) In the analysis, a threshold value (taken from the background measurement of the confocal image of pristine PMMA) was used to determine whether there was a tube bundle (designated as "1") or not (designated as "0") in each cell of about  $90 \text{ nm} \times 90 \text{ nm} \times 100 \text{ nm}$  size. However, we did not determine whether there was more than one tube bundle or not. The analysis clearly requires further refinement to include the relationship between intensity and the number of tube bundles.

The analysis based on absorbance measurement is relatively easy and does not take too much time. However, this approach may not be used for samples with higher concentration of tubes because the absorbance becomes too high to allow application of the Beer–Lambert law described by Eq. (4). For

a comparison of dispersion between two different resins and/or different nanoparticles, this approach requires multiple calibrations and consequently it could become more complicated. It would appear to be most suited for comparison of the dispersion of the same type of nanoparticles with different sample preparation conditions, for example different mixing times, but keeping the same composition. Although the analysis using confocal microscopy might need further improvements to remove the above uncertainties, it can apply to higher concentration samples and it might also be possible to compare two different sample types based on different resins and/or different types of particles. Although a uniform distribution of tubes in nanocomposites is one of the requirements for better physical properties, electrical conductivity of nanocomposites can be significantly increased with specific alignment of tubes [42] or the formation of interconnected agglomerates [19]. Therefore, three-dimensional reconstructed images by X-ray transmission could be used to obtain detailed morphology including distribution, orientation, size, if the spatial resolution of this method were to be improved [43].

## 5. Conclusions

Relation between our relative dispersion metric and the properties of PMMA/SWNT nanocomposites was obtained at a fixed SWNT concentration of 0.5%. When the sample preparation method led to large range of dispersions in the samples, the dispersion metric of SWNTs was determined by two different methods, one was an absorbance measurement by UV–vis spectroscopy and the other was a statistical analysis of 100 images taken by confocal microscopy. The observation domain of the former was about  $3\text{ mm} \times 10\text{ mm} \times 200\text{ }\mu\text{m}$  thickness and that of the latter was about  $92\text{ }\mu\text{m} \times 92\text{ }\mu\text{m} \times 10\text{ }\mu\text{m}$  thickness. Quantitative spatial dispersion levels were obtained through image analysis to obtain a ‘relative dispersion index’ representing the uniformity of the dispersion of SWNTs in the samples and through the absorbance. The storage modulus, electrical conductivity, and flammability property (normalized peak mass loss rate) of the PMMA/SWNT (0.5%) nanocomposites are well correlated with respect to the quantified dispersion levels determined by the two different analyses. The relation between the quantified dispersion levels and physical properties shows about four orders of magnitude variation in the storage modulus, almost eight orders of magnitude variation in electrical conductivity, and about 70% reduction in peak mass loss rate at the highest dispersion level used in this study. With the profound effects of dispersion of SWNTs, objective dispersion metrics in an appropriate scale must be measured to understand how the properties of nanocomposites depend on the concentration, shape and size of the nanotubes and the reproducibility of the properties in the preparation of samples under nominally fixed preparation conditions.

## Acknowledgements

We thank Mr. John R. Shields and Mr. Jason Marple at NIST for helping with the flammability test, taking TGA data, and

preparing sample discs. We also thank Dr. Shinnosuke Nishiki for his help to make the three-dimensional images shown in Fig. 1 and Carbon Nanotechnologies Incorporated and Foster Miller Company for providing SWNTs. T.K. acknowledges funding from NIST with Grant no. 5D1022.

## References

- [1] Iijima S. *Nature* 1991;354:603–5.
- [2] Schadler LS, Giannaris SC, Ajayan PM. *Appl Phys Lett* 1998;73:3842–4.
- [3] Stephan C, Nguyen TP, Lahr B, Blau W, Lefrant S, Chauvet OJ. *Mater Res* 2002;17:396–400.
- [4] Dalton AB, Collins S, Munoz E, Razzal JM, Ebron VH, Ferraris JP, et al. *Nature* 2003;423:703.
- [5] Barrau S, Demont P, Peigney A, Laurent C, Lacabanne C. *Macromolecules* 2003;36:5187–94.
- [6] Thostenson ET, Chou T-W. *J Phys D Appl Phys* 2003;36:573–82.
- [7] Coleman JN, Khan U, Blau WJ, Gun'ko YK. *Carbon* 2006;44:1624–52.
- [8] Moninuzzaman M, Winey KI. *Macromolecules* 2006;39:5194–205.
- [9] Mitchell CA, Bahr JL, Arepalli S, Tour JM, Krishnamoorti R. *Macromolecules* 2002;35:8825–30.
- [10] Ramanathan T, Liu H, Brinson LC. *J Polym Sci Part B Polym Phys* 2005;43:2269–79.
- [11] Vaisman L, Marom G, Wagner HD. *Adv Funct Mater* 2006;16:357–63.
- [12] Schaefer DW, Zhao J, Brown JM, Anderson DP, Tomlin DW. *Chem Phys Lett* 2003;375:369–75.
- [13] Du F, Scogna RC, Zhou W, Brand S, Fischer JE, Winey KI. *Macromolecules* 2004;37:9048–55.
- [14] Liao Y-H, Marietta-Tondin O, Liang Z, Zhang C, Wang B. *Mater Sci Eng A* 2004;385:175–81.
- [15] Song W, Windle AH. *Macromolecules* 2005;38:6181–8.
- [16] Song YS, Youn JR. *Carbon* 2005;43:1378–85.
- [17] Park C, Ounaies Z, Watson KA, Crooks RE, Smith Jr J, Lowther SE, et al. *Chem Phys Lett* 2002;364:303–8.
- [18] Park SJ, Cho MS, Lim ST, Choi HJ, Jhon MS. *Macromol Rapid Commun* 2003;24:1070–3.
- [19] Martin CA, Sandler JKW, Shaffer MSP, Schwarz MK, Bauhofer W, Schulte K, et al. *Compos Sci Technol* 2004;64:2309–16.
- [20] Huang YY, Ahir SV, Terentjev EM. *Phys Rev B* 2006;73:125422.
- [21] Sennett M, Welsh E, Wright JB, Li WZ, Wen JG, Ren ZF. *Appl Phys A* 2003;76:111–3.
- [22] Kashiwagi T, Grulke E, Hilding J, Groth K, Harris R, Butler K, et al. *Polymer* 2004;45:4227–39.
- [23] Krishnamoorti R. *MRS Bull* 2007;32:341–7.
- [24] Balazs AC, Emrick T, Russell TP. *Science* 2006;314:1107–10.
- [25] Fagan JA, Landi BJ, Mandelbaum I, Simpson JR, Bajpai V, Bauer BJ, et al. *J Phys Chem B* 2006;110:23801–5.
- [26] Bellayer S, Gilman JW, Eidelman N, Bourbigot S, Flambar X, Fox DM, et al. *Adv Funct Mater* 2005;15:910–6.
- [27] Ratinae KR, Gilbert RG, Ye L, Jones AL, Ringer SP. *Polymer* 2006;47:6337–61.
- [28] Tan Y, Resasco DE. *J Phys Chem B* 2005;109:14454–60.
- [29] Yalcin B, Cakmak M. *Polymer* 2004;45:6623–38.
- [30] Konishi Y, Cakmak M. *Polymer* 2006;47:5371–91.
- [31] Morishita M. *Memories of the faculty of science series E, Biology*, vol. 2. Fukuoka, Japan: Kyushu University; 1959. 215.
- [32] Nikolaev P, Bronikowski MJ, Bradley RK, Rohmund FR, Colbert DT, Smith KA, et al. *Chem Phys Lett* 1999;313:91.
- [33] Du F, Fischer JE, Winey KI. *J Polym Sci Part B Polym Phys* 2003;41:3333–8.
- [34] Fortin M-J, Dale M. *Spatial analysis: a guide for ecologist*. Cambridge, UK: Cambridge University Press; 2005.
- [35] Blom G, Holst L, Sandell D. *Problems and snapshots from the world of probability*. New York: Springer-Verlag; 1991.

- [36] Kashiwagi T, Du F, Winey KI, Groth KM, Shields JR, Bellayer SP, et al. *Polymer* 2005;46:471–81.
- [37] Kashiwagi T, Harris RH, Zhang X, Briber RM, Cipriano BH, Raghavan SR, et al. *Polymer* 2004;45:881–91.
- [38] Austin PJ, Buch RR, Kashiwagi T. *Fire Mater* 1998;22:221–37.
- [39] Kharchenko SB, Douglas JF, Obrzut J, Grulke EA, Milger KB. *Nat Mater* 2004;3:564–8.
- [40] Bicerano J, Douglas JF, Brune DA. *J Macromol Sci Rev Macromol Chem Phys* 1999;C39:561–642.
- [41] Kashiwagi T, Du F, Douglas JF, Winey KI, Harris Jr RH, Shields J. *Nat Mater* 2005;4:928–33.
- [42] Du F, Fischer JE, Winey KI. *Phys Rev B* 2005. 121404(R).
- [43] Larson BC, Lengeler B. *MRS Bull* 2004;29:152–6.



## Effects of aspect ratio of MWNT on the flammability properties of polymer nanocomposites<sup>☆</sup>

Bani H. Cipiriano<sup>a</sup>, Takashi Kashiwagi<sup>b,\*</sup>, Srinivasa R. Raghavan<sup>a</sup>, Ying Yang<sup>c</sup>,  
Eric A. Grulke<sup>c</sup>, Kazuya Yamamoto<sup>b</sup>, John R. Shields<sup>b</sup>, Jack F. Douglas<sup>d</sup>

<sup>a</sup> Department of Chemical and Biomolecular Engineering, University of Maryland, College Park, MD 20742, USA

<sup>b</sup> Fire Research Division, National Institute of Standards and Technology, Gaithersburg, MD 20899, USA

<sup>c</sup> Department of Chemical and Materials Engineering, University of Kentucky, Lexington, KY 40506, USA

<sup>d</sup> Polymers Division, National Institute of Standards and Technology, Gaithersburg, MD 20899, USA

Received 6 July 2007; received in revised form 30 July 2007; accepted 31 July 2007

Available online 6 August 2007

---

### Abstract

The effects of the aspect ratio of multi-walled carbon nanotubes (MWNTs) on the rheology and flammability of polystyrene/MWNT nanocomposites are studied using two MWNTs having average aspect ratios (length to outer diameter) of 49 and 150. Dynamic rheological experiments show that the particles with the larger aspect ratio impart much higher storage moduli and complex viscosities to the nanocomposites compared to equivalent mass loadings of particles with the smaller aspect ratio. Additionally, in flammability experiments, the larger aspect ratio particles lead to a greater reduction in mass loss rate, i.e., they are more effective at reducing flammability. These results demonstrate that the aspect ratio of MWNTs is a key parameter in controlling the rheology and flammability of polymer nanocomposites.

Published by Elsevier Ltd.

**Keywords:** Aspect ratio; Flammability; Nanocomposites

---

### 1. Introduction

Polymer nanocomposites have attracted a great deal of interest due to their ability to improve physical properties of polymers such as mechanical and thermal properties. In particular, polymer–carbon nanotube nanocomposites have been extensively studied to explore their unique electronic, thermal, optical, and mechanical properties [1–5], as summarized in recent review articles [6,7]. Furthermore, an improvement in the flammability properties of polymers has been achieved with polymer–carbon nanotube nanocomposites, which could provide an alternative to conventional flame retardants [8–15].

The outstanding improvement of physical properties with carbon nanotubes is in part attributed to their extremely high aspect ratio (length to outer diameter ratio) of up to 1000. An increase in the aspect ratio of single-walled carbon nanotube (SWNT) increases Young's modulus [16] and reduces critical concentration for the formation of a percolation network [17]. Other evidence includes higher electric and thermal conductivities of epoxy–carbon nanotube nanocomposites with high aspect ratio of the tubes [18] and higher thermal conductivity of poly  $\alpha$ -olefin/multi-walled carbon nanotube nanocomposites [19]. Furthermore, polymer–clay nanocomposites with higher aspect ratios (length to thickness ratio) of clay particles are also found to have enhanced barrier [20,21] and mechanical properties [22–24].

Although many studies have shown enhanced physical properties of polymer nanocomposites with increasing aspect ratio, only a limited study on the effects of aspect ratio of nanoparticles on flammability properties of polymer

---

<sup>☆</sup> This was carried out by the National Institute of Standards and Technology (NIST), an agency of the US Government which, by statute, is not subject to copyright in US.

\* Corresponding author.

E-mail address: [takashi.kashiwagi@nist.gov](mailto:takashi.kashiwagi@nist.gov) (T. Kashiwagi).

nanocomposites has been reported. In particular, the measurement has been limited to clay nanocomposites [25]. The objective of this study is to determine the effects of aspect ratio of MWNT on the flammability properties of polystyrene. It has been demonstrated that the formation of a jammed network composed of carbon nanotubes in the initial composite samples is critical to significantly reduce the heat release rate of the composites [15]. Therefore, dynamic measurement of storage modulus of the samples is made at an elevated temperature to determine the effects of aspect ratio of MWNT on network formation in these materials.

## 2. Experimental

### 2.1. Materials

The matrix polymer used in this study was PS (Styron 666D, Dow Chemical, melt mass flow rate of 8.0 g/10 min at 200 °C).<sup>1</sup> Two different MWNTs were used; one was purchased from Hyperion Catalyst International in the form of a master batch with a mass concentration of 20% in PS. Other MWNTs were made using xylene as a carbon source and ferrocene as a catalyst at about 675 °C by a chemical vapor deposition, CVD, method at the University of Kentucky [26].

### 2.2. Composites

Composites were prepared at the University of Kentucky by melt blending the MWNT–polystyrene mixture in a Haake PolyLab shear mixer. The mixture temperature was set at 180 °C and the polystyrene pellets were added to the mixer running at a speed of 20 rpm. The pellets melted in about 3 min, and the MWNTs were added at this time and mixing was continued for 40 min. For the Hyperion master batch, appropriate amounts of the PS pellets and of the master batch pellets were mixed and fed into a B & P Process Equipment and Systems twin-screw extruder (co-rotating, intermeshing, *L:D* equals 25:1) at NIST. Operating conditions were 400 rpm screw speed and 185 °C barrel temperature in all zones except the last zone (195 °C). Samples with mass concentrations of 0.2%, 0.5%, 1%, 2%, and 4% MWNT were prepared with the two MWNTs. All samples for measuring flammability properties (discs of 75 mm diameter and 4 mm thickness) were compression molded at 200 °C under a pressure of about 1.4 MPa for a duration of 15 min.

### 2.3. Sample characterization

The morphologies of the nanotubes in the melt blended samples were evaluated using a laser confocal microscope (Model LSM510, Carl Zeiss Inc.) to image the MWNTs in the PS matrix. The confocal microscope utilizes coherent laser

light and collects reflected light exclusively from a single plane with a thickness of 100 nm (a pinhole sits conjugated to the focal plane and rejects light out of the focal plane). A red laser ( $\lambda = 633$  nm) was used as the coherent light and images were taken at 100 $\times$  magnification with an Epiplan-Neofluar 100 $\times$ /1.30 oil-pool objective. An LP385 (Rapp Opto Electronic) filter was used to limit the lower spectra of reflected light. One hundred two-dimensional images (optical slices with 512 pixels  $\times$  512 pixels), with scan size 92.1  $\times$  92.1  $\mu$ m, were taken at a spacing of 100 nm by moving the focal plane.

The aspect ratio of the MWNTs was evaluated using scanning and transmission electron microscopies (SEM and TEM). The SEM, Phillips ESEM – E3, was operated at a voltage of 30 kV. The TEM, Hitachi H-600, was operated at a voltage of 100 kV. MWNTs were isolated from the nanocomposite by extraction of polystyrene in tetrahydrofuran, THF. The MWNTs were then dried and redispersed at very low concentrations ( $\sim 0.01$  mg/mL) in THF by stirring. Ultrasonication was avoided since it is known to modify nanotube length. Drops of the MWNT dispersion in THF were dried onto the freshly cleaved mica surfaces for evaluation using SEM. Nitrogen was blown on the drops to vaporize the THF quickly and prevent substantial tube aggregation. For evaluation using TEM, drops of the dispersion were dried onto a copper grid covered with carbon film (Ted Pella, Redding, CA).

Rheological experiments were performed on an RDAIII strain-controlled rheometer (TA Instruments) equipped with a convection oven. A parallel plate geometry (25 mm diameter) was used with a gap of 0.9 mm. Samples were prepared by melt-pressing nanocomposite pellets at 150 °C and a pressure of about 0.93 MPa. All rheological experiments were performed at 200 °C and in a nitrogen atmosphere to avoid oxidative degradation of polystyrene. The gap reference was set at 200 °C. Dynamic rheological experiments were conducted to measure the storage and loss moduli as a function of frequency (0.01–100 rad/s) at a constant strain of 0.5% (this value of strain was verified to be in the linear viscoelastic regime of the sample). Thermogravimetric analysis (TGA) was conducted using a TA Instruments TGA Q500 at a heating rate of 5 °C/min from 90 °C to 500 °C in nitrogen (flow rate of 60 cm<sup>3</sup>/min) for the original nanocomposite samples (about 5 mg) in a platinum pan.

### 2.4. Flammability property measurement

A cone calorimeter built by NIST was used to measure ignition characteristics, heat release rate, and sample mass loss rate according to ASME E1354/ISO 5660. An external radiant heat flux of 50 kW/m<sup>2</sup> was applied. All of the samples were measured in the horizontal position and wrapped with a thin aluminum foil except for the irradiated sample surface. The standard uncertainty of the measured heat release rate was  $\pm 10\%$ .

A radiant gasification apparatus, somewhat similar to a cone calorimeter, was designed and constructed at NIST to study the gasification processes of samples by measuring

<sup>1</sup> Certain commercial equipment, instruments, materials, services or companies are identified in this paper in order to specify adequately the experimental procedure. This in no way implies endorsement or recommendation by NIST.

mass loss rate and temperatures of the sample exposed to a fire-like heat flux in a nitrogen atmosphere (no burning). The apparatus consists of a stainless-steel cylindrical chamber that is 1.70 m tall and 0.61 m in diameter. In order to maintain a negligible background heat flux, the interior walls of the chamber are painted black and the chamber walls are water-cooled to 25 °C. All experiments were conducted at 50 kW/m<sup>2</sup>. The unique nature of this device is threefold: (1) observation and results obtained from it are only based on the condensed phase processes due to the absence of any gas phase oxidation reactions and processes; (2) it enables visual observations of gasification behavior of a sample using a video camera under a radiant flux similar to that of a fire without any interference from a flame; (3) the external flux to the sample surface is well-defined and nearly constant over the duration of an entire experiment (and over the spatial extent of the sample surface) due to the absence of heat feedback from a flame. A more detailed discussion of the apparatus is given in a previous study [27]; the standard relative uncertainty of the measured mass loss rate is  $\pm 10\%$ .

### 3. Results

#### 3.1. Aspect ratio and morphology of the MWNTs in PS

TEM images of the two types of MWNTs studied here (from Kentucky and Hyperion, respectively) are shown in Fig. 1. In order to determine the aspect ratio for both types of MWNTs, it is important to extract the MWNTs from compounded PS/MWNT samples because particle sizes might be modified during extrusion. A minimum of 140 measurements of diameter and of 200 measurements of length was conducted for both types of MWNTs. Histograms of MWNT length and diameter are shown in Fig. 2 for the extracted Kentucky MWNTs and in Fig. 3 for the Hyperion MWNTs. The average diameter and length of the Kentucky MWNTs were obtained by SEM (images not shown) and they are  $75 \pm 54$  nm and  $11.3 \pm 5.6$   $\mu\text{m}$ , respectively. The dimensions of the Hyperion MWNTs were determined by using TEM and they are  $7.1 \pm 2.5$  nm and  $351 \pm 195$  nm, respectively. The large standard deviation was mainly due to a few large or extremely

long and large tubes, as shown in Figs. 2 and 3. The average aspect ratio obtained by dividing the average length by the average diameter is 150 for the Kentucky MWNTs and 49 for the Hyperion MWNTs. Henceforth, the Kentucky MWNTs will be designated as MWNT-150 and the Hyperion MWNTs as MWNT-49.

Since a good dispersion of the nanotubes in the polymer matrix is crucial for the reduction in flammability [14,28], the distribution of the tubes in the PS/MWNT samples was examined by confocal microscopy to globally observe the dispersion of the MWNTs, as shown in Fig. 4. Each MWNT-150 tube can be seen in the figure and these tubes are well dispersed in PS without forming many agglomerates. However, the confocal microscopy has barely enough spatial resolution to see each MWNT-49 tube due to its much smaller size than MWNT-150. All images show no formation of agglomerates except some possibility in the image of Fig. 4(b). From these images and others (not shown), we consider that both tubes were reasonably well dispersed in PS.

#### 3.2. Thermal stability

Thermogravimetric analysis was conducted in nitrogen at a heating rate of 5 °C/min. Although previous studies did not conclusively exclude the effects of oxygen in surrounding air on thermal degradation of polymeric materials during burning of polymers, oxidation reactions of the polymers appear to be insignificant (oxygen is mainly consumed by gas phase reactions, i.e., the flame). An exception is the case in which the flame does not cover the entire burning surface or the burning/pyrolysis rate is extremely low [29,30]. Addition of either MWNT-150 or MWNT-49 to PS does not show significant effects on thermal stability of PS even with significant mass concentration of MWNTs, as shown in Fig. 5.

#### 3.3. Viscoelastic properties

We previously found that nanocomposites based on carbon nanotubes are capable of forming a continuous network-structured protective layer that mainly consists of the tubes without the formation of any opening/cracks [14,15]. (Vigorous

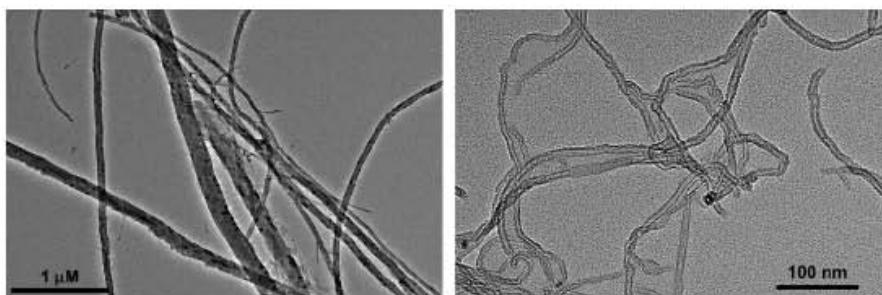


Fig. 1. TEM images of the MWNTs extracted from the composites, left is MWNTs in PS/MWNT prepared at University of Kentucky and right is MWNTs in PS/MWNT compounded with the Hyperion master batch.

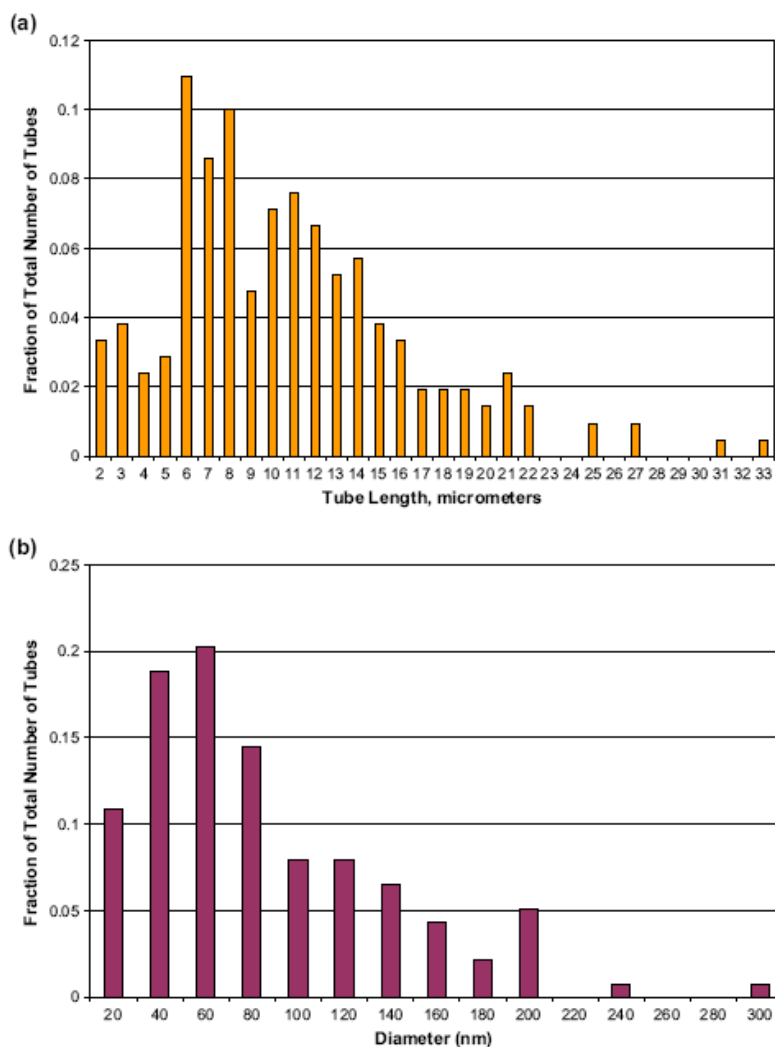


Fig. 2. Histogram plots of the dimension of MWNT, prepared at the University of Kentucky, extracted from the compounded PS/MWNT: (a) tube length and (b) tube diameter.

bubbling through any opening/cracks supplies evolved combustible degradation products to a flame, which compromises the flame retardant effectiveness.) This results in a significant reduction in heat release rate (a flammability measure related to the intensity/size of fire; the lower the heat release rate, the smaller the size of fire) with a carbon nanotube mass concentration as low as 0.5% [15]. Since the network is formed in the initial composite samples, flame retardant effectiveness could be estimated from the measurement of storage modulus of the initial samples. The storage modulus  $G'$  provides a measure of nanocomposites' 'stiffness' and its frequency dependence characterizes whether the material is liquid-like or solid-like.

Fig. 6 plots  $G'$  for PS/MWNT composites made from the MWNTs of two different aspect ratios. At 200 °C, the  $G'$  curve

of PS shows the typical response of a viscous liquid with  $G' \sim \omega^2$  at low frequencies  $\omega$ . At a 1% MWNT loading, the  $G'$  of PS/MWNT-49 is slightly higher than that of PS, while the  $G'$  of PS/MWNT-150 is even higher. At higher mass concentrations of MWNTs, the liquid-like low-frequency scaling of  $G'$  disappears and  $G'$  becomes nearly constant at low frequencies. We term the composition at which this rheological state is achieved as the 'gel concentration',  $\varphi_g$ . We define  $\varphi_g$  as the concentration at which  $G'$  becomes independent of  $\varphi$  for an extended low-frequency range. The  $\varphi_g$  of the composites with MWNT-150 is between 1% and 2% compared to about 4% with MWNT-49.

Fig. 7 plots the storage modulus measured at a frequency of 0.5 rad/s for PS/MWNT-150 and PS/MWNT-49 as a function

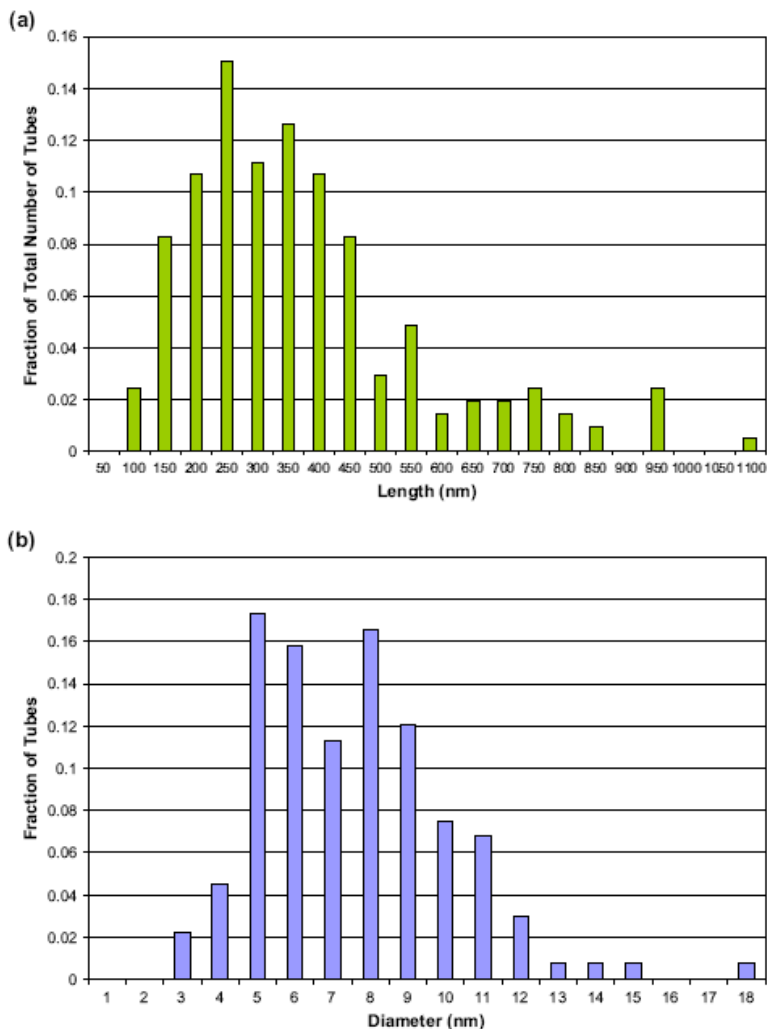


Fig. 3. Histogram plots of the dimension of MWNT in PS/MWNT compounded with the Hyperion master batch: (a) tube length and (b) tube diameter.

of MWNT concentration. This data reiterate that the  $G'$  for MWNT-150 composites is significantly larger than that for MWNT-49 at all mass concentrations studied. Note that at a mass concentration of 0.1% with MWNT-150 and 0.1% and 0.2% with MWNT-49 the  $G'$  of the composites are less than that of pristine PS. This reduction in  $G'$  is due to a small reduction in molecular weight of PS during compounding, and similar reduction in  $G'$  has been observed for extruded polymer–clay composites at low clay concentrations [31,32]. If we define a percolation concentration of MWNT,  $\varphi_c$ , as the concentration when the intertube interactions dominate over polymer chain interactions,  $\varphi_c$  for PS/MWNT-150 is about 0.35% and that for PS/MWNT-49 is 0.62%. It has been known

that a bulk ‘stiffness’  $G'$  of the composites varies phenomenologically with mass concentration according to a power law [17,33]

$$G'/G'_{\text{PS}} \sim [(\varphi - \varphi_c)/\varphi_c]^\beta$$

The inset in Fig. 7 shows that the above relationship adequately describes the  $G'$  data for both PS/MWNT-150 and PS/MWNT-49, with the value of  $\beta = 2$  for the former and 2.3 for the latter. Indeed,  $\beta = 2$  is a typical experimental value for networks of stiff fibers [35].

We now consider the effects of aspect ratio and mass concentration of MWNT on complex viscosity at 200 °C (Fig. 8).

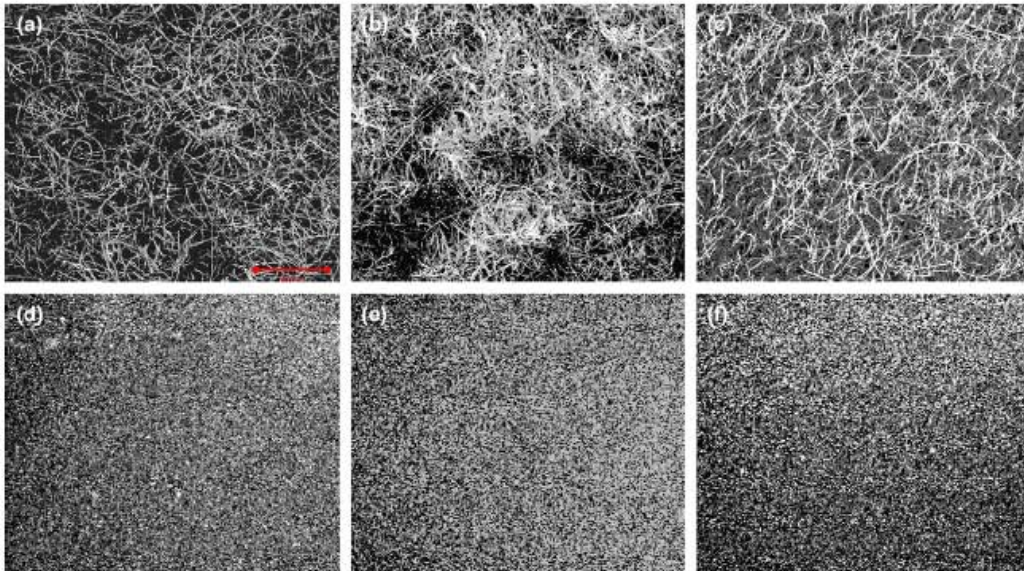


Fig. 4. Confocal microscopic images with a scale bar of 20  $\mu\text{m}$  : (a) PS/MWNT-150 (1%), (b) PS/MWNT-150 (2%), (c) PS/MWNT-150 (4%), (d) PS/MWNT-49 (1%), (e) PS/MWNT-49 (2%), and (f) PS/MWNT-49 (4%).

Since suppression of bubbling caused by the nucleation of degradation products in the polymer melt [34] is required for effective flame retardant performance, the melt viscosity of the composites at elevated temperatures might play an important role in this process. The data in Fig. 8 show an increase by about two orders of magnitude in the complex viscosity at low frequencies upon addition of 4% MWNTs. This significant increase in complex viscosity indicates an increasing importance of tube–tube interactions in dictating the rheological

response [35,36]. Fig. 8 also shows that the complex viscosities of the composites with MWNT-150 are higher than those with MWNT-49 at the same mass concentration (similar to the trend in Figs. 6 and 7 for  $G'$ ). These results suggest that the PS/MWNT-150 samples should be less flammable than those of PS/MWNT-49 at the same MWNT concentration.

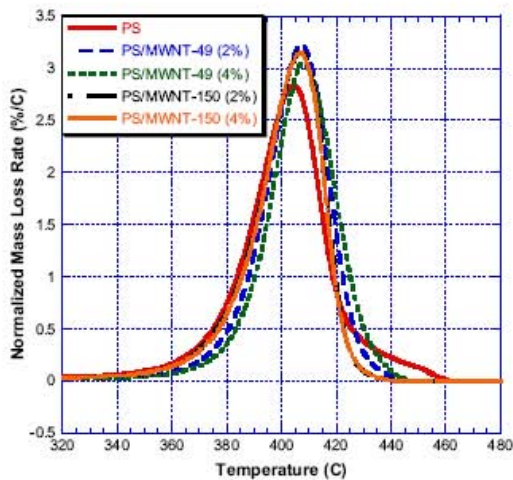


Fig. 5. Derivative thermogravimetric mass loss rates of selected samples.

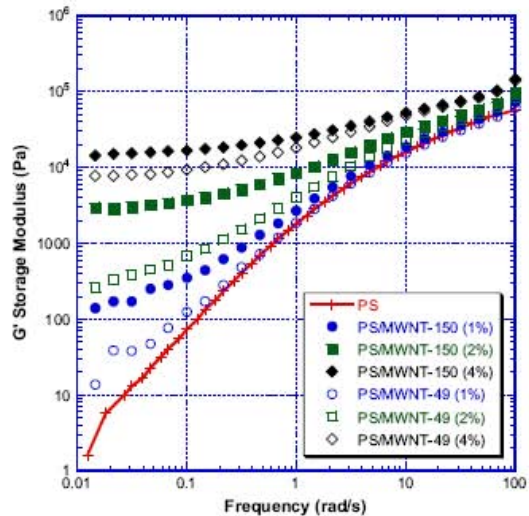


Fig. 6. Effects of aspect ratio and of mass concentration of MWNT on storage modulus of PS/MWNT nanocomposites at 200  $^{\circ}\text{C}$ .

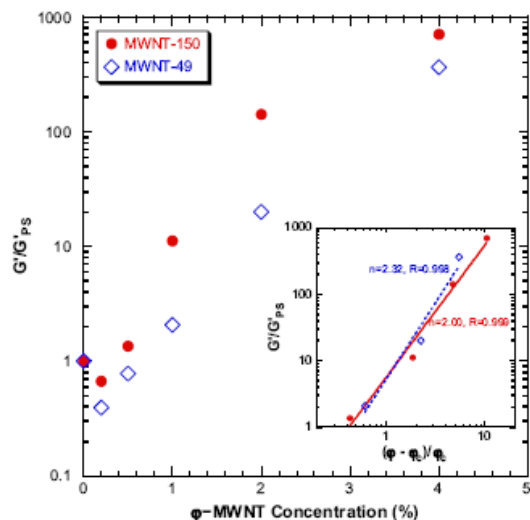


Fig. 7. The relationship between mass concentration of MWNT and normalized storage modulus of PSMWNT nanocomposites at a frequency of 0.05 rad/s and 200 °C with that of PS. Inset is the power law relationship between the normalized storage modulus and normalized mass concentration of MWNT with percolation mass concentration  $P_c$ .

### 3.4. Flammability properties

The mass of a sample was continuously measured under an external radiant flux of 50 kW/m<sup>2</sup> in a slow flowing nitrogen atmosphere and mass loss rate was calculated by taking the time derivative of the measured weight change. The results

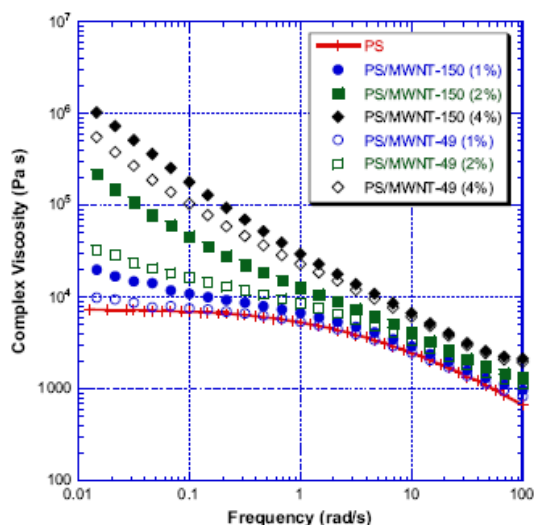


Fig. 8. Effects of aspect ratio and of mass concentration of MWNT on complex viscosity of PSMWNT nanocomposites at 200 °C.

with PS/MWNT-150 and with PS/MWNT-49 at various mass concentrations of the MWNT are shown in Fig. 9(a) and (b), respectively. At low mass concentrations of both MWNTs, the reduction in mass loss rate was relatively small. The nanocomposites behaved like a liquid with numerous bubbles

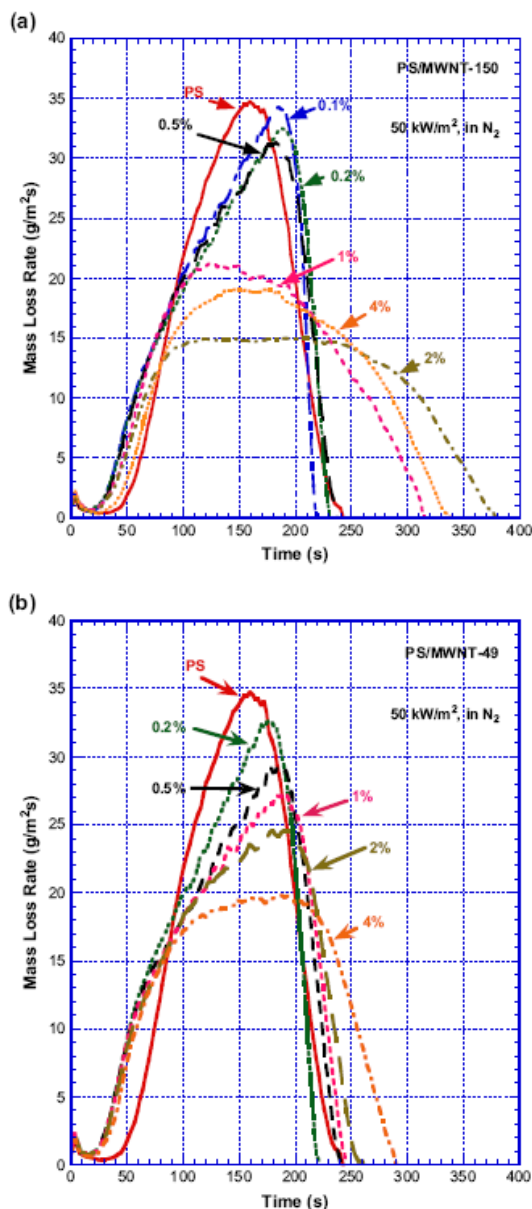


Fig. 9. Effects of mass concentration of MWNT on mass loss rate of PS/MWNT nanocomposites at 50 kW/m<sup>2</sup> in nitrogen: (a) samples with MWNT-150 and (b) with MWNT-49.

during the test and no char was left in the container. Also, samples with low mass concentrations of either of the MWNTs behaved like a viscous liquid with accompanying formation and bursting of many large bubbles and formation of many small black islands. Such islands were left at the end of the test as can be seen in the images shown in Fig. 10. The number and size of the islands increased with an increase in mass concentration of MWNTs. With 1% of MWNT-150, the sample behaved almost like a solid with a wavy surface contour; PS/MWNT-150 (2%) and PS/MWNT-150 (4%) also behaved like a solid forming a uniform protective layer with a smooth surface without any openings. This protective layer has a randomly interlaced network structure mainly consisting of the MWNTs [10,14]. PS/MWNT-150 (2%) has the lowest mass loss rate as shown in Fig. 11. However, PS/MWNT-150 (4%) has higher peak mass loss rate than that of PS/MWNT-150 (2%). The measured transmitted heat flux through the residue of PS/MWNT-150 (4%) collected after the gasification test was about 15 kW/m<sup>2</sup> compared to about 12.5 kW/m<sup>2</sup> for the residue of PS/MWNT-150 (2%). This higher transmitted heat flux for the residue of PS/MWNT-150 (4%) is due to an increase in thermal conductivity of the sample at high MWNT mass concentration [10]. The sample with higher thermal conductivity tends to slow the increase in initial mass loss rate but to increase it later after accumulation of energy in the sample. The mass loss rate of PS/MWNT-49 decreases with an increase in mass concentration of the tubes, but the peak mass loss rate tends to be higher than that of PS/MWNT-150 at the same mass concentration of tubes. It appears that true percolation-like behavior is not responsible for the reduction in mass loss rate of PS/MWNT-49. The residue even at 4% mass concentration consisted of numerous granular, coarse particles, as shown in Fig. 10, instead of a uniform protective

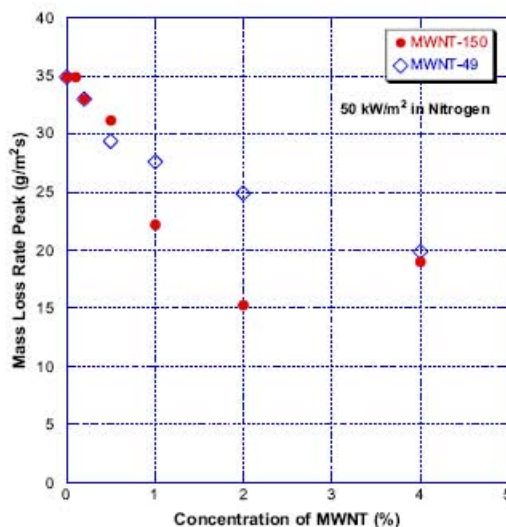


Fig. 11. The effects of aspect ratio of MWNT on the relationship between mass loss rate peak and mass concentration of MWNT.

layer. Bubbling in the space between the particles could be seen during the test.

It has been demonstrated that the flame retardant performance of polymer-carbon nanotube nanocomposites is mainly due to the physical process of heat shielding by the formation of a network-structured protective layer in the condensed phase [10,14,15]. Therefore, it is expected that the heat release rate curves of these samples would be similar to the mass loss rate curves shown in Fig. 9. Observed heat

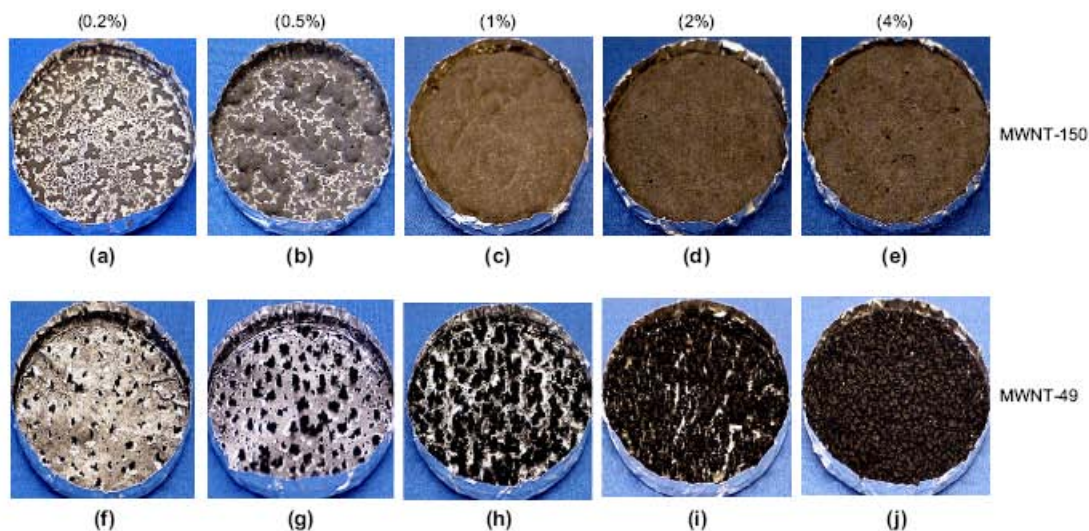


Fig. 10. Comparison of residues of PS/MWNT nanocomposites, based on MWNT-150 and MWNT-49, collected after the gasification test at 50 kW/m<sup>2</sup> in nitrogen.

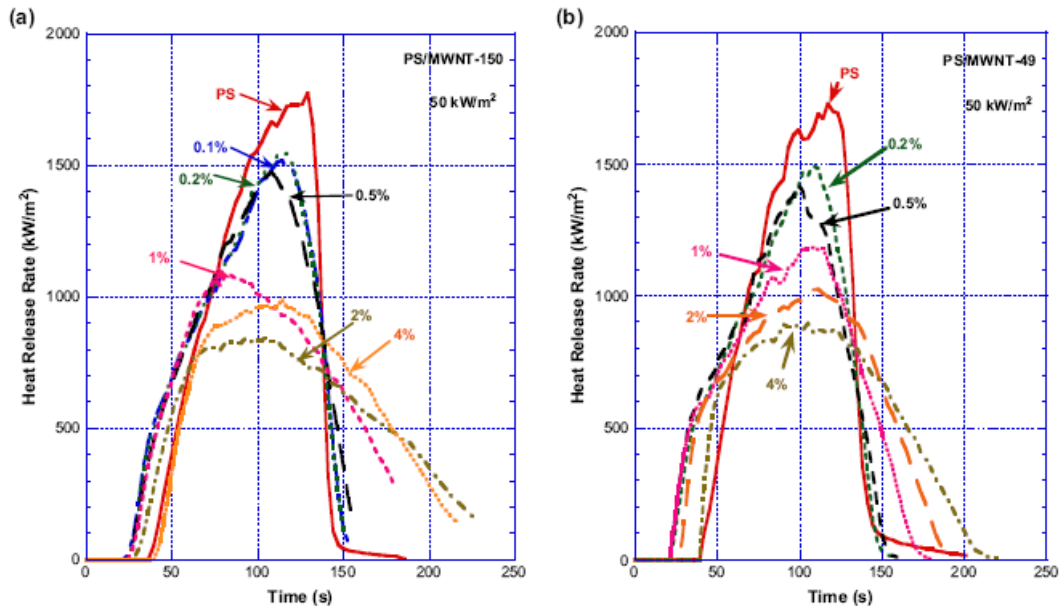


Fig. 12. Heat release rate curves of PS/MWNT nanocomposites at various mass concentrations of MWNT at  $50 \text{ kW/m}^2$ : (a) with MWNT-150 and (b) with MWNT-49.

release rate curves with the two different MWNTs at various mass concentrations of the tubes are shown in Fig. 12. The observed trends are very similar to those observed in Fig. 9, including lower peak heat release rates for PS/MWNT-150 as compared to those of PS/MWNT-49 at the same tube mass concentration. Furthermore, the peak heat release rate of PS/MWNT-150 (4%) is higher than that of PS/MWNT-150 (2%) as observed in Fig. 9 due to an increase in thermal conductivity for PS/MWNT-150 (4%) as described above.

#### 4. Discussion

The above results clearly show the importance of aspect ratio of MWNT on viscoelastic properties and flammability properties of PS/MWNT nanocomposites. Since the sizes of the two MWNTs are quite different, it is interesting to explore the significant effects of the aspect ratio. We estimate the difference in the total number of MWNTs in PS/MWNT-150 (average length of  $11 \mu\text{m}$  and average outer diameter of  $97 \text{ nm}$ ) and PS/MWNT-49 (average length of  $347 \text{ nm}$  and average diameter of  $7.1 \text{ nm}$ ) at the same mass concentration of MWNT. With the assumptions that the outer diameter is much larger than the inner diameter of both tubes and that both the densities of the two MWNTs are the same, the total number of MWNT-49 is roughly 6000 times more than that of MWNT-150 in the same volume of PS/MWNT. Furthermore, the total outer surface area of MWNT-49 in PS/MWNT-49 is about 14 times greater than that of MWNT-150 in PS/MWNT-150. However, the results show that the effects of aspect ratio of MWNT are more dominant than the total number of nanotubes

or their total surface area. Then, if two MWNT types having the same outer diameter but different aspect ratios (different lengths of tube) were used, it is possible that the effects of aspect ratio on flammability properties might be larger than those observed in this study.

The importance of aspect ratio of nanoparticles on the formation of the network-structured layer and flammability properties was also demonstrated in our previous study with plate shaped nanoparticles of clay [25]. In that study three different types of clays were used in polypropylene/polypropylene-g-maleic anhydride (PP/PP-g-MA): synthetic mica (aspect ratio of about 1200 [37]), montmorillonite (MMT) (about 200 [37]) and synthetic hectorite (about 50 [37]). The sample was a  $10 \text{ cm} \times 10 \text{ cm} \times 0.3 \text{ cm}$  thick plate and it was tested in nitrogen at  $50 \text{ kW/m}^2$ . The lowest mass loss rate was observed for the sample with synthetic mica, which generated a significantly lower mass loss rate than with MMT and synthetic hectorite, as shown in Fig. 13. The figure shows pictures of the residues of the four samples collected after the tests. The surface of the residue of the sample with synthetic mica is relatively smooth without any large cracks. However, the two samples with the other two clays show large cracks (in particular, with synthetic hectorite). Melting and vigorous bubbling were observed in the cracks during the test. It has demonstrated that the addition of carbon nanotubes or clay having a large aspect ratio into polymers tends to generate residues having a smooth surface without any openings/cracks and to reduce significantly the flammability properties of the polymers.

In Fig. 6, the storage modulus of PS/MWNT-49 (4%) is seen to be nearly independent of frequency at low frequencies,

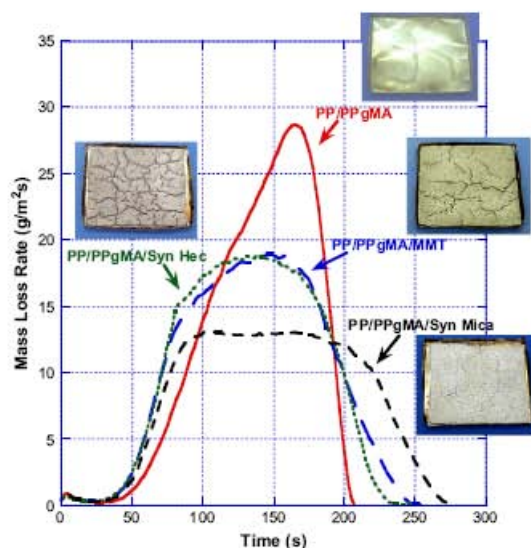


Fig. 13. Effects of clay type on mass loss rate of PP (92.3%)/PP-g-MA (7.7%) and PP (84.6%)/PP-g-MA (7.7%)/clay (7.7%) samples in nitrogen at  $50 \text{ kW/m}^2$ .

which indicates the formation of network structure and such nanocomposite samples having a relatively high complex viscosity formed a protective heat shield layer covering the sample surface without any cracks [10,12,15]. However, it appears that the residue of PS/MWNT-49 (4%) collected after the gasification test in nitrogen at  $50 \text{ kW/m}^2$  is made of a collection of numerous discrete agglomerates, as shown in Fig. 10j. Vigorous bubbling was observed around the agglomerates during the test and the mass loss rate of this sample is not as low as that of PS/MWNT-150 (2%) which did form a smooth, network-structured protective layer, as shown in Fig. 10d. In our previous study, the formation of the network-structured protective layer was observed with poly(methyl methacrylate)/single-walled carbon nanotube (PMMA/SWNT) nanocomposite at a mass concentration of 0.5% [15]. The aspect ratio of the bundled SWNT was about 45 based on the average diameter of about 7 nm and average length of 310 nm. Since these SWNT bundles and MWNT-49 are about the same size, the size of MWNT-49 is not the reason why PS/MWNT-49 does not form the protective layer. If the dispersion of MWNT-49 in PS/MWNT-49 (4%) is much worse than that of MWNT-150 in PS/MWNT-150 (this does not appear in Fig. 4), the storage modulus of PS/MWNT-49 (4%) should not be so high as shown in Fig. 6. At present, it is not clear why a fully effective protective layer was not formed for PS/MWNT-49.

## 5. Conclusions

The effects of the aspect ratio of MWNT on viscoelastic properties and flammability properties of PS/MWNT nanocomposites were studied with two different MWNTs in the

mass concentration from 0.1% to 4%. The samples were prepared using twin-screw extruders. The average aspect ratios of the two MWNTs, 49 and 150, were determined by analyzing the images of the tubes extracted from the compounded nanocomposites, which were taken by SEM and TEM. No significant effects of aspect ratio on thermal stability of PS/MWNT nanocomposites were observed. However, storage modulus and complex viscosity of PS/MWNT-150 are larger than those of PS/MWNT-49 at the same mass concentration of MWNT. PS/MWNT-150 samples with 2% and 4% mass concentration of MWNT-150 form solid-like network structures but only PS/MWNT-49 (4%) forms this structure. The mass loss rate of PS is more reduced with PS/MWNT-150 and the lowest mass loss rate is observed with PS/MWNT-150 (2%). Slightly higher mass loss rate of PS/MWNT-150 (4%) is probably due to an increase in thermal conductivity. With increasing concentration of MWNT-150, the residue of PS/MWNT-150 changes from the formation of discrete islands to a smooth surface layer without any openings, which is generated at concentrations of 2% and 4%. All PS/MWNT-49 samples used in this study did not generate such residues. These results show that the addition of MWNT with large aspect ratios significantly reduces the flammability of polymers.

## Acknowledgements

B.H.C. and S.R.R. gratefully acknowledge funding from the NIST BFRL extramural grants program through grant no. 70NANB4H1001. T.K. is funded by NIST under Grant 5D1022.

## References

- [1] Schadler L.S., Giannaris S.C., Ajayan P.M. *Appl Phys Lett* 1998;73:3842–4.
- [2] Stephan C., Nguyen T.P., Lahr B., Blau W., Lefrant S., Chauvet O. *J Mater Res* 2002;17:396–400.
- [3] Dalton A.B., Collins S., Munoz E., Razal J.M., Ebron V.H., Ferraris J.P., et al. *Nature* 2003;423.
- [4] Barrau S., Demont P., Peigney A., Laurent C., Lacabanne C. *Macromolecules* 2003;36:5187–94.
- [5] Thostenson E.T., Chou T.-W. *J Phys D Appl Phys* 2003;36:573–82.
- [6] Coleman J.N., Khan U., Blau W.J., Gun'ko Y.K. *Carbon* 2006;44:1624–52.
- [7] Moniruzzaman M., Winey K.I. *Macromolecules* 2006;39:5194–205.
- [8] Kashiwagi T., Grulke E., Hilding J., Harris R.H., Awad W.H., Douglas J.F. *Macromol Rapid Commun* 2002;23:761–5.
- [9] Beyer G. *Fire Mater* 2002;26:291–3.
- [10] Kashiwagi T., Grulke E., Hilding J., Groth K., Harris R.H., Butler K., et al. *Polymer* 2004;45:4227–39.
- [11] Peeterbroeck S., Alexandre M., Nagy J.B., Pirlot C., Fonseca A., Morea N., et al. *Compos Sci Technol* 2004;64:2317–23.
- [12] Schartel B., Pötschke P., Knoll U., Abdel-Goad M. *Eur Polym J* 2005;41:1061–70.
- [13] Gao F., Beyer G., Yuan Q. *Polym Degrad Stab* 2005;89:559–64.
- [14] Kashiwagi T., Du F., Winey K.I., Groth K.M., Shields J.R., Bellayer S.P., et al. *Polymer* 2005;46:471–81.
- [15] Kashiwagi T., Du F., Douglas J.F., Winey K.I., Harris R.H., Shields J.R. *Nat Mater* 2005;4:928–33.
- [16] Ashrafi B., Hubert P., Vengallatore S. *Nanotechnology* 2006;17:4895–903.
- [17] Munson-McGee S.H. *Phys Rev B* 1991;43(4):3331–6.
- [18] Gojny F.H., Wichmann M.H.G., Fiedler B., Kinloch I.A., Bauhofer W., Windle A.H., et al. *Polymer* 2006;47:2036–45.
- [19] Yang Y., Grulke E.A., Zhang Z.G., Wu G. *J Appl Phys* 2006;99:114307.

- [20] Osman MA, Mittal V, Lusti HR. *Macromol Rapid Commun* 2004;25: 1145–9.
- [21] Lu C, Mai Y-W. *Phys Rev Lett* 2005;95:088303.
- [22] Miyagawa H, Rich MJ, Drzal LT. *J Polym Sci Part B Polym Phys* 2004;42:4391–400.
- [23] Stretz HA, Paul DR, Li R, Keskkula H, Cassidy PE. *Polymer* 2005;46: 2621–37.
- [24] Weon J-I, Sue H-J. *Polymer* 2005;46:6325–34.
- [25] Kashiwagi T. In: Le Bras M, Wilkie CA, Bourbigot S, Duquesne S, Jama C, editors. *Fire retardancy of polymers*. Cambridge, UK: Royal Society of Chemistry; 2005. p. 81–99 [chapter 6].
- [26] Andrews R, Jacques D, Rao AM, Derbyshire F, Qian D, Fan X, et al. *Chem Phys Lett* 1999;303:467–74.
- [27] Austin PJ, Buch RR, Kashiwagi T. *Fire Mater* 1998;22:221–37.
- [28] Kashiwagi T, Fagan J, Douglas JF, Yamamoto K, Heckert AN, Leigh SD. *Polymer* 2007;48:4855–66.
- [29] Brauman SK. *J Polym Sci Part B Polym Phys* 1988;26:1159–71.
- [30] Kashiwagi T, Ohlemiller TJ. *Proc Combust Inst* 1982;19:815–23.
- [31] Wang K, Lian S, Deng J, Yang H, Zhang Q, Fu Q, et al. *Polymer* 2006; 47:7131–44.
- [32] Treece MA, Oberhauser JP. *Polymer* 2007;48:1083–95.
- [33] Gingold DB, Lobb CJ. *Phys Rev B* 1990;42:8220–4.
- [34] Kashiwagi T. *Proc Combust Inst* 1994;25:1423–37.
- [35] Kharchenko SB, Douglas J, Obrzut J, Grulke EA, Migler KB. *Nat Mater* 2004;3:564–8.
- [36] Hu G, Zhao C, Zhang S, Yang M, Wang Z. *Polymer* 2006;47:480–8.
- [37] Yano K, Usuki A, Okada A. *J Polym Sci Part A Polym Chem* 1997;35: 2289–94.

## Chapter 10 New fire retardant nanocomposites<sup>1</sup>

Takashi Kashiwagi

Fire Research Division, NIST, Gaithersburg, MD 20899-8665 USA

### 10.1. Introduction

While the incorporation of microscale particles as fillers into polymers has been scientifically well explored, the decrease in size of particles to nanometers, and the simultaneous increase of the interface area, results in new extraordinary material properties<sup>i,ii,iii,iv</sup>. In one such application, the flammability properties of polymers have been improved with the addition of nanoscale particles. These filled nanocomposites provide an attractive alternative to conventional flame retardants. At present, the most common approach for improving flammability is the use of layered silicates such as clays, as described in Chapter 3. However, there are many different shapes/types of nanoparticles. (Here, a nanoscale particle is defined as having at least one dimension on the nanometer scale.) When all three dimensions are of the order of nanometers, we are dealing with true nanoparticles, such as spherical silica particle, having an aspect ratio of 1. Another type of nanoparticle has only one dimension on the nanometer scale. Such nanoscale particles are sheet/layers, such as layered silicate or graphite, which are one to a few nanometers thick and hundreds to thousands of nanometers in the other two dimensions. When two dimensions are on the nanometer scale and the third is larger, the particles form elongated structures such as nanotubes, whiskers, or rods with a high aspect ratio.

It is of interest to determine the flame retardant effectiveness of these shapes/types of nanoparticles, other than layered silicates to find what shape/type of nanoparticles is the most effective for improving flammability properties of commodity polymers. In this chapter, flammability properties of nanocomposites containing nanoscale oxides such as nano silica particles and metal oxides, polyhedral oligomeric silsesquioxanes (POSS), and carbon based nanoparticles such as graphite, single-walled carbon nanotubes (SWNT), multi-walled carbon nanotubes (MWNT), and carbon nano fibers (CNF) are described and a flame retardant mechanism of these nanoparticles is discussed.

### 10.2. Nano scale oxide based nanocomposites

#### 10.2.1. Nano silica particles

Nanoscale silica particles can have a huge interfacial area as long as the diameter of the particles is in the range of nanometers. Although they do not have the narrow gallery structure of a layered clay, an improvement in physical properties<sup>v,vi,vii,viii</sup> and also an improvement in thermal stability<sup>ix,x</sup> by the addition of nanoscale silica particles to polymer were reported. This latter improvement was attributed to the formation of tightly

---

<sup>1</sup> This article is a US Government work and as such, is in the public domain in the United States of America.

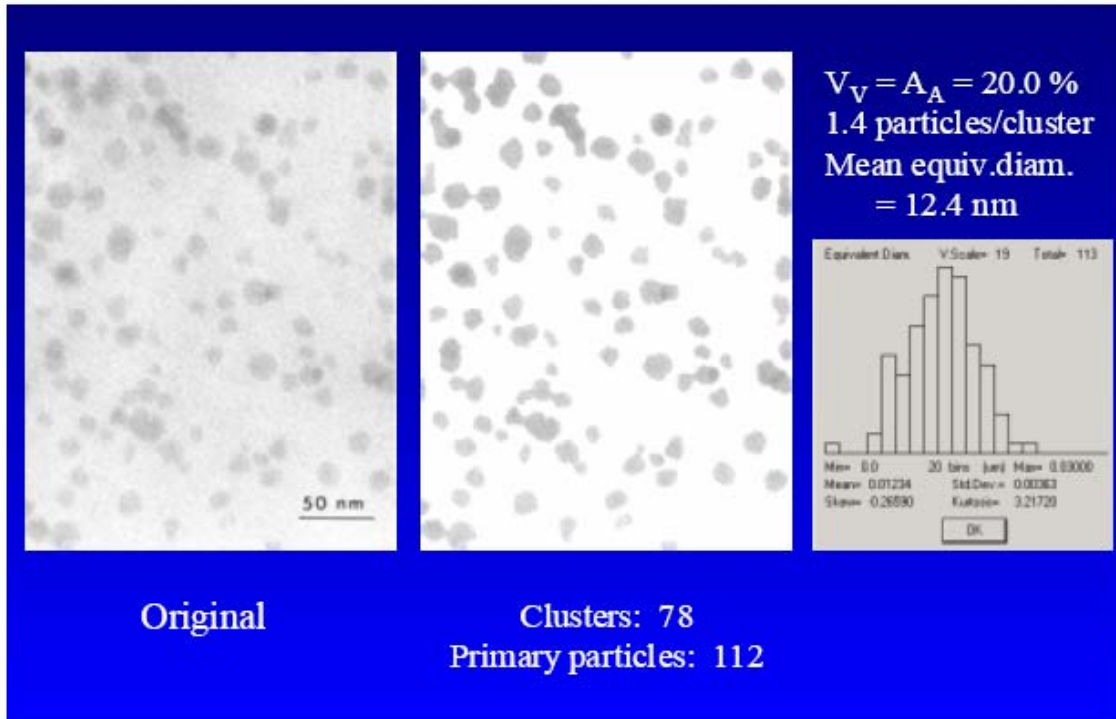


**Figure 1.** TEM image of the PMMA/nanosilica nanocomposite (left), analyzed image (middle) and a histogram distribution of diameter (right).

packed particles to various polymers significantly reduced heat bound and loosely bond polymer chains around the particles<sup>xi</sup>. It was also reported that the addition of mesoscale silica to various polymers significantly reduced the heat release rate of the polymers<sup>xii,xiii</sup>. Flammability properties of poly(methyl methacrylate) (PMMA)/nano silica nanocomposites<sup>xiv,xv,xvi</sup> and polyimide/nano silica nanocomposites<sup>xvii</sup> have been reported. Samples have been prepared by solvent blending<sup>xiv,17</sup>, melt blending utilizing single screw extrusion<sup>xvi</sup>, or in situ polymerization<sup>xv</sup> in order to obtain well-dispersed nanosilica particles in the sample. The dispersion of the particles in the polymer is

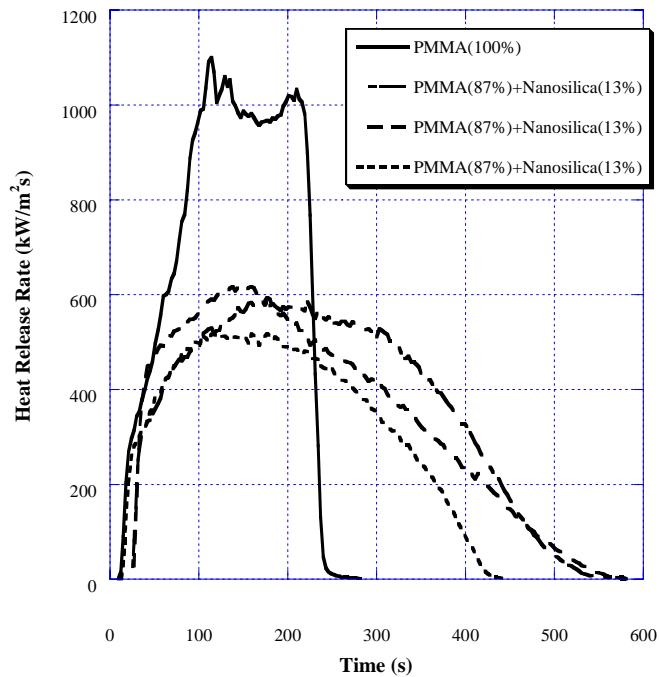


**Figure 2.** The effects of the addition of nanosilica on heat release rate of PMMA at 50 kW/m<sup>2</sup>.

critical for obtaining better flame retardant performance, as described in previous chapters. Transmission electron microscopy (TEM) was used to determine the dispersion. An example is shown in Figure 1<sup>xv</sup> and it indicates well-dispersed particles having an average diameter of about 12 nm. Roughly a 50 % reduction of the peak heat release rate was reported with the addition of 13 % mass fraction of the silica particles<sup>xv</sup>, as shown in Figure 2 and little to no improvement was reported in a limiting oxygen index (LOI) measurement<sup>xiv</sup> with up to 10 % mass fraction of silica particles having a diameter as small as 7 nm (the dispersion of these particles was not shown). Although LOI increased from 36 to 44, the addition of 28 % mass fraction of silica particles (a diameter of 50-300 nm) was required. In the heat release rate curves shown in Figure 2, the addition of the nano silica particles hardly reduced the heat release rate at the early stage of burning and it was demonstrated that the addition of nanoscale silica particles did not significantly modify the UL-94 rating<sup>xvi</sup>. Therefore, the overall flame retardant effectiveness of nanosilica particles appears to be less than that of clay particles, as described in the previous chapters.

The observation of the sample behavior during the gasification in a nitrogen atmosphere at an external radiant flux of 40 kW/m<sup>2</sup> reported the formation of many small bubbles followed by the formation of many rigid white islands<sup>xv</sup>.



**Figure 3.** The residue of the PMMA/Nanosilica nanocomposite after the gasification test in nitrogen at 40 kW/m<sup>2</sup> [15].

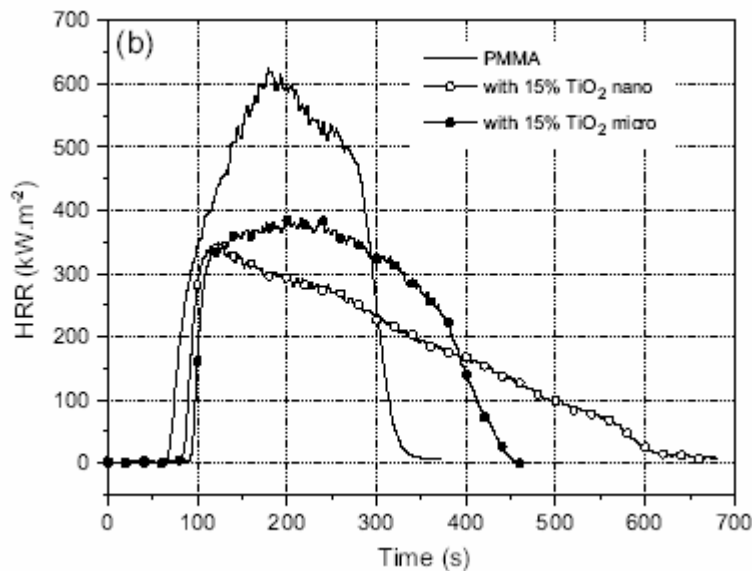


**Figure 4.** Effect of the particle size on heat release rate for PMMA/TiO<sub>2</sub> at 35 kW/m<sup>2</sup> [19].

Vigorous bursting of small bubbles was observed around the islands. The islands appeared to be made of coarse, granular particle clumps. Since the sample surface was only partly covered by these loose granular particles/clumps, part of the sample surface was still exposed to the external heat between the coarse particles and barrier performance of the layer to slow the evolution of the degradation products of PMMA was not effective.

A similar behavior was observed with polycarbonate containing 15 nm coated silica particles<sup>xviii</sup>. At the end of the test, a dark, coarse powdery layer was left at the bottom of the sample container (Figure 3.). No network structured protective layer covering the entire sample surface was formed. One possible approach to forming such an *in situ* silica network during gasification would be to enhance the formation of crosslinks among the particles by appropriate surface treatments on the surface of the nanosilica particles but no work along these lines has been reported.

### 10.2.2. Metal Oxides

The flammability properties of nanocomposites consisting of nanoscale titanium oxide ( $\text{TiO}_2$ , a median diameter of 21 nm) and iron oxide ( $\text{Fe}_2\text{O}_3$ , a median diameter of 23 nm) in PMMA were measured<sup>xix</sup>. The nanocomposites were prepared by melt blending. A morphology study of the nanocomposites showed that the particles were well distributed in the sample, but with some

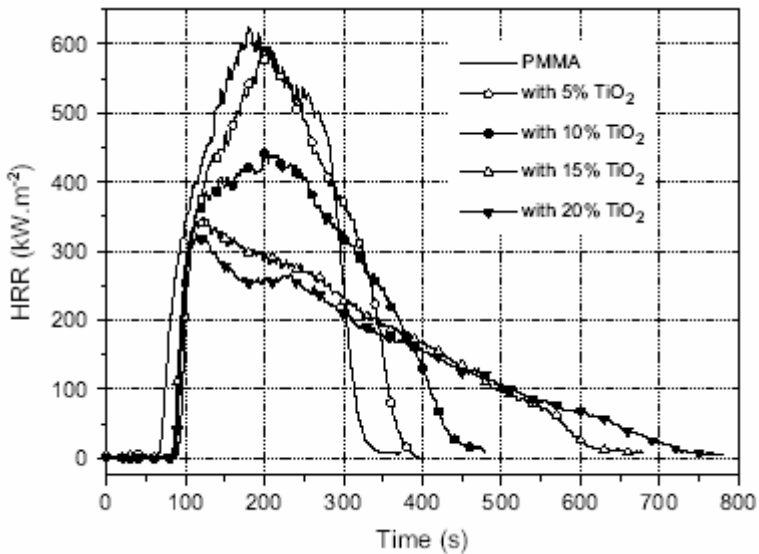


**Figure 5.** Effect of  $\text{TiO}_2$  nanoparticle concentration on heat release rate of PMMA at  $35 \text{ kW/m}^2$  [19].

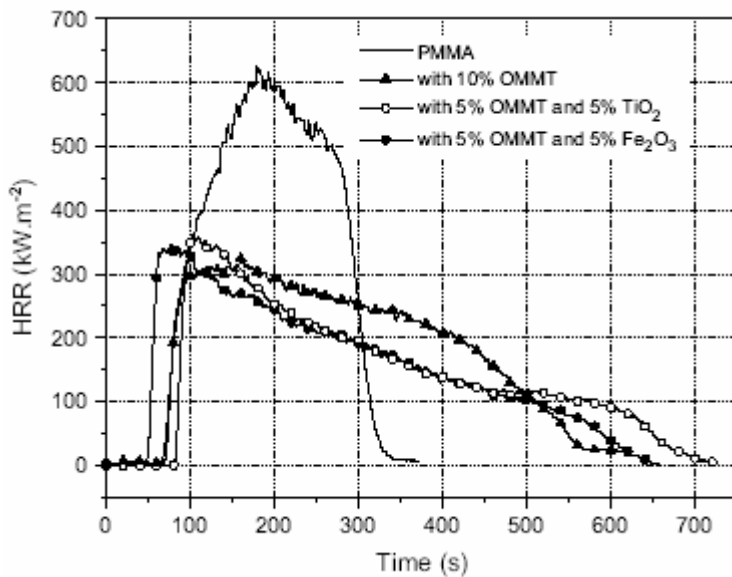


**Figure 6.** Comparison of heat release rates of the nanocomposites with OMMT, OMMT- $\text{TiO}_2$ , and OMMT- $\text{Fe}_2\text{O}_3$  at  $35 \text{ kW/m}^2$  [19].

tendency to aggregate since no surface treatment was done on the oxides. The effect of particle size was studied by comparing heat release rate of the nanocomposite with the nanoscale  $\text{TiO}_2$  particles to that of the microcomposite with micrometer scale  $\text{TiO}_2$  ( $0.2 \mu\text{m}$ ); the comparison is shown in Fig. 4. The peak heat release rate of the nanocomposite was about 10 % lower than that of the microcomposite. A similar result was also observed for PMMA/ $\text{Fe}_2\text{O}_3$  samples. An increase in nanoparticle  $\text{TiO}_2$

concentration reduced the heat release rate of PMMA, as shown in Figure 5, but the amount of the reduction is not as significant as with other types of nanoparticles such as clay or carbon nanotubes, as described later. The combination of these nanoparticles with organo-modified montmorillonite (OMMT) was used to determine the synergistic effect on the reduction in the heat release rate of PMMA; the results are shown in Figure 6. The observed improvement via the incorporation of the oxide particles was explained by several effects; (1)  $\text{TiO}_2$  to act as a “heat shield” which can limit the thermal conduction into the sample, (2) limitation of evolved gas release due to an increase in melt viscosity, and (3) enhanced wetting of mineral particles by the molten polymer.

### 10.2.3. Polyhedral Oligomeric Silsequioxanes (POSS)

With the recent development of nanostructured chemical feedstocks based on POSS<sup>xx,xxi,xxii</sup>. POSS based hybrid nanocomposites have received increasing attention because of the unique three-dimensional structure of the POSS macromonomer<sup>xxiii</sup>, as shown in Figure 7. POSS represents an intermediate structure between that of silicone and that of silica, explaining its excellent oxidation stability and reaction to fire. It consists of an inorganic silica-like core ( $\text{Si}_8\text{O}_{12}$ ) surrounded by eight organic groups at the corners to enhance compatibility with organic polymers. Its nanoscale enables the POSS segment to effectively reinforce polymer chain-segments and to control polymer chain motion at the molecular level through

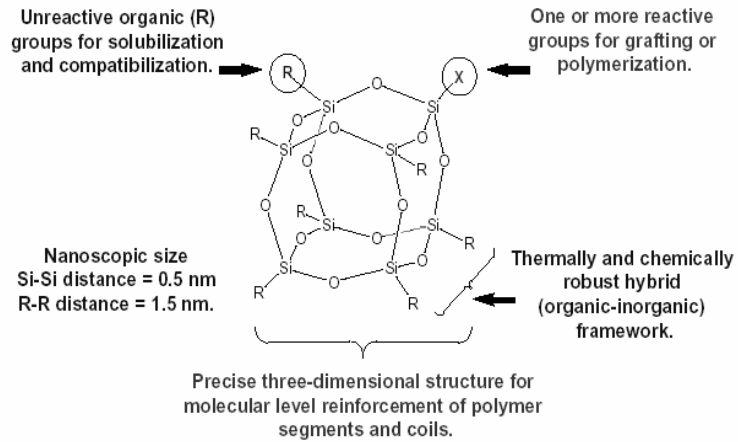


**Figure 7.** General structure of POSS [23].

maximizing the interface area and chemical interactions of reinforcement with polymers. Early examples were presented with siloxanes<sup>xxiv,xxv</sup> followed by numerous applications showing enhancement of thermal stability and improving flammability properties of polymers.

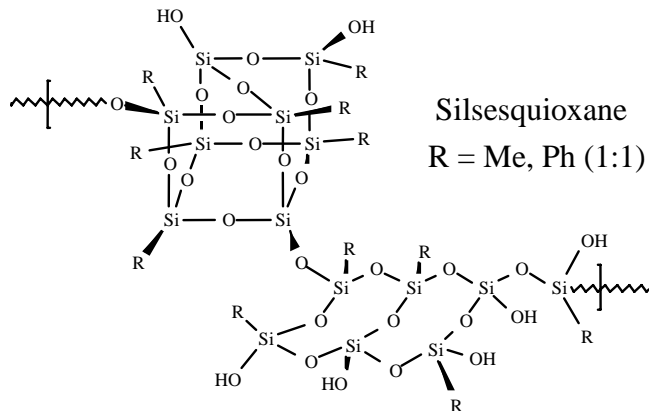


**Figure 8.** The structure of the POSS.

POSS macromers generally sublime at high temperatures provided that they contain functionalities which do

not readily undergo cross-linking reactions. Once incorporated into a polymeric form, POSS macromers do not sublime; rather they decompose primarily through partial loss of their organic substituents without significantly affecting the degradation of the matrix polymers<sup>xxvi</sup> or with subsequent cross-linking reactions which incorporates the remaining

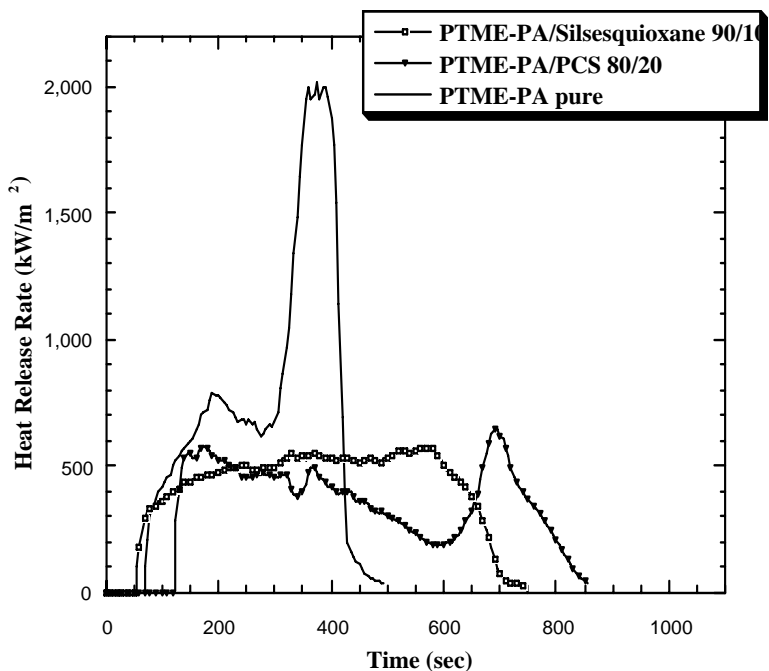


**Figure 9.** Heat release rate curves of PTME-PA with siloxane and the POSS at 35 kW/m<sup>2</sup> [30].

composition into SiO<sub>x</sub>C<sub>y</sub> network (residue) in POSS-Siloxane copolymer<sup>xxvii</sup>. Thermal gravimetric analysis of these nanocomposites shows that the initial decomposition temperatures and residue (ceramic and/or char) yield increased with increasing POSS concentration<sup>24,xxvi,xxviii,xxix</sup>. In terms of the initial decomposition temperature and residue yield the thermal stability of the nanocomposites was significantly enhanced with increasing inorganic component.

The above thermal analysis study demonstrated the enhanced thermal stability of POSS-polymer nanocomposites and suggested there is potential to improve flammability properties of matrix polymers. However, studies clearly demonstrating such improvement via the use of POSS based nanocomposites are rather limited. One study<sup>xxx</sup> is of nanocomposites consisting of polytetramethyleneether-glycol-*b*-polyamide-12, 1% polyimide-12 (PTME-PA), polystyrene-polybutadiene-polystyrene (SBS), and polypropylene (PP) prepared with POSS (structure is described in Figure 8) ranging from 10 to 20% via solution blending in tetrahydrofuran (THF). For comparison purposes, composites based on other silicone compounds such as polycarbosilane (PCS) and polysilastyrene (PSS) were also prepared by solution blending. The flammability properties of these blends were characterized using a Cone Calorimeter. The results, shown in Figure 9 and Table 1, reveal that both PCS (although twice higher concentration than that of the POSS) and POSS are reasonably effective for reducing the heat release rate measured at 35 kW/m<sup>2</sup>. However, the total heat release (integrating the heat release rate with respect to time) of the nanocomposites was not significantly reduced from that of the matrix resins. Furthermore, the residue yields are about the same as the calculated yields listed in the Table 1 (in parentheses). This means that the addition of the POSS in the nanocomposites does not significantly increase the yield of carbonaceous char. The residue is mainly the inorganic component of the POSS.

Simultaneous significant reduction of heat release rate and of the total heat release was achieved with polyurethane (PU) POSS nanocomposites (POSS 10% mass fraction) used as a coating on polyethylene terephthalate (PET) knitted fabric<sup>xxx1</sup>, as shown in Figure 10. Two different POSSs were used in this study. One was octamethyl POSS (POSS MS) with R = methyl in the structure described in Figure 7 and the other was poly vinylsilsequioxane (POSS FQ) with R = vinyl in the structure described in Figure 8 (all ends are vinyl). For comparison purposes, clay (Closite 30 B) was also used as a nanocomposite filler. It was observed that a significant reduction of heat release rate and of the total heat release of the PET knitted fabric was achieved with POSS FQ2 ( 2 means incorporation of the nano additives in the second stage during the sample preparation) but no reduction was observed with POSS MS2. The thermal stability of the coated knitted fabric containing POSS MS2 was lower than that of the fabric coated by virgin PU in the TGA measurement. Destabilization of the fabric at 200 °C by POSS MS2 and sublimation of POSS MS2 at around 300 °C could explain the lack of FR performance shown in Figure 10. On the other hand, POSS FQ showed a remarkable thermal stability without mass loss up to 380 °C and only a mass loss of 6 % occurred at 700 °C due to the formation of crosslinks. In the case of the PU POSS FQ2 coating, the residue (consisting of carbonaceous char and possible preceramic components) was more uniform, and only small cracks were observed on the surface. This residue was more resistant and could suppress the flame<sup>31</sup>. The formation of a hard uniform barrier over a polycarbonate surface was also reported with the polycarbonate/coated POSS nanocomposites<sup>18</sup>. However, PP-POSS multifilament yarns prepared from PP POSS FQ

**Table 1.** Summary of Cone Calorimeter Data of PP, PTME-PA, and SBS with Siloxanes and the POSS at 35 kW/m<sup>2</sup> [30].

Sample	Residue Yield %	Mean Mass Loss Rate g/s m <sup>2</sup>	Peak HRR (Δ %) kW/m <sup>2</sup>	Mean HRR (Δ%) kW/m <sup>2</sup>	Hc MJ/kg	SEA m <sup>2</sup> /kg	Mean CO yield kg/kg
PP	0	25.4	1,466	741	34.7	650	0.03
PP/POSS 80/20	17 (16)	19.1	892 (40%)	432 (42%)	29.8	820	0.03
PTME-PA	0	34.2	2,020	780	29.0	190	0.02
PTME-PA/PCS 80/20	15 (15)	14.8	699 (65%)	419 (46%)	28.5	260	0.02
PTME-PA /POSS 90/10	6 (8)	19.8	578 (72%)	437 (44%)	25.2	370	0.02
SBS	1	36.2	1,405	976	29.3	1,750	0.08
SBS /PCS 80/20	20 (15)	18.5	825 (42%)	362 (63%)	26.4	1,550	0.07
SBS/POSS 90/10	6 (8)	31.2	1,027 (27%)	755 (23%)	26.9	1,490	0.07

Hc = Mean Heat of Combustion; SEA = Specific extinction area (smoke measurement)

Uncertainties: ± 5 % of reported value for residue yields, HRR and Hc data; ± 10% for the carbon monoxide and SEA data. Theoretical residue yields in ( ).

nanocomposites did not show either any reduction of heat release rate or of the total heat release, but the ignition delay time was much longer than that of PP, as shown in Figure 11<sup>xxxiii</sup>. These results suggest that POSS FQ did not act as a flame retardant for PP but only as a thermal stabilizer. These results reveal that flammability of polymer/POSS nanocomposites depends on the type of polymer matrix, the structure of POSS, and

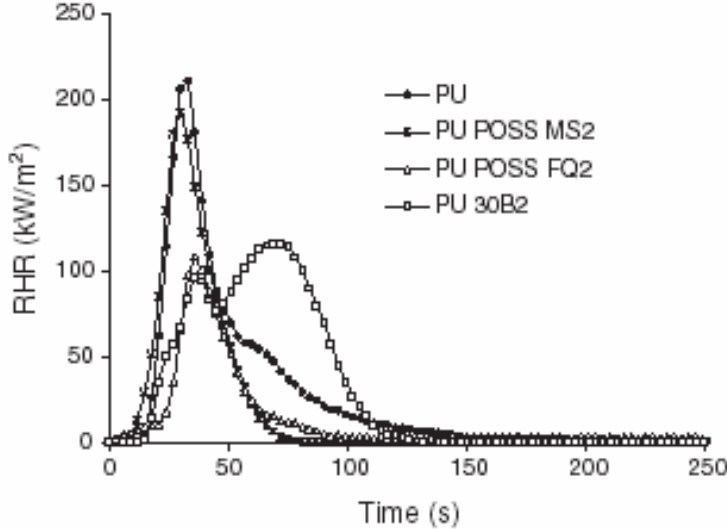


**Figure 10.** Heat release rate curves of PU-nanocomposites on PET knitted fabrics at 35 kW/m<sup>2</sup>, incorporation of the nanoadditives in second stage during sample preparation [31].

incorporation of POSS into the polymer structure. If a certain POSS structure significantly enhances crosslinks with a matrix polymer to form a significant amount of SiO<sub>x</sub>C<sub>y</sub> network, not only reduction of heat release rate but also reduction of the total heat

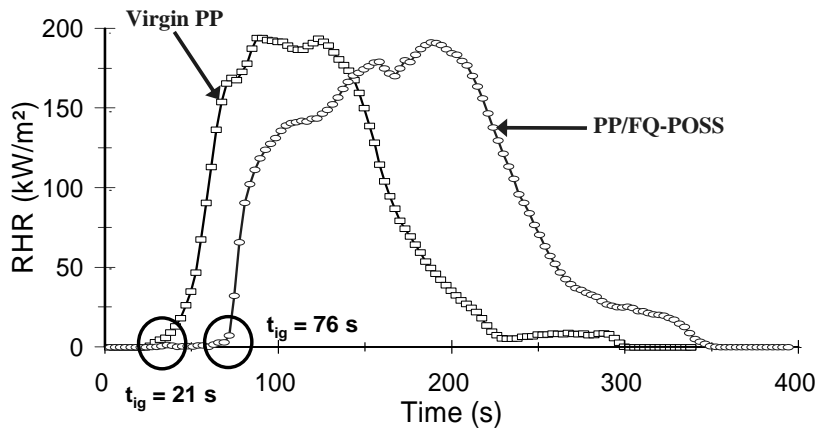


**Figure 11.** Heat Release rate curves of PP and PP/POSS-FQ knitted fabrics at 35 kW/m<sup>2</sup> [32]

release could be achieved. Another important factor for the previous inconsistent flame retardant performance of POSS could be due to difference in the dispersion of POSS in the matrix polymer. The importance of the dispersion of POSS on the flame retardant performance was described for the formation of

oxidatively stable, uniformly covered nonpermeable surface char layer<sup>xxxiii</sup>. Some previous studies demonstrated reasonably effective flame retardant performance of POSS, but a recent study with trisylanol phenyl POO in PMMA did not show any FR performance as measured in a Cone Calorimeter<sup>xxxiv</sup>. It was suggested that POSS has a potential to reduce heat release rate but one must be careful in selecting the POSS material to be evaluated.

### 10.3. Carbon based nanocomposites

There are several different types of carbon-based nanoparticles. One is graphite which is a layered material having a thickness of a nano meter, similar to clay particles, and others are based on a tubular shape having a diameter of nano meters. Since expandable graphite (an intumescent material) is discussed in Chapter 6, it is not discussed in this chapter.

#### 10.3.1. Graphite Oxide(GO)

The graphite structure consists of carbon layers in a stacked configuration. The carbon atoms are bonded covalently in a hexagonal arrangement within each layer and these layers are weakly bonded by Van der Waals forces between the layers which makes intercalation possible. Graphite does not undergo any ion exchange process but graphite oxide can add organophilic ammonium cations between the layers. Molecular dynamics simulations of the thermal degradation of a series of PP/graphite nanocomposites at 873 °K were performed as a function of the distance of the separation between the graphite sheets<sup>xxxv</sup>. The mass loss curves obtained from these simulations indicate that there is a pronounced stabilization of the polymer at a distance of 3.0 nm that results from both PP-PP and PP-graphite interactions. Below a distance of 2.5 nm, the Van der Waals repulsions between the atoms destabilize the polymer due to high density in the narrow space between the graphite sheets. However, at larger spacing between the sheets, the interactions with the polymer melt do not provide sufficient resistance to prevent the rapid escape of the degradation products from the spaces between the sheets.

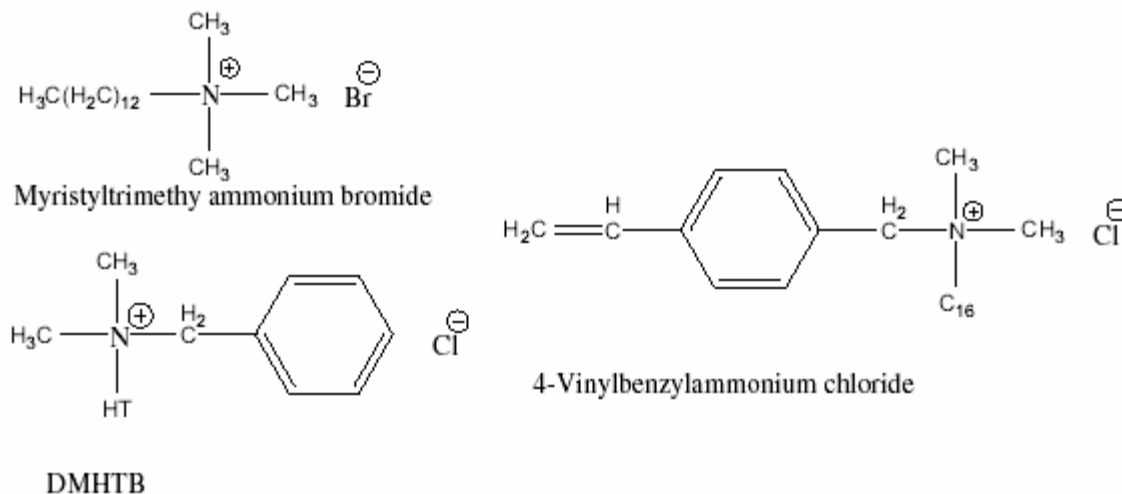


**Figure 12.** Structures of the surfactants .

Motivated by the above study, Uhl and Wilkie studied the thermal stability and flammability properties of polystyrene(PS)/graphite nanocomposites<sup>xxxvi,xxxvii</sup>. Nanocomposites with graphite concentrations of 1 %, 3 %, and 5 % were prepared by two different methods, one was by in situ polymerization in the presence of graphite oxide and the other was by melt blending. Graphite oxide was organically modified using three different surfactants (GO-C14, GO-10A, and GO-VB16), the structures of which

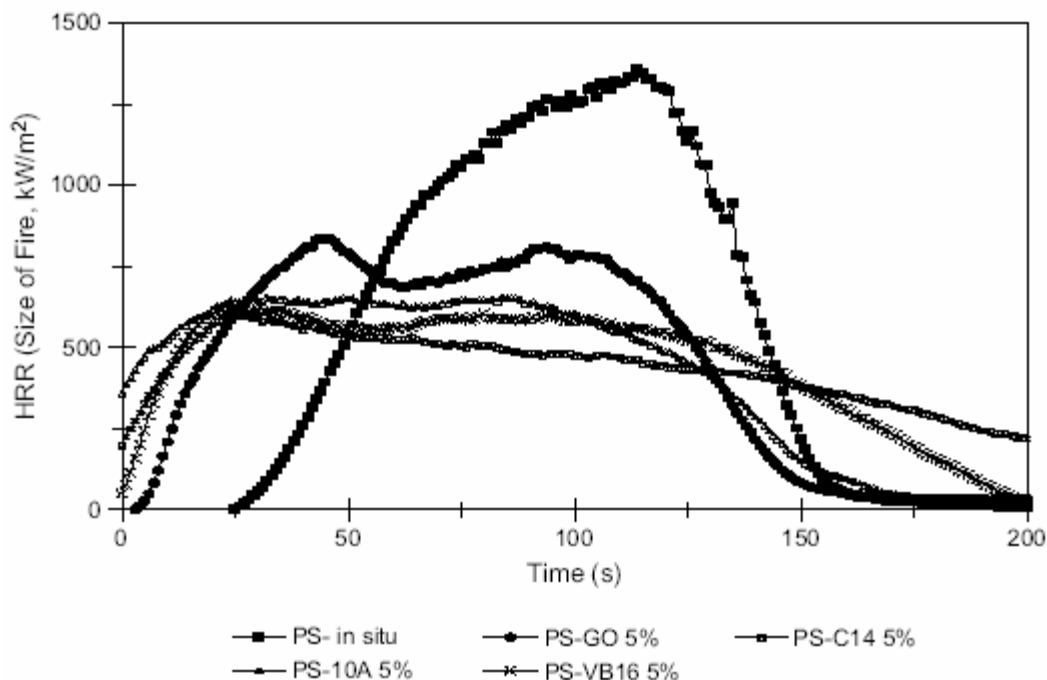


**Figure 13.** Heat release rate curves for in situ polymerized PS/GO nanocomposites at 35 kW/m<sup>2</sup> ref.[37].

are shown in Fig. 12. The XRD data showed no peaks were observed at 1 % for all three modified graphite oxides indicating their exfoliation and also for two of the three modified graphite oxides at 3% loading; at 5% loading XRD peaks were clearly seen with the d-spacing (plate-to-plate spacing) much larger than that in the GO (non-modified). Intercalation of graphite oxide plates was suggested for those samples having the XRD peaks. Similar results were observed for the melt blended samples with narrower d-spacing than those observed in the in situ polymerized samples. The reduction in peak heat release rate ranged from 27% to 54% as shown in Fig 13; the reduction increased as the loading of GO increased. It was also observed that GO as well as modified GOs gave qualitatively similar reduction (from 1% to 27%) in the peak heat release rate. The time to ignition was drastically decreased for the in situ polymerized nanocomposites compared to pristine PS. The amount of the reduction in time to ignition for the melt blended samples was less than that for the in situ polymerized nanocomposites. Since there were no significant difference in thermal stability among all samples (actually there was a slight increase in thermal stability for both in situ polymerized nanocomposites and the melt blended samples), the observed reduction in time to ignition must be due to some other reason. Some other works claimed a more significant increase in thermal stability for epoxy/graphite composites<sup>xxxviii</sup> and poly(vinyl alcohol)/graphite oxide nanocomposites<sup>xxxix</sup>. One possible reason for the reduction in time to ignition by graphite-based nanocomposites will be discussed in Section 10.4.1. in this chapter. The observed reduction in peak heat release rate for the in situ polymerized PS/graphite nanocomposites is comparable to the roughly 50% reduction for PS/clay nanocomposites with the 3 % and 5 % clay content<sup>xl</sup>.

Mixed FR performance of polymer/graphite samples was reported for phenolic/graphite and epoxy/graphite composites compared to fiberglass and aramid as a filler. Phenolic/graphite had the highest flame resistance but epoxy/graphite had the lowest flame resistance<sup>xli</sup>. Since there was no discussion on the dispersion of graphite in the polymers, it is not clear whether the samples studied were nanocomposites or microcomposites.

Very effective FR data were obtained with styrene-butyl acrylate copolymer/graphite oxide (St-BA/GO) nanocomposites<sup>xlii,xliii</sup>. The GO was prepared by oxidation of expandable graphite and the St-BA/GO nanocomposites (GO content of up to 4 % mass fraction) were synthesized by exfoliation/adsorption of monomer followed by in situ emulsion polymerization. The distribution of the GO particles were examined by XRD, TEM, and electron diffraction; exfoliated GO layers in crystalline structures were observed. The TGA data show a slight increase in thermal stability (up to 15 °C with 3 % mass fraction of GO).

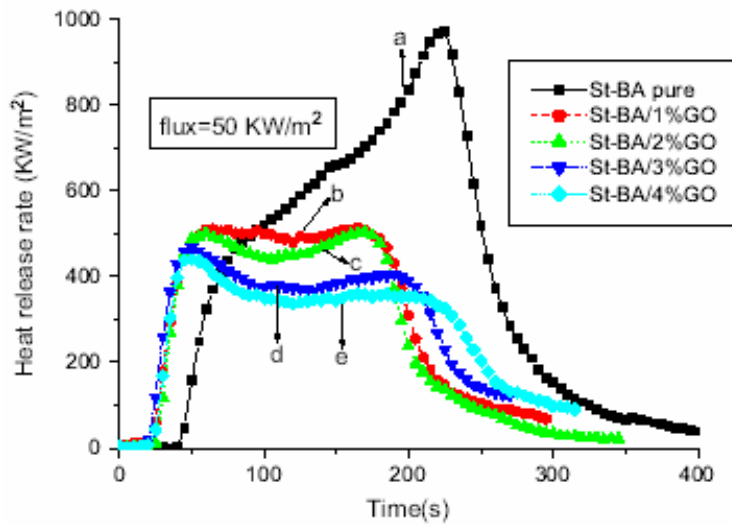


**Figure 14.** Heat release rate curves of St-BA and St-BA/GO nanocomposites<sup>xlii</sup>.

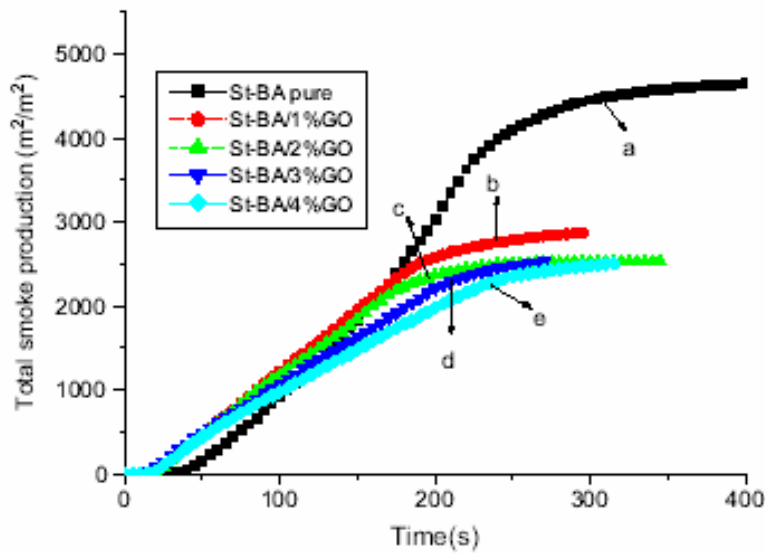


**Figure 15.** Total heat released for St-BA and St-BA nanocomposites at 50 kW/m<sup>2</sup> [ref.xlii].

Significant reduction in heat release rate by increasing content of GO has been reported; all nanocomposites reduced about 40 % of total heat released compared with that of St-BA, as shown in Figures 14 and 15. However, ignition delay times for the nanocomposites were shorter than that of the pristine sample and it was suggested that this could be caused by the thermal degradation of its organic emulsifier resulting in the formation of volatile

combustibles<sup>xliv</sup> or a catalytic effect by Lewis or Bronsted acid sites on the GO layer on the initial stages of thermal degradation of the nanocomposites compared to the pristine sample. The proposed FR mechanism of the addition of GO is that the formation of a char layer consisting of GO acts as a thermal insulator and a mass transport barrier slowing the escape of the volatile products generated from the degradation of St-BA.

### 10.3.2. Carbon Nanotubes

Since carbon nanotubes were first synthesized in 1991<sup>xlv</sup>, there have been numerous studies on the preparation of carbon nanotubes and their many different applications which take advantage of their unique physical properties such as high thermal conductivity (more than 3,000 W/mK<sup>xlvi</sup>), high electrical conductivity, etc. There are two different types of carbon nanotubes, one is single-walled (SWNT) with small diameters (1 nm ~ 2 nm) and the other is multi-walled (MWNT) with larger diameters (10 nm ~ 100 nm). The manufacturing processes of the nanotubes include direct-current arc discharge<sup>xlvii</sup>, laser ablation<sup>xlviii</sup>, thermal and plasma enhanced chemical vapor-growth deposition<sup>xlix,1</sup> and flame synthesis<sup>li</sup>. After the synthesis of these nanotubes, the tubes contain various impurities such as residual catalysts, amorphous carbons, and fullerenes. Therefore, these tubes are generally purified by various processes such as oxidation in concentrated acids<sup>lii</sup>, wet-air oxidation<sup>liii</sup> or high temperature treatment<sup>liv</sup>. Detailed studies of the effects of cleaning on the characteristics of carbon nanotubes have been reported over the last several years<sup>lv,lvi,lvii,lviii,lix</sup>. Cleaning of the tubes is critical for obtaining thermal stability and for the preparation of nanocomposites with well-dispersed tubes.

#### 10.3.2.1. SWNT

A TEM picture of SWNTs is shown in Fig. 16<sup>lx</sup>. Generally SWNTs form bundles (or ropes) due to Van der Waals forces between the tubes. The black spots in the picture are residual catalyst particles. There have been many studies on the enhancement of physical properties of polymers by polymer/SWNT nanocomposites such as electric conductivity<sup>lxi,lxii</sup> and mechanical strength<sup>lxiii,lxiv,lxv</sup>. There are also several papers reporting on the thermal stability of nanocomposites<sup>62,65,lxvi,lxvii</sup> but as far as this author is aware only two papers reporting on the flammability of polymer/SWNT nanocomposites<sup>60,lxviii</sup>. Significantly enhanced thermal stability in air was reported for the PMMA/SWNT nanocomposites<sup>lxii</sup>. However, a decrease in thermal stability in nitrogen was reported for epoxy-fluorinated SWNT nanocomposites compared to the

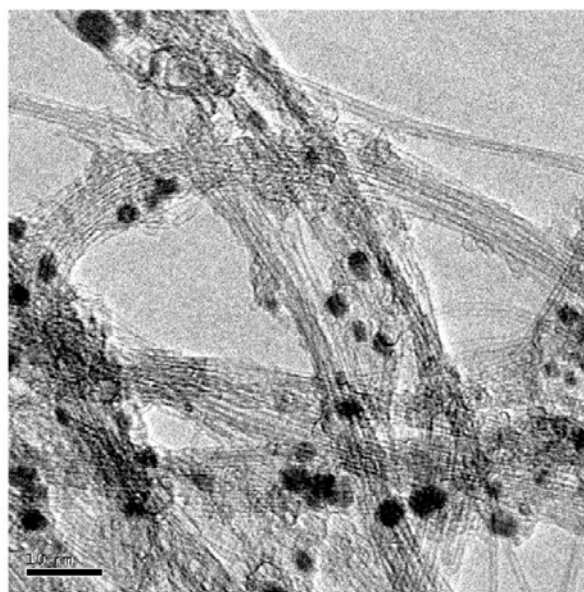


**Figure 16.** TEM image of SWNT ropes, scale bar 10 nm [60].

pristine epoxy and no significant change in thermal stability in nitrogen was observed for PMMA/SWNT nanocomposites<sup>60, 65</sup> compared to the pristine PMMA.

SWNTs for the flammability study of PMMA/SWNT nanocomposites were synthesized by the high-pressure carbon monoxide method (HiPCo)<sup>xlix</sup> and

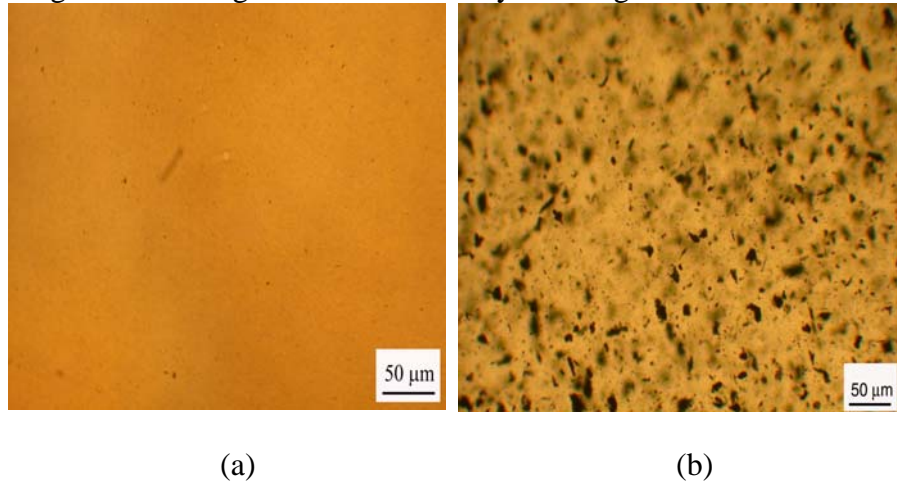


**Figure 17.** Optical microscopy images of PMMA/SWNT(0.5%) with two different dispersion of nanotubes, (a) ‘good dispersion’ and (b) ‘poor dispersion’ with numerous agglomerates [60].

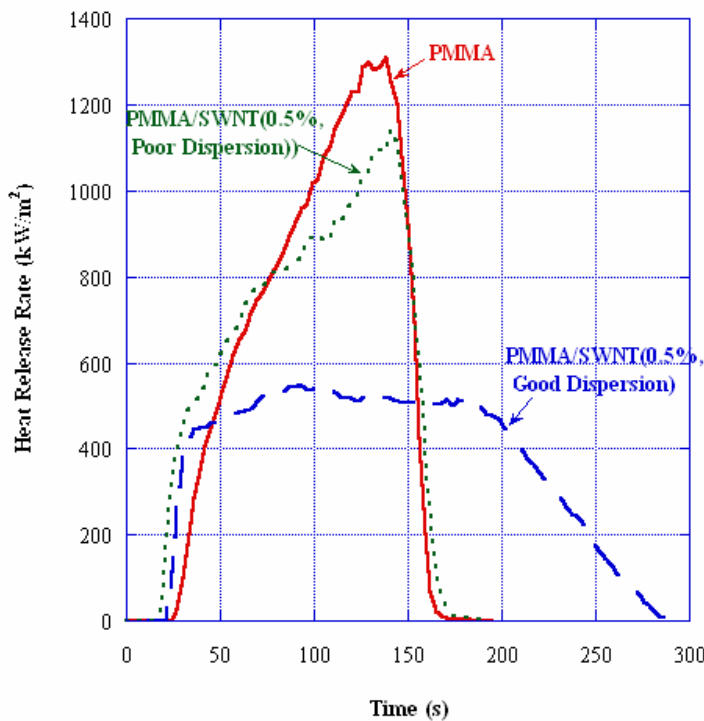


**Fig. 18.** Effect of SWNT dispersion on heat release rate of PMMA/SWNT(0.5%) nanocomposites at external radiant flux of 50 kW/m<sup>2</sup> [60].

the coagulation method was used to produce the PMMA/SWNT nanocomposites<sup>62</sup> in order to control the dispersion of the SWNTs in the nanocomposites. In the coagulation method, dimethylformamide (DMF) was chosen to dissolve the PMMA and to permit dispersion of the SWNT by bath sonication. The nanotube dispersion in the nanocomposites was controlled by changing the nanotube concentration in DMF. The effects of the nanotube dispersion in the nanocomposites on the flammability properties of the nanocomposites were investigated by comparing the flammability properties of the nanocomposite with poor nanotube dispersion to those

with good tube dispersion. The global nanotube dispersion was determined by optical microscopy; images are shown in Fig. 17. Fig. 17a indicates that the nanotubes are relatively uniformly distributed within the polymer matrix on a micrometer scale. By using a higher concentration of SWNT in the DMF suspension, the sample in Fig. 17b

shows regions of nanotube aggregation. The former sample is designated as having ‘good dispersion’ and the latter sample is designated as having ‘poor dispersion’. A TEM image of the purified original SWNT shows many nanotube bundles with a small amount of amorphous carbon and of large carbon fullerenes with many iron particles in the nanotubes from the residual catalyst; see Fig. 16.

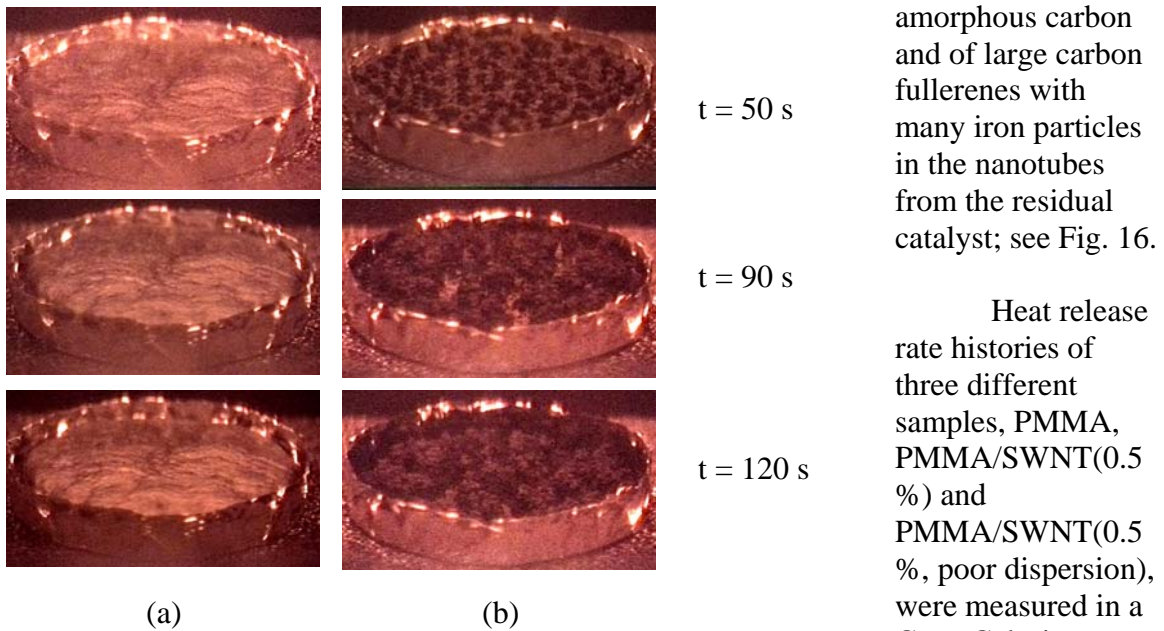


**Fig. 19.** Selected video images of PMMA/SWNT(0.5%) during gasification tests at 50 kW/m<sup>2</sup> in nitrogen; (a) with good nanotube dispersion and (b) with poor nanotube dispersion. [60].

The heat release rate of the sample with good nanotube dispersion is much lower than those of pristine PMMA and of the sample with poor nanotube dispersion. The heat release rate of the sample with poor nanotube dispersion is not appreciably reduced from that of pristine PMMA. However, the total heat release values of all samples are comparable. This indicates that the sample with relatively good nanotube dispersion burns much slower than that with poor nanotube dispersion but both samples eventually burn almost completely at an external radiant flux of 50 kW/m<sup>2</sup>.

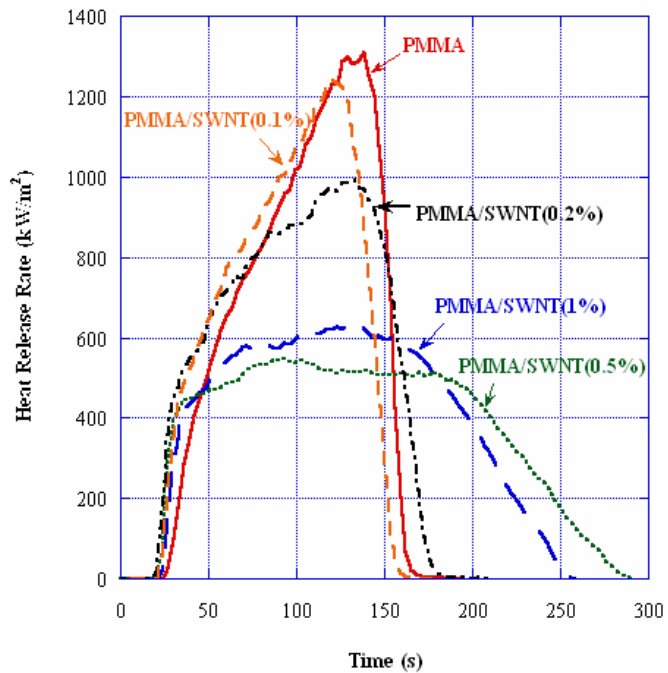


**Fig. 20.** Effects of SWNT concentration on heat release rate curve of PMMA/SWNT at 50 kW/m<sup>2</sup>.

In order to understand how the difference in dispersion of the nanotubes affects the heat release rate of the nanocomposite, the behavior of the two samples during a gasification test in nitrogen atmosphere at an external radiant flux of  $50 \text{ kW/m}^2$  was observed by taking video images. Selected pictures from the video images are shown in Fig. 19. For the sample with good nanotube dispersion, numerous small bubbles formed initially and their bursting was observed at the surface. This was shortly followed by formation of a solid-like behavior with no overt fluid motion. The final residue was a continuous dark layer covering the entire sample container. The sample with poor nanotube dispersion formed initially many small bubbles and their bursting at the surface was followed by the formation of many small black islands. Vigorous bubbling was subsequently observed between the islands. At a later time, the islands coalesced into a

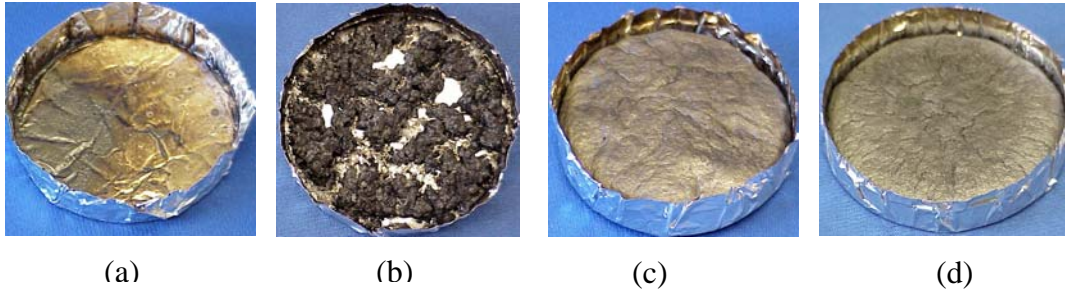


**Fig. 21.** Pictures of the residues of PMMA/SWNT after the gasification tests in a nitrogen atmosphere at  $50 \text{ kW/m}^2$ ; (a) PMMA, (b) PMMA/SWNT(0.2%), (c) PMMA/SWNT(0.5%), and (d) PMMA/SWNT(1%).

connected structure and their size gradually increased during the course of the test. The mass loss rate curves of the samples with good and poor nanotube dispersion in the gasification tests have very similar trends as the heat release rate curves shown in Fig. 18.

The effects of SWNT concentration on flammability properties of the nanocomposites were determined by measuring heat release rate curves of PMMA/SWNT nanocomposites having good dispersion of the nanotubes at levels from 0.1 % to 1 %, prepared by the coagulation method. The results are shown in Fig. 20. The addition of 0.1% mass fraction of SWNT did not significantly reduce the heat release rate of PMMA. The most reduction in heat release rate was achieved by 0.5 % mass fraction. The amount of the reduction with 0.5 % SWNT (about 60 % reduction) is much larger than that with clay (about 28 % reduction) even at 3 % loading<sup>lxix</sup>. The behavior of the nanocomposite sample with

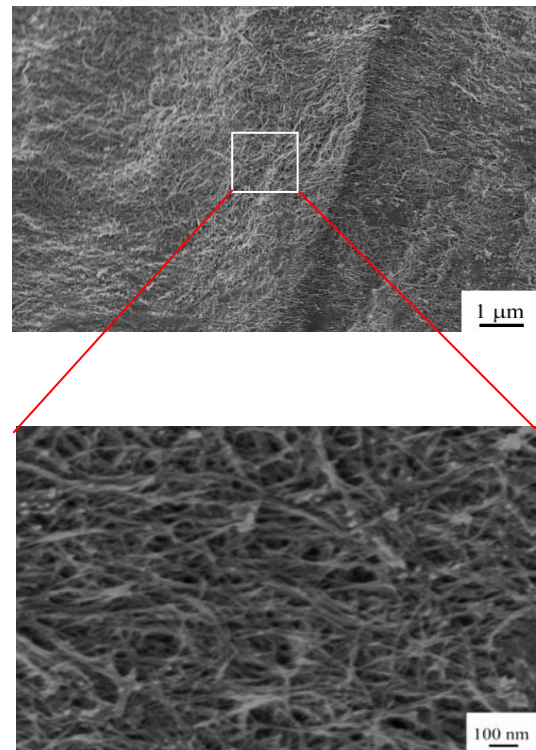


**Fig. 22.** SEM image of the residue of PMMA/SWNT(1%) collected after gasification test in nitrogen.

0.2 % SWNT during a gasification test in nitrogen atmosphere was similar to that of PMMA/SWNT(0.5%, poor dispersion) i.e., formation of many small, black discrete islands after initial numerous small bubbles and their bursting at the surface. Bubbling was observed between islands. It appeared that bubbling pushed nanotubes to the islands and the size of islands gradually became larger and eventually some of the islands were connected to each other. The connected black islands were left behind at the end of test, as shown in Fig. 21 (b). For the samples with 0.5 % and 1 %, both samples appeared to be solid-like throughout their gasification; a network structured layer covered the sample surface during the entire test period and was left behind as a residue without any major, open cracks, as shown in Fig. 21 (c) and (d). A SEM image of the residue of PMMA/SWNT(1%) shows a network structure consisting of bundled, inter-wined carbon nanotubes, as shown in Fig. 22. The residue was strong enough to be readily handled without breaking. The amount of each residue collected after the gasification test was measured. The results indicate that the addition of the nanotubes only slightly increases the amount of the residue from PMMA.

Despite of an effective FR performance by the previous study<sup>lx</sup>, another recent study shows no FR effectiveness for PE/SWNT samples with the SWNT concentration of 5 % and 10 %<sup>lxxviii</sup>. These samples were prepared by a melt blending and the dispersion of the SWNTs in the sample was not determined. Considering the difficulty of the dispersion of SWNTs in a polymer, the results could be due poor dispersion of the SWNTs.

#### 10.3.2.2. MWNT

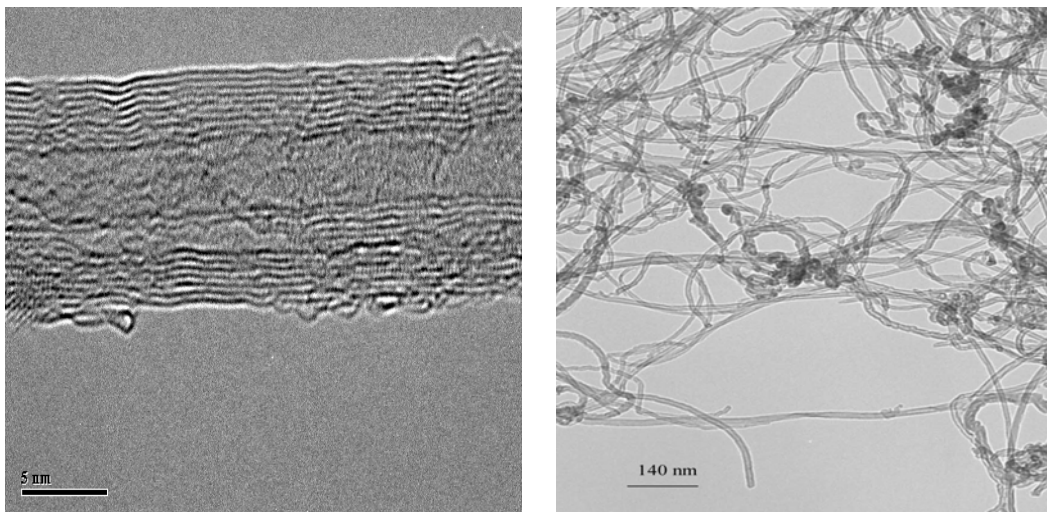


**Fig. 23.** TEM images of MWNT; left - scale bar 5 nm and right – scale bar 140 nm.

TEM images of MWNT are shown in Fig. 23. The lower magnification picture in the figure shows that the tubes appear to be flexible and have more of an appearance of noodles than rods. Many studies have been published on the enhancement of electric conductivity<sup>lxx,lxxi,lxxii,lxxiii</sup>, mechanical properties<sup>lxxiv,lxxv,lxxvi,lxxvii</sup> of polymers by

polymer/MWNT nanocomposite and papers on the flammability of polymer/MWNT nanocomposites<sup>lxxviii,lxxix,lxxx,lxxxi,lxxxii,lxxxiii</sup>. It was also reported that the oxidation of PS, PP, poly(vinylidene fluoride) (PFV) is retarded by the addition of carbon nanotubes<sup>lxxxiv</sup>.

PP/MWNT nanocomposite samples with MWNT loading of 1 %, 2 %, and 4 % by mass were melt blended in a shear mixer. The MWNTs were prepared by CVD using xylene as a carbon source and ferrocene as a catalyst at about 675 °C<sup>lxxxv</sup>. The distribution of the nanotubes in the blended samples was examined by two different methods and magnifications. A SEM picture of the MWNT dispersion in the PP/MWNT(4%) nanocomposites after solvent removal is shown in Fig. 24(a). The optical microscopy

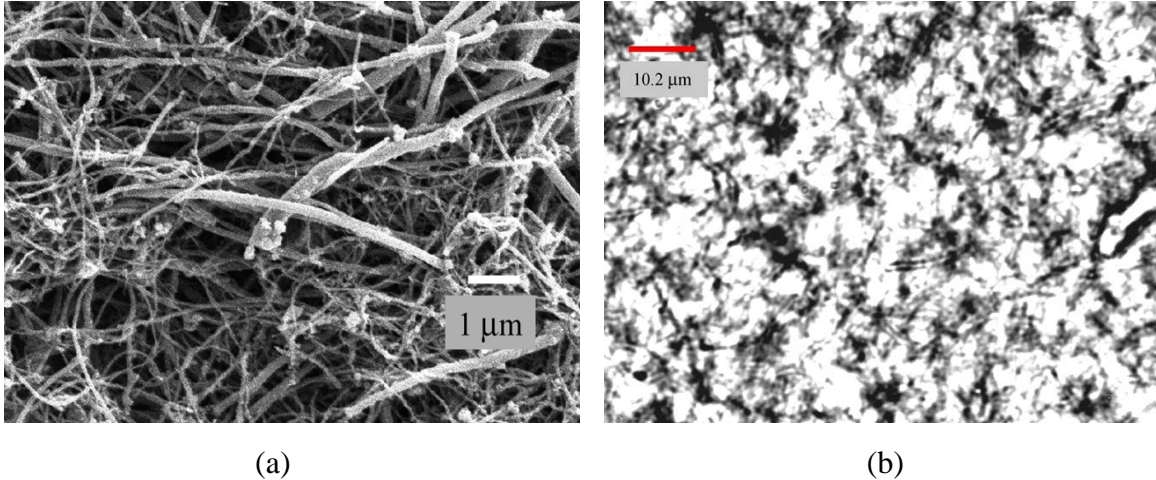


**Fig. 24.** (a) SEM picture of PP/MWNT(4%) after solvent removal of PP, (b) optical microscopy image of PP/MWNT(1%) nanocomposite in the melt<sup>lxxx</sup>.

image of PMMA/MWNT(1%) is shown in Fig. 24(b), which shows globally well-

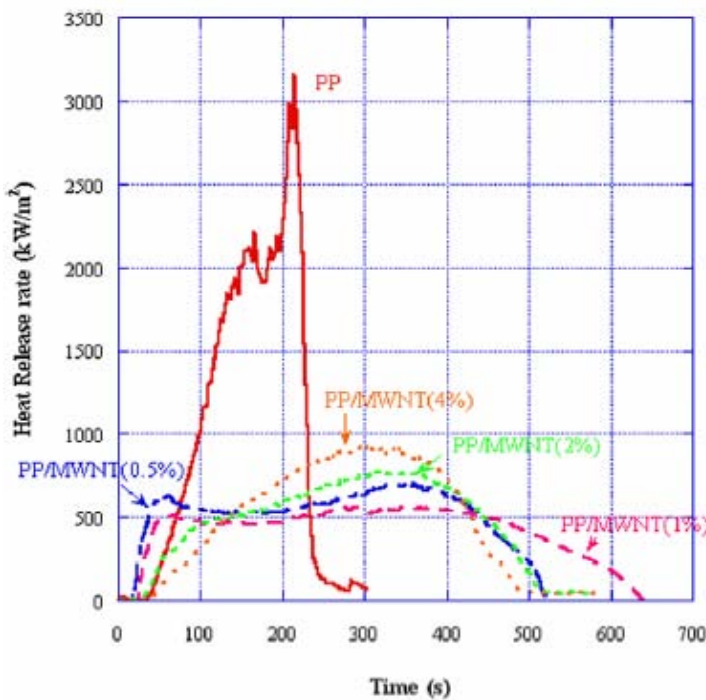


**Fig. 25.** Effects of concentration of MWNT in PP on heat release rate of PP/MWNT nanocomposites at 50 kW/m<sup>2</sup>.

dispersed nanotubes in PP at large scales and a wide range of diameters and lengths of nanotubes as shown in Fig. 24(a). The residual catalyst particles (iron) are encapsulated at various locations inside the nanotubes, and also at the nanotube tips, as shown in Fig. 24(a). Nanoparticulate iron is pyrophoric, and could reduce the thermal oxidative stability of MWNT, as well as possibly acting as a catalyst during the oxidative degradation of the PP/MWNT nanocomposites. Since the heat release rate curves of the PP/graphitized MWNT nanocomposites (with

iron particles removed by high temperature annealing<sup>liv,lxxxvi</sup>) were similar to those of PP/MWNT (with iron particles), it was concluded that residual iron particles did not have significant effects on heat release rate of PP/MWNT nanocomposites during flaming combustion<sup>lxxx</sup> (little oxygen reaches the sample surface because oxygen is consumed by gas phase oxidation reactions). However, strong glowing combustion (smoldering) of the sample residues (PP/MWNT with iron) was observed after flaming combustion was over (oxygen could then reach the residue surface) during the cone calorimeter tests. (Smoldering was not observed with the residue of PP/graphitized MWNT under the same conditions).

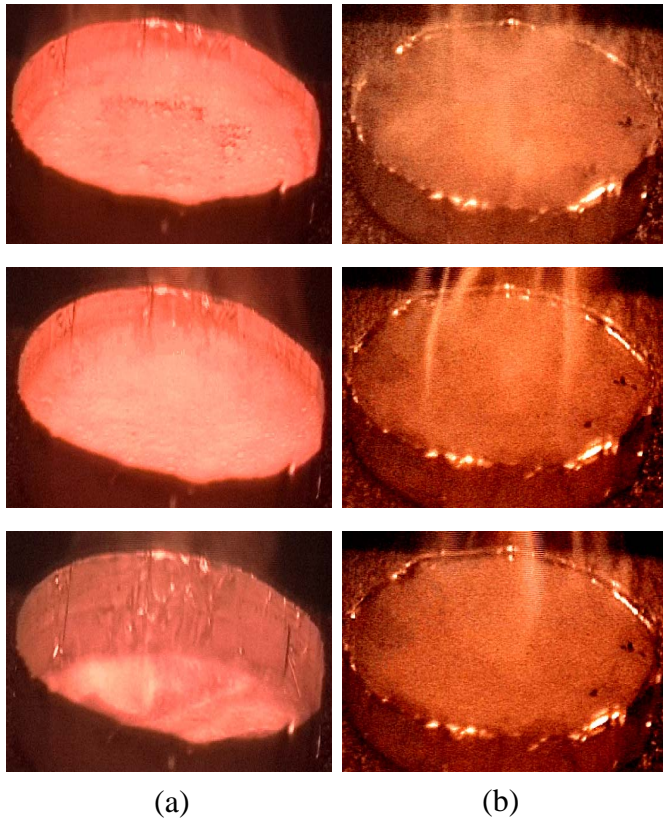


**Fig.26.** Sample behavior in the gasification test at  $50 \text{ kW/m}^2$  in nitrogen, (a) PP, and (b) PP/MWNT(1%).

above 1 % appears to be due to an increase in thermal conductivity of the nanocomposite<sup>lxxx</sup>.

The physical behavior

The effects of the concentration of MWNTs in PP on the heat release rate curves of the nanocomposites are shown in Fig. 25. The results show two distinct characteristics brought on by the addition of MWNTs; first, there is a shortened ignition delay time with the PP/MWNT(0.5%) followed by an increase in ignition delay time with an increase in the concentration of MWNT; second, there is a gradual increase in peak heat release rate above about 1 % by mass of MWNT. A similar trend was also observed for the PMMA/SWNT nanocomposites (less obvious for PMMA/SWNT due to lower concentration of SWNT, as shown in Fig. 20.). The lowest heat release rate curve for PP/MWNT is achieved with about 1 % by mass of MWNT compared to about 0.5 % by mass of SWNT. The increase in peak heat release rate with concentration of MWNT



**Fig. 27.** The cross section of the residue of the PP/MWNT (1%).

of the PP/MWNT nanocomposites was significantly different from that of PP during the gasification test in a nitrogen atmosphere, as shown in Fig. 26. The PP sample behaved

like a liquid with a fine froth top layer generated by the bursting of numerous small bubbles at the sample surface. No char was left at the end of the test. However, all the PP/MWNT samples behaved like a solid without any visible melting except at the very beginning of the test and the shape of the sample or size of the sample did not change significantly during the test. The residue of each sample was collected. No cracks were observed in any residue of the PP/MWNT nanocomposites. The network-structured layer of the PP/MWNT samples covered the entire sample surface and extended to the bottom of the residue as shown in Fig. 27. The residue consisted of tangled and roped

carbon nanotubes. The tubes in the residue were more intertwined and larger than those in the original sample. The network layer was porous but had physical integrity and did not break when lightly picked by one's fingers. The structure of the residue of the PP/MWNT was very similar to that of the residue of the PMMA/SWNT nanocomposites. The mass of the network-structured layer was very close to the initial mass of carbon nanotubes in the original nanocomposites. This indicates that the network structured layer did not enhance char formation from PP. The importance of the formation of a network structure and of melt viscosity on flame retardant effectiveness were reported for the PA6/MWNT nanocomposites prepared from a commercially available master batch sample<sup>lxxxii</sup>.

Since carbon black (CB) has been used as a filler to enhance the physical properties of rubbers, the observed flame retardant performance of MWNT and of SWNT could possibly be due to the addition of carbon alone, independent of its size or/and shape. In order to test this hypothesis, two different carbon blacks having different surface areas were compounded with PP at the same level of carbon concentration in PP as those of the

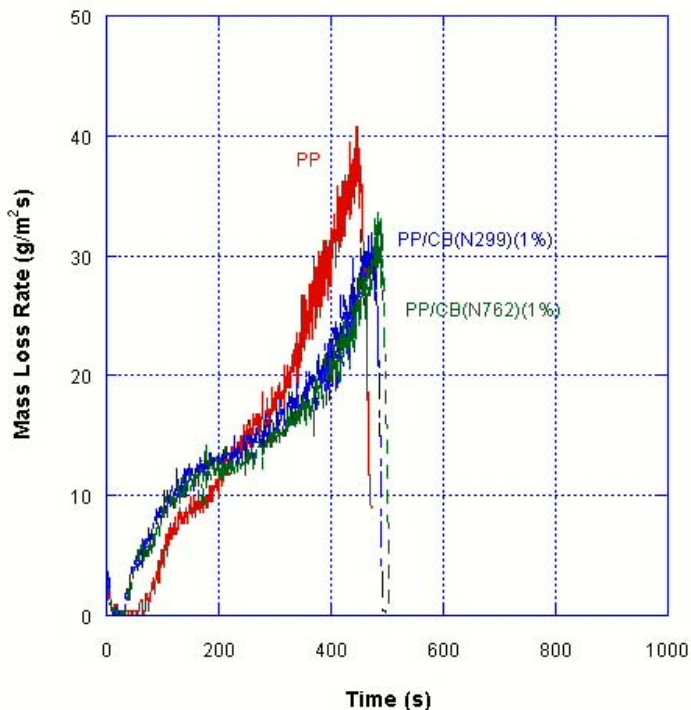


**Fig. 28.** The effects of addition of carbon black on mass loss rate of PP at 50 kW/m<sup>2</sup> in nitrogen.



**Fig. 29.** The residue of PP/CB(N299)(1%) after gasification test at 50kW/m<sup>2</sup> in nitrogen.

PP/MWNT nanocomposites. The surface area of the carbon black designated as N299 was 102 m<sup>2</sup>/g and that designated as N762 was 27.3 m<sup>2</sup>/g. The mass loss rate curves of the PP/CB measured at 50 kW/m<sup>2</sup> in a nitrogen atmosphere were compared with that of PP in Fig. 28. The addition of either carbon black increased the initial mass loss rate compared to that of PP. This trend is similar to the addition of MWNTs to PP as shown in Fig. 25 (the trend of the heat release rate was very similar to the mass loss rate<sup>lxxviii</sup>), but the reduction in the peak mass loss rate was much less than that for PP/MWNT(1%).

During the gasification test in a nitrogen atmosphere with the PP/CB samples, the sample behaved like a viscous liquid with the formation of large bubbles, which frequently burst at the sample surface. The residue of the PP/MWNT(1%) was a smooth layer filling the sample container without any cracks (almost the same size as the original sample). However, both residues of the PP/CB samples consisted of dispersed, aggregated granular particles left at the bottom of the sample container, as shown in Fig.

Sample	MWNT(purified) (% by mass)	MWNT(crude) (% by mass)	Organo-clay (% by mass)	Ignition time (s)	PHRR (kW/m <sup>2</sup> )
1				84	580
2	2.4			85	520
3	4.8			83	405
4			2.4	70	530
5			4.8	67	470
6	2.5		2.5	71	370
7		4.8		83	403

Table 2. Properties of samples with MWNT at 35 kW/m<sup>2</sup>, ref. [79].

29. These results indicate that the flame retardant effectiveness of the PP/MWNT (and also PMMA/SWNT) nanocomposites is mainly due to extended shape of the carbon nanotubes.

There were three studies<sup>lxxviii,lxxix,lxxxi</sup> to investigate the synergistic flame retardant performance of combined organoclay–MWNT/EVA

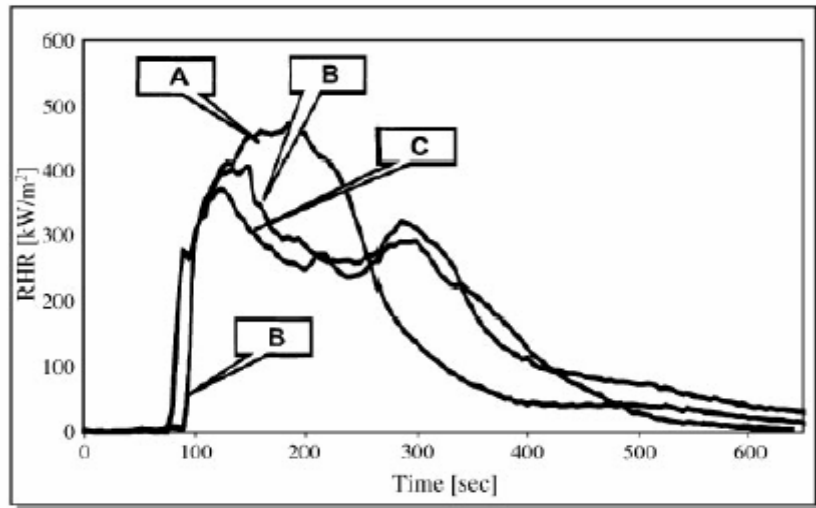


**Fig. 30.** Heat release rate curves of EVA/clay(4,8%) [A]. EVA/MWNT(4.8%) [B], EVA/clay(2.4%)/MWNT(2.4%) [C] at external flux of 35 kW/m<sup>2</sup>. ref. [79]

nanocomposites prepared by melt blending. The MWNTs were prepared by catalytic decomposition of acetylene with cobalt and iron as catalysts supported on alumina. The synthesized MWNTs were directly used as a crude sample and purified MWNTs were also made by boiling concentrated sodium hydroxide water solution and removing mainly alumina in concentrated hydrochloric acid water solution. For the same filler content, either the purified or the crude MWNTs act as better flame retardant than organo-clay, with a larger reduction in the peak heat release rate and no significant influence on the time of ignition, as shown in Table 2. The crude MWNT was as effective in the reduction of the peak heat release rate as the purified MWNT. The peak heat release rate of the ternary nanocomposites, filled with 2.4 % of an organo-clay and 2.4 % of purified MWNTs was slightly less than that of the nanocomposites with either the purified MWNT(4.8%) or the crude MWNT(4.8%). A comparison of the heat release rate curves for EVA/clay(4.8%), EVA/MWNT(4.8%), and VA/clay(2.4%)/MWNT(2.4%) is shown in Fig. 30. It was speculated that the formation of graphitic carbon in char is enhanced when both carbon nanotubes and clay particles are

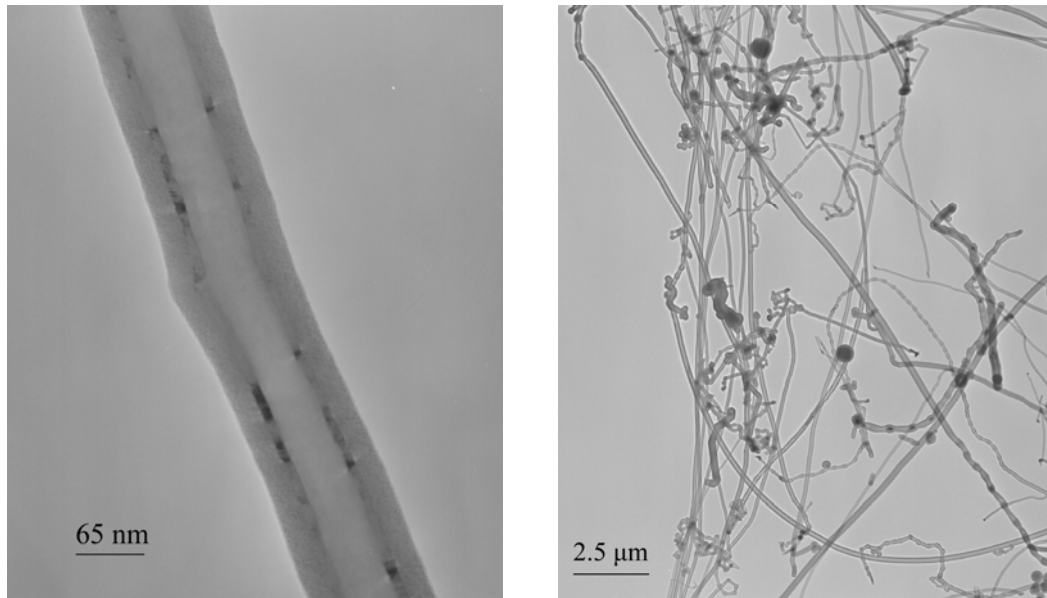


**Fig. 31.** TEM images of CNF at two different magnifications.

applied and this may contribute directly to the reduction of the peak heat release rate. The nanotubes also tend to reduce surface cracks of chars, as demonstrated above, leading to an increase of barrier resistance to the evolution of flammable volatiles and oxygen ingress to the condensed phase<sup>lxxxiii</sup>.

### 10.3.2.3 Carbon Nanofibers

Another type of nanoscale carbon-based particles is vapor grown carbon nanofibers (VGCFs) (or carbon nanofibers (CNF)). These diameters are in the range of 60-200 nm and lengths are tens to hundreds of microns, which are much larger than SWNT and MWNT. They are commercially readily available at the level of kg and furthermore with different levels of purified samples. TEM images of these nanofibers

are shown in Fig. 31. Many polymer nanocomposites were prepared with CNF by melt blending for rheological studies<sup>lxxxvii,lxxxviii,lxxxix</sup>, reinforcement of physical properties<sup>xc</sup>, and enhancement of electric conductivity<sup>lxxxvii,xc</sup>. However, published studies on the flammability properties of polymer/CNF nanocomposites are rare. Since the enhancement of the physical properties by the polymer/CNF has been demonstrated, it was expected that flame retardant performance by the addition of CNF could be as effective as that of SWNT and MWNT probably with a higher loading level of CNF than SWNT or MWNT. Our recent results of PMMA/CNF nanocomposites and PP/CNF are discussed in this chapter.

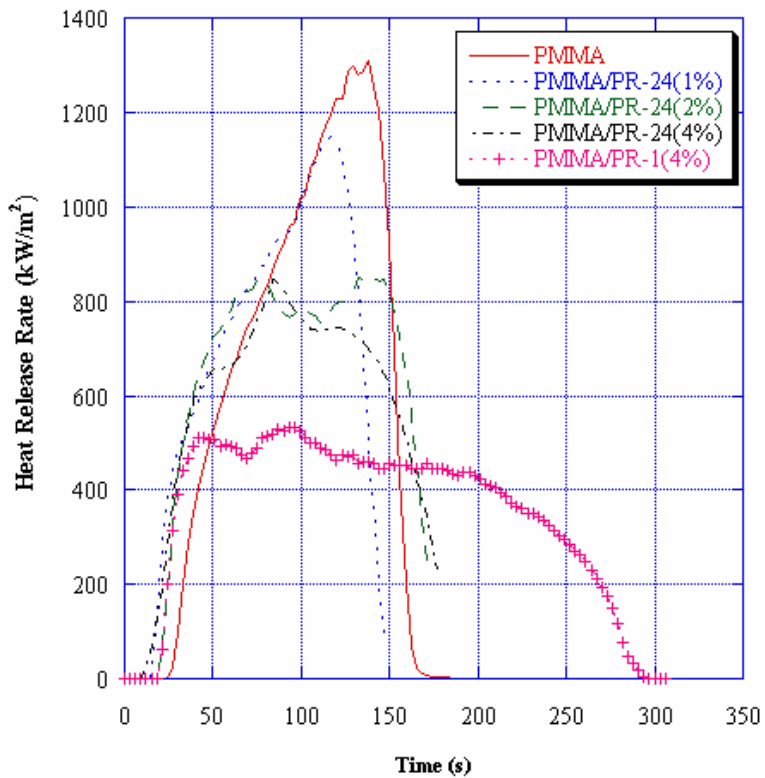


**Fig. 32.** Mass loss rate curves of PMMA/CNF nanocomposites at 50 kW/m<sup>2</sup> in a nitrogen

The PMMA/CNF nanocomposites were prepared by the coagulation method using DMF as a solvent. The method was the same as that used for the PMMA/SWNT discussed in the Section of 10.3.2.1. Two different CNFs were used; one was PR-1 and the other was PR-24LHT. The TEM images of PR-24LHT are shown in Fig. 31. According to the manufacture of the CNFs (Applied Science Incorporated), PR-1 is as

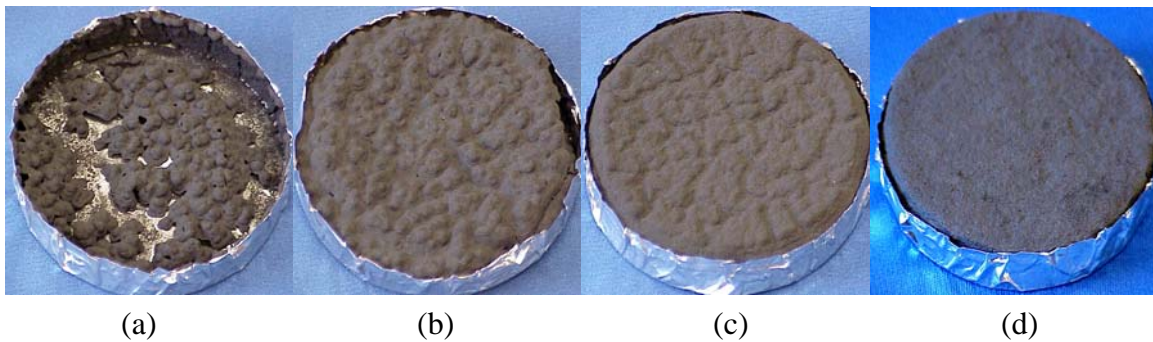


**Fig. 33.** Pictures of the residues after the gasification tests at 50 kW/m<sup>2</sup> in nitrogen; (a) with PR-24(1%), (b) with PR-24(2%), (c) with PR-24(4%), (d) with PR-1(4%).

grown materials with diameters of 100-200 nm containing amorphous carbons, and PR-24LHT is graphitized fiber by a heat treatment with diameters of 60-150 nm without amorphous carbons. The flame retardant effectiveness of these nanofibers was investigated by measuring heat release rates of PMMA/CNF nanocomposites at 50 kW/m<sup>2</sup>. The results are shown in Fig. 32. An increase in loading of the PR-24 reduced the heat release rate of the nanocomposites up to 4 % by mass (although the reduction in heat release from 2 % mass fraction to 4 % mass fraction becomes less than that from 1 % mass fraction to 2 % mass fraction). The PMMA/PR-24(1%) nanocomposite showed a muddy liquid-like behavior followed by the formation of many small black islands during the test. The islands gradually coalesced with the progress of the test and a thin connected mass of black islands was left on the bottom of the sample container at the end of the test, as shown in Fig. 33 (a). Similar behavior was observed for the PMMA/PR-24(2%) nanocomposite but it appeared to be more viscous, with the formation of large islands followed by a rugged, solid-like appearance accompanied with large bubbles and their bursting. A rugged layer without any cracks was left at the end of test, as shown in Fig. 33 (b). The PMMA/PR-24(4%) nanocomposite appeared to be solid-like, accompanied with several large bubbles and their bursting followed by small swelling. A slightly rugged surfaced solid layer without any cracks was left at the end of the test, as shown in Fig. 33 (c). On the other hand, the PMMA/PR-1(4%)

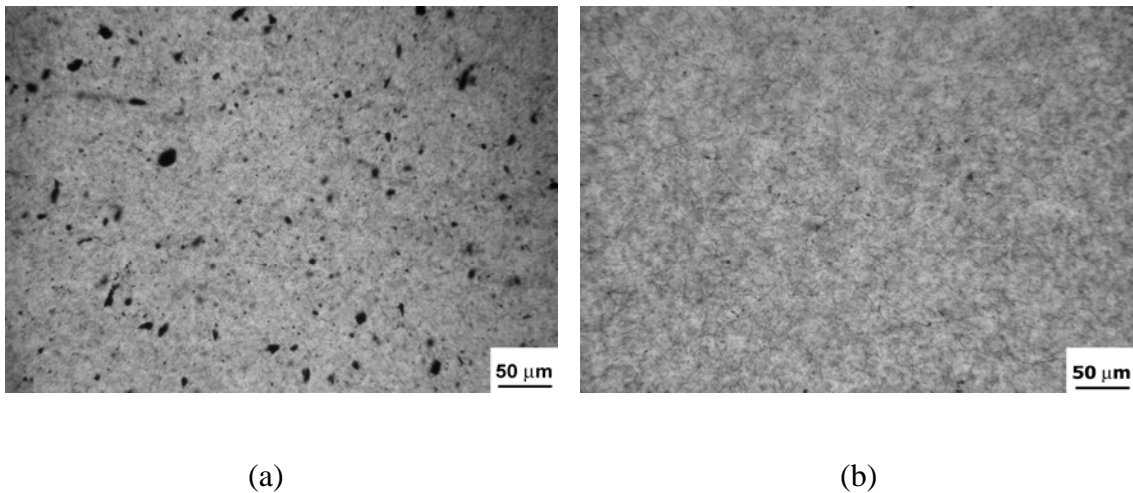


**Fig. 34.** Optical microscopy images; (a) PMMA/PR-24(2%), (b) PMMA/PR-1(2%).

nanocomposite remained solid-like with a smooth surface without forming any significant amount of bubbles over the entire duration of the test. The shape of the residue was nearly the same as that of the original sample, as shown in Fig. 33 (d).

The heat release rate of the PMMA/PR-1(4%) is much less than that of the PMMA/PR-1, as shown in Fig. 32. Considering the high purity nature of the PR-24 (without amorphous carbons) compared to the PR-1 which contains amorphous carbons, it is surprising to observe better flame retardant effectiveness of the PR-1 than the PR-24 in PMMA. The heat treatment for PR-24 could remove any defects and –COOH and –OH from the fibers if they existed on the nanofibers<sup>lviii</sup>. If so, the PR-24 could be less polar than the PR-1. Then, the PR-24 in polar PMMA may not be dispersed as well as the PR-

1dispersed in PMMA. Optical microscopy image of the PMMA/PR-24 (2%) shows well-dispersed nanofibers with some agglomerated nanofibers, as seen in Fig. 34 (a). However, the image of the PMMA/PR-1(2%) shows well-dispersed nanofibers without any agglomerates, as seen in Fig. 34 (b). Another possibility to explain the difference in flame retardant effectiveness of the two nanofibers is the difference in the size of the two nanofibers. The images indicate that the PR-24 might be much smaller diameter and much shorter length fibers than the PR-1. Therefore, the observed better flame retardant performance of the PR-1 in PMMA as compared to that of the PR-24 could be due to better dispersion of the PR-1 in PMMA and also due to the difference in the size of the nanofibers.

Another example for the excellent flame retardant performance by PR-1 could be seen with PP. A PP/PR-1(4%) nanocomposite was prepared by melt mixing. The mass loss rate of the PP/PR-1(4%) nanocomposite was measured at 50 kW/m<sup>2</sup> in a nitrogen atmosphere. The nanocomposite appeared to be solid-like with a smooth surface without any cracks during the most of the test period except for an initial, brief period of formation of numerous small bubbles and their bursting at the surface. The size of the residue collected at the end of the test was nearly the same as that of the original sample. The measured mass loss rate curve is compared with those of

PP/MWNT nanocomposites described in the previous section and the comparison is shown in Fig. 35. The mass loss rate of the PP/PR-1(4%) is slightly less than those of PP/MWNT(0.5%) and PP/MWNT(1%). Thus, the heat release rate curve (Fig. 32) and the mass loss rate curve (Fig. 35) show effective flame retardant performance by an *appropriate CNF* as long as CNFs are *well dispersed without any agglomerates*. The flame retardant effectiveness of such CNF appears to be as good as those of SWNT and of MWNT except CNF requires higher loading than those of SWNT and of MWNT (roughly 4 to 8 times by mass). This indicates that the use of CNF is much more economical (at least 1/1000) than SWNT to obtain a similar FR performance.

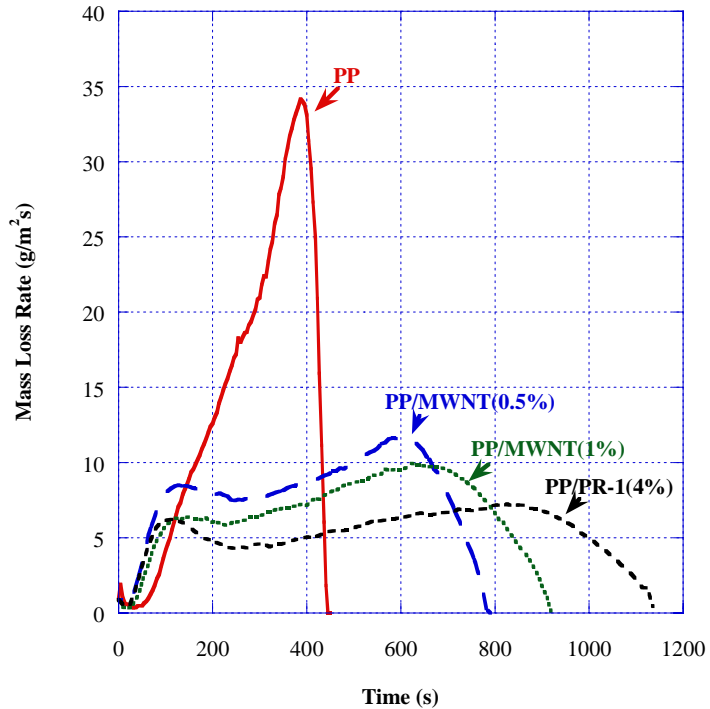


**Fig. 35** Comparison of mass loss rate curves for PP, PP/MWNTs, and PP/PR-1 nanocomposites at 50 kW/m<sup>2</sup> in nitrogen.

#### 10.4. Discussion

### 10.4.1. FR Mechanism

It appears that the FR mechanism for the nanoparticles discussed in this chapter is the formation of a continuous protective layer consisting of a *network* of the nanoparticles and the layer appears to act as a heat shield. All data shown in this chapter show that the peak heat release rate could be reduced significantly using nanoscale tube shape particles as long as these particles are well dispersed in a polymer matrix as a filler. Recent study indicates the direct relationship between viscoelastic measurement (storage modulus) and reduction in heat release rate<sup>xcii</sup>. This suggests that we might be able to screen for promising flame retarded polymer nanocomposites by performing viscoelastic measurements on the initially fabricated samples. Although heat release rate is the key parameter for fire growth<sup>xciii</sup>, total heat releases of these nanocomposites are not significantly reduced except in the results shown in Figure 15. This means that burning rate or flame size of these nanocomposites would be low or small but they would burn slowly for a longer time and eventually most of the matrix would be thermally decomposed to provide flammable gaseous products. Furthermore, ignition delay times of the nanocomposites based on carbons measured in a Cone Calorimeter tend to be shorter than those of polymer matrixes despite little difference in thermal stability between the nanocomposite and the polymer matrix (In some cases the thermal stability of the nanocomposite is slightly higher than that of the matrix.). This shorter ignition delay time for the carbon based nanocomposite can be explained with the case of PP/MWNT as an example.

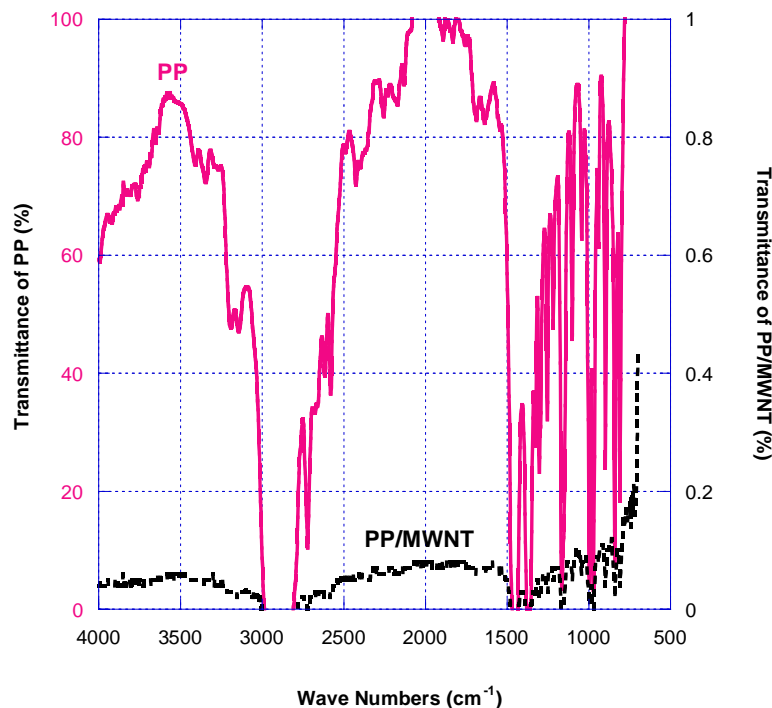


**Figure 36.** Comparison of transmission spectra between PP and PP/MWNT (1%) through 200  $\mu\text{m}$  thick film.

In a Cone Calorimeter test, ignition is initiated by thermal radiation from an electrically heated element at a temperature of about 750 °C. It is expected that the emission spectra from the heater element is that of a gray body covering from the visible to the far infrared but peaking at about 2.7  $\mu\text{m}$ . Therefore, there might be significant difference in absorption characteristics of the external emission by PP/MWNT as compared to that of PP. The measured infrared transmission spectra of the PP sample was

compared with that of the PP/MWNT(1 %) nanocomposite; see Figure 36<sup>lxxx</sup>. The PP shows many absorption bands based on various vibrational modes but there is substantial transmission between these bands. This indicates that the external thermal radiant flux of 50 kW/m<sup>2</sup> is absorbed by the PP sample over some depth. On the other hand, the PP/MWNT nanocomposite shows no significant transmission bands and all of the 50 kW/m<sup>2</sup> flux is absorbed very near the sample surface, within a distance of 200 μm. Therefore, a narrow layer in the vicinity of the PP/MWNT sample surface is rapidly heated and its temperature becomes high enough to initiate thermal degradation of PP and to generate evolved degradation products of monomer dimer, trimer, and oligomers to initiate ignition. On the other hand, the PP sample is heated over a greater depth and it thereby takes a longer time to heat the sample to initiate degradation. Thus, the ignition delay time of PP/MWNT, in particular at low concentration of MWNT, tends to be shorter than that of PP. This explanation applies to any polymer –carbon based nanocomposites because of absorption of incident radiant energy by *discrete* bands based on the polymer structure.

It is also observed that the heat release rates of the nanocomposites during the *early stage* of burning from the onset of ignition (until the establishment of a protective layer) are not significantly different from those of the matrix. (A similar trend was observed with the polymer nanocomposites with nanoclay particles as a filler. However, it appears that the FR effectiveness of carbon nanotubes determined by the reduction in heat release rate is better than those with nanoclay particles per unit mass base<sup>xciv</sup>.) This might be the reason why these particles might not be considered as an all-around fire retardant since they fail to pass the UL-94 type small ignition test<sup>lxxxii</sup>. However, a performance-based fire safety approach instead of a single go/no - go type test is becoming increasingly considered in many countries looking at material flammability characteristics of ignition, heat release rate, CO production rate, etc as inputs. Therefore, these nanocomposites can help to reduce heat release and slow down fire growth but further improvement in their FR effectiveness is needed for a wider application of these nanoparticles. An improvement in FR effectiveness could be achieved by significantly enhancing the formation of char (more carbons in the polymer matrix remain in the condensed phase) or by a combined use with conventional FR additives.

#### 10.4.2. Morphology

The dispersion of nanoparticles in polymer nanocomposites has a significant effect on their flammability properties as shown in Figure 18. Many studies used TEM and/or SEM images to demonstrate the quality of the dispersion of the nanoparticles in the nanocomposites. However, these images tend to observe an extremely small area of the samples, on the order of 100 nm by 100 nm. These images show the shape, the size, and interaction of the nanoparticles but they do not show the overall dispersion of the nanoparticles in the samples. Furthermore, there are two aspects which affect the effectiveness of TEM analysis. First is the sample preparation. The sample prepared is extreme small as described above and the observed area may not represent overall dispersion characteristics. The people preparing the sample may select the "good" region to cut. The second is the fact that we all prone to look at what we want. So from TEM pictures we always see what the observer want.

It appears looking at that the dispersion on a  $\mu\text{m}$  scale (for example, in the order of 100

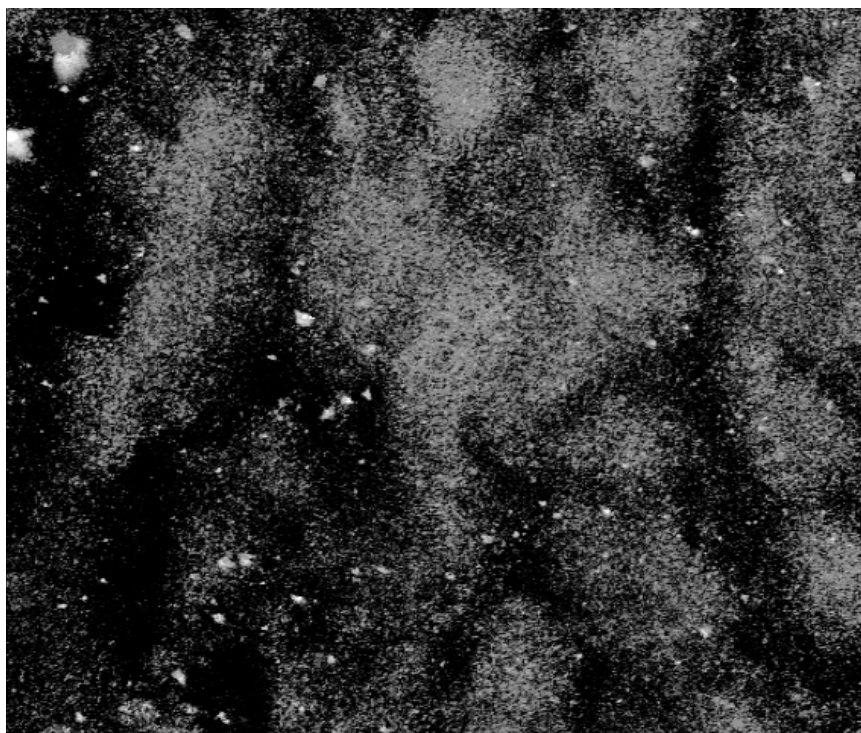


**Fig. 37.** A confocal microscopy image of PA6/Clay(2%). The image dimension is about  $100\ \mu\text{m}$  by  $100\ \mu\text{m}$  with the thickness of  $30\ \mu\text{m}$ .

$\mu\text{m}$  by  $100\ \mu\text{m}$ ) to observe the formation of agglomerates of the nanoparticles tends to be more appropriate for the FR effectiveness. Such measurements could be made with confocal microscopy or optical microscopy at various locations in the sample. An image by confocal microscopy of the polyamide 6 nanocomposite with 2 % clay particles is shown in Figure 37 as an example. This image was constructed from the 300 images

taken from the surface of a  $200\ \mu\text{m}$  thick sheet looking inside the sample in  $0.1\ \mu\text{m}$  steps. This image shows a large scale distribution pattern of clay particles including several agglomerates, which cannot be determined by TEM or SEM. If an image on a scale of  $100\ \text{nm}$  by  $100\ \text{nm}$  were taken, the distribution of the clay particles would be mostly judged to be qualitatively reasonable. Ideally, a statistical analysis should be conducted on these images to quantify the dispersion of the nanoparticles instead of the qualitative image observation which has been commonly used.

#### 10.4.3. Thermal Gravimetric Analysis, TGA

The measurement of the thermal stability of the polymer nanocomposites by TGA is useful for understanding their FR mechanism. Since oxygen is mostly consumed by the gas phase oxidation reactions during flaming burning of the nanocomposites, oxygen hardly reaches the thermally degrading sample surface beneath the evolved gaseous products. Therefore, it is recommended that TGA be conducted in an inert atmosphere instead of air. The results of TGA conducted in air would apply to smoldering combustion instead of flaming combustion. Heating rates in TGA are generally at least one to three orders magnitude slower than heating rates in fire conditions. The composition of the degradation products can be significantly modified by the heating rate of the sample. Furthermore, a TGA sample is generally very small (few mg). Then,

secondary reactions of degradation products passing through the sample (real material is thicker than that for TGA) are not encountered. Therefore, one needs to be cautious in extrapolating the TGA results, in particular, degradation products, to fire conditions.

### **Acknowledgement**

The author would like to thank Ms. Severine Bellayer at NIST, Mr. Fangming Du at the University of Pennsylvania, Ms. Ying Yang at University of Kentucky, and Dr. Kazuya Yamamoto and Dr. Kathryn Butler at NIST for their help by taking various TEM images, the confocal microscopy image, and the image analysis shown in this chapter. The author also thanks Dr. Tom Ohlemiller at NIST for his careful review of this chapter. The author acknowledges funding from NIST with the grant number 5D1022.

## References

- <sup>i</sup> Kojima Y, Usuki A, Kawasumi M, Okada A, Fukushima Y, Kurauchi T, Kamigaito O, *J Mater Res* 1993;8:1185-9.
- <sup>ii</sup> Novak BM, *Adv Mater* 1993;5:422-33.
- <sup>iii</sup> Giannelis E, *Adv Mater* 1996;8:29-35.
- <sup>iv</sup> Alexandre M, Dubois P, *Mater Sci Eng* 2000;R28, 1.
- <sup>v</sup> Landry C.J.T, Coltrain B.K, Landry M.R, Fitzgerald J. J, Long V.K. *Macromolecules* 1993; 26:3702-12.
- <sup>vi</sup> Hajji P, David L, Gerard J.F, Pascault J.P, Vigier G. J, *Poly. Sci. Part B* 1999; 37:3172-87.
- <sup>vii</sup> Ou Y, Yang F, Yu Z-Z, *J.Poly. Sci., Part B*, 1998;36:789-95.
- <sup>viii</sup> Reynaud E, Jouen T, Gauthier C, Vigier G, Varlet J, *Polymer*, 2001; 42:8759-68.
- <sup>ix</sup> Hsiue G-H, Kuo W-J, Huang Y-P, Jeng R-J, *Polymer* 2000; 41:2813-25.
- <sup>x</sup> Liu YL, Hsu CY, Wei WL, Jeng RJ, *Polymer* 2003; 44: 5159-67.
- <sup>xi</sup> Tsagaropoulos G, Eisenberg A, *Macromolecules* 1995; 28: 396-8.
- <sup>xii</sup> Kashiwagi T, Gilman J.W, Butler K.M, Harris R.H, Shields J.R, *Fire Mater.*, 2000; 24: 277-89.
- <sup>xiii</sup> Kashiwagi T, Shields J.R, Harris R.H, Davis R.D, *J. Appl. Polym. Sci.* 2003; 87: 1541-53.
- <sup>xiv</sup> Yang F, Nelson GL, *J. Appl. Polym. Sci.* 2004; 91:3844-50.
- <sup>xv</sup> Kashiwagi T, Morgan AB, Antonucci, JM, VanLandingham MR, Harris RH, Awad WH, Shields JR, *J. Appl. Polym. Sci.* 2003; 89:2072-8.
- <sup>xvi</sup> Yang F, Yngard R, Nelson GL, *J. Fire Sci.* 2005; 23:209-226.
- <sup>xvii</sup> Liu J, Gao Y, Wang F, Wu M, *J. Appl. Polym. Sci.* 2000; 75:384-9.
- <sup>xviii</sup> Okoshi M, Nishizawa H, *Fire Mater.* 2004; 28:423-9.
- <sup>xix</sup> Laachachi A, Leroy E, Cochez M, Ferriol M, Lopez Cuesta JM, *Polym. Degrad. Stab.* 2005; 89:344-52.
- <sup>xx</sup> Lichtenhan JD, Vu NQ, Carter JA, Gilman JW, Feher FJ, *Macromolecules* 1993; 26:2141-2.
- <sup>xxi</sup> Lichtenhan JD, Otonari YA, Carr MJ, *ibid* 1995; 28:8435-7.
- <sup>xxii</sup> Haddad TS, Lichtenhan JD, *ibid* 1996; 29:7302-4.
- <sup>xxiii</sup> <http://www.hybridplastics.com>.
- <sup>xxiv</sup> Mantz RA, Jones PF, Chaffee KP, Lichtenhan JD, Gilman JW, Ismail IMK, Burmeister MJ, *Chem. Mater.* 1996; 8:1250-9.
- <sup>xxv</sup> Schwab JJ, Lichtenhan JD, *Appl. Organometal. Chem.* 1998; 12:707-13.
- <sup>xxvi</sup> Ni Y, Zheng S, *Chem. Mater.* 2004; 16:5141-8.
- <sup>xxvii</sup> Mantz RA, Jones PF, Chaffee KP, Lichtenhan JD, Gilman JW, Ismail IMK, Burmeister MJ, *Chem. Mater.* 1996; 8:1250-9.
- <sup>xxviii</sup> Zheng L, Kasi RM, Farris RJ, Coughlin EB, *J. Polym. Sci. Part A, Polym. Chem.* 2002; 40:885-91.
- <sup>xxix</sup> Huang JC, He Cb, Xiao Y, Mya KY, Dai J, Siow YP, *Polymer* 2003; 44:4491-9.
- <sup>xxx</sup> Kashiwagi T, Gilman JW, in Grand AF, Wilkie CA, eds. *Fire Retardancy of Polymeric Materials*. New York, Marcel Dekker, 2000, Chapt. 10: 353-89.

- 
- xxx<sup>i</sup> Devaux E, Rochery M, Bourgiot S, *Fire Mater.* 2002; 26:149-54.
- xxx<sup>ii</sup> Bourgiot S, Flambar X, Rochery M, Le Bras M, Devaux E, Lichtenhan JD,
- xxx<sup>iii</sup> Guputa SK, Schwab JJ, Lee A, Fu BX, Hsiao BS, in “Affordable Materials Technology – Platform to Global Value and Performance” Rasmussen BM, Pilato LA, Kliger HS eds., SAMPE Pub. 2002; 47(2)1517-26.
- xxx<sup>iv</sup> Jash P, Wilkie CA, *Polym. Degrad. Stab.* 2005; 88:401-6.
- xxx<sup>v</sup> Nyden MR, Gilman JW, *Comp. and Theor. Polymer Science*, 1997; 7:191-8.
- xxx<sup>vi</sup> Uhl FW, Wilkie CA, *Polym. Degrad. Stab.*, 2002; 76:111-22.
- xxx<sup>vii</sup> Uhl FM, Wilkie CA, *ibid.* 2004; 84:215-26.
- xxx<sup>viii</sup> Xu J, Hu Y, Song L, Wang Q, Fan W, Liao G, Chen Z, *ibid.* 2001; 73: 29-31.
- xxx<sup>ix</sup> Yasmin A, Daniel IM, *Polymer* 2004; 45:8211-9.
- x<sup>l</sup> Zhu J, Wilkie CA, *Polym. Int.* 2000; 49:1158-63.
- x<sup>li</sup> Hshieh FY, Beeson HD, *Fire Mater.* 1997; 21:41-9.
- x<sup>lii</sup> Zhang R, Hu Y, Xu J, Fan W, Chen Z, *Polym Degrad Stab* 2004; 85:583-8.
- x<sup>liii</sup> Zhang R, Hu Y, Xu J, Fan W, Chen Z, Wang Q, *Macromole. Mater. Eng.* 2004; 289:355-9.
- x<sup>liv</sup> Zanetti M, Kashiwagi T, Falqui L, Camino G, *Chem Mater* 2002; 14:881-7.
- x<sup>lv</sup> Iijima S, *Nature* 1991; 354: 56-8.
- x<sup>lvi</sup> Kim P, Shi L, Majumdar A, McEuen PL, *Phys. Rev Lett* 2001; 87:215502
- x<sup>lvii</sup> Journet C, Maser WK, Bernier P, Loiseau A, Lamy de la Chapelle M, Lefrant A, Deniard P, Lee R, Fischer JE, *Nature* 1997; 388:756-8.
- x<sup>lviii</sup> Rinzler AG, Liu J, Dai H, Nikolaev P, Huffman CB, Todriguez\_Macias FJ, Boul PJ, Lu AH, Heymann D, Colbert DT, Lee RS, Fischer JE, Rao AM, Eklund PC, Smalley RE, *Appl Phys, A* 1998; 67:29-37.
- x<sup>lix</sup> Nikolaev P, Bronikowski MJ, Bradley RK, Fohmund F, Colbert DT, Smith KA, Smalley RE, *Chem Phys Lett* 1999; 313:91-7.
- <sup>l</sup> Hata K, Futaba DN, Mizuno K, Namai T, Yumura M, Iijima S, *Science* 2004; 306: 1362-4.
- <sup>li</sup> Height MJ, Howard JB, Tester JW, Vander Sande JB, *Carbon* 2004; 42:2295-307.
- <sup>lii</sup> Furtado CA, Kim UJ, Gutierrez HR, Pan L, Dickey EC, Eklund PC, *J. Am. Chem. Soc.* 2004; 126: 6095-105.
- <sup>liii</sup> Chiang IW, Brinson BE, Huang AY, Willis PA, Bronikowski MJ, Margrave JL, Smalley RE, Hauge RH, *J Phys Chem B* 2001; 105: 8297-
- <sup>liv</sup> Andrews R, Jacques D, Qian D, Dickey EC, *Carbon* 2001; 39:1681-7.
- <sup>lv</sup> Monthieux M, Smith BW, Burtex B, Claye A, Fischer JE, Luzzi DE, *ibid.* 2001; 39:1251-72.
- <sup>lvi</sup> Zhang M, Yudasaka M, Koshio A, Iijima S, *Chem Phys Lett* 2002; 364:420-6.
- <sup>lvii</sup> Jang J, Bae J, Yoon SH, *J Mater Chem* 2003; 13:676-81.
- <sup>lviii</sup> Futado CA, Kim UJ, Gutierrez HR, Pan L, Dickey EC, Eklund PC, *J Am Chem Soc* 2004; 126:6095-105.
- <sup>lix</sup> Ziegler KJ, Gu Z, Peng H, Flor EL, Hauge RH, Smalley RE, *ibid.* 2005; 127:1541-7.
- <sup>lx</sup> Kashiwagi T, Du F, Winey KI, Groth KM, Shields JR, Bellayer SP, Kim H, Douglas JF, *Polymer* 2005; 46: 471-81.
- <sup>lxi</sup> Tchmutin IA, Ponomarenko AT, Krinichnaya EP, Kozub GI, Efimov ON, *Carbon* 2003; 41:1391-5.

- 
- lxii Du F, Fischer JE, Winey KI, *J Polym Sci B Polymer Physics* 2004; 41:3333-8.
- lxiii Ajayan PM, Schadler LS, Giannaris C, Rubio A, *Adv Mater* 2000; 12:750-3.
- lxiv Chang TE, Jensen LR, Kisliuk A, Pipes RB, Pyrz R, Sokolov AP, *Polymer* 2004; 46:439-44.
- lxv Putz KW, Mitchell CA, Krishnamoorti R, Green PF, *J Polym Sci B Polymer Physics* 2004; 42:2286-93.
- lxvi Yang S, Castilleja JR, Barrera EV, Lozano K, *Polym Degrad Stab* 2004; 83:383-8.
- lxvii Miyagawa H, Drzal LT, *Polymer*; 45:5163-70.
- lxviii Beyer G, *Fire Mater.* 2005; 29:61-9.
- lxix Zhu J, Start P, Mauritz KA, Wilkie CA, *Polym Degrad Stab* 2002; 77:253-8.
- lxx Stephan C, Nguyen TP, Lahr B, Blau W, Lefrant S, Chauvet O, *J Mater Res* 2002; 17:396-400.
- lxxi Kilbride BE, Coleman JN, Fraysse J, Fournet P, Cadek M, Drury A, Hutzler S, Roth S, Blau WJ, *J Appl Phys* 2002; 92:4024-30.
- lxxii Barrau S, Demont P, Peigney A, Laurent C, Lacabanne C, *Macromolecules* 2003; 36:5187-94.
- lxxiii Hsu WK, Koteva V, Watts PCP, Chen GZ, *Carbon*; 2004; 42:1707-12.
- lxxiv Ruan SL, Gao P, Yang XG, Yu TX, *Polymer*; 44:5643-54.
- lxxv Breton Y, Desarmot G, Salvetat JP, Delpeux S, Sinturel C, Beguin F, Bonnamy S, *Carbon* 2004; 42:1027-30.
- lxxvi Meincke O, Kaempfer D, Weickmann H, Friedrich C, Vathauer M, Warth H, *Polymer* 2004; 45:739-48.
- lxxvii Liu T, Phang IY, Shen L, Chow SY, Zhang WD, *Macromolecules* 2004; 37:7214-22.
- lxxviii Kashiwagi T, Grulke E, Hilding J, Harris JrRH, Awd WH, Douglas J, *Macromol Rapid Commun* 2002; 23:761-5.
- lxxix Beyer G, *FireMater* 2002; 26:291-3.
- lxxx Kashiwagi T, Grulke E, Hilding J, Groth K, Harris RH, Butler K, Shields J, Kharchenko S, Douglas J, *Polymer* 2004; 45:4227-39.
- lxxxi Peeterbroeck S, Alexandre M, Nagy JB, Pirlot C, Fonseca A, Morea N, Philippin G, Delhalle J, Mekhalif Z, Sporken R, Beyer G, Dubois Ph, *Comp Sci Tech* 2004; 64:2317-23.
- lxxxii Schartel B, Pötschke P, Knoll U, Abdel-Goad M, *European Polym. J.* 2005; 41:1061-70.
- lxxxiii Gao F, Beyer G, Yuan Q, *Polym. Degrad. Stab.* 2005; 89:559-64.
- lxxxiv Watts PCP, Fearon PK, Hsu WK, Billingham NC, Kroto HW, Walton DRM, *J Mater Chem* 2003; 13:491-5.
- lxxxv Andrews R, Jacques D, Rao AM, Derbyshire F, Qian D, Fan X, Dickey EC, Chen J, *Chem Phys Lett* 1999; 303:467-74.
- lxxxvi Bom D, Andrews R, Jacques D, Anthony J, Chen B, Meier MS, Selegue JP, *Nano Lett* 2002; 2(6):615-9.
- lxxxvii Lozano K, Bonilla-Rios J, Barrera EV, *J Appl Polym Sci* 2001; 80:1162-72.
- lxxxviii Zeng J, Saltysiak B, Johnson WS, Schiraldi DA, Kumar S, *Composites Part B* 2004; 35:173-8.
- lxxxix Lozano K, Yang S, Zeng Q, *J Appl Polym Sci* 2004; 93:155-62.
- xc Gauthier C, Chazeau L, Prasse T, Cavaille JY, *Composit Sci Tech* 2005; 65:335-43.

---

<sup>xc</sup><sub>i</sub> Xu Y, Higgins B, Brittain J, Polymer 2005; 46:799-810.

<sup>xc</sup><sub>ii</sub> Kashiwagi T, Du F, Douglas JF, Winey KI, Harris RH, Shields, JR, Nature Materials, 2005;

<sup>xc</sup><sub>iii</sub> Quintiere JQ, "Surface Flame Spread" in the SFPE Handbook of Fire Protection Engineerin, Society of Fire Protection Engineerin, Third Edition, Chapt. 2-12, 2002.

<sup>xc</sup><sub>iv</sub> Kashiwagi, T. "Flammability of Nanocomposites: Effects of the Shape of Nanoparticles" in Fire Retardancy of Polymers, edited by Le Bras, M. Wilkie, CA, Bourbigot, S., Duquesne, S., and Jama C, The Royal Society of Chemistry, Cambridge, UK, Chapter 10, 2005.